Descriptive Statistics and Spatial Distributions of Geochemical Variables Associated with Manganese Oxide-Rich Phases in the Northern Pacific

U.S. GEOLOGICAL SURVEY BULLETIN 1863

Descriptive Statistics and Spatial Distributions of Geochemical Variables Associated with Manganese Oxide-Rich Phases in the Northern Pacific

By JOSEPH MOSES BOTBOL and GERALD I. EVENDEN

Tables, ogives, scatter plots, and gray-scale maps portray frequency characteristics, correlations, and spatial distributions of northern Pacific manganese oxide-rich phase geochemical data

U.S. GEOLOGICAL SURVEY BULLETIN 1863

DEPARTMENT OF THE INTERIOR
MANUEL LUJAN, JR., Secretary

U.S. GEOLOGICAL SURVEY
Dallas L. Peck, Director

UNITED STATES GOVERNMENT PRINTING OFFICE: 1989

For sale by the Books and Open-File Reports Section,
U.S. Geological Survey, Federal Center,
Box 25425, Denver, CO 80225

Library of Congress Cataloging in Publication Data

Botbol, Joseph Moses.
Descriptive statistics and spatial distributions of geochemical variables associated with manganese oxide-rich phases in the northern Pacific.

(U.S. Geological Survey bulletin ; 1863)
Bibliography: p.
Supt. of Docs. no.: I 19.3:1863
1. Manganese nodules—North Pacific Ocean. 2. Manganese ores—North Pacific Ocean. I. Evenden, Gerald Ian. II. Title. III. Series.
QE75.B9 no. 1863 557.3 s 88-600293
[QE390.2.M35] [553.4'629'091644]

CONTENTS

OVERLAY

FIGURES

TABLES

Descriptive Statistics and Spatial Distributions of Geochemical Variables Associated with Manganese Oxide-Rich Phases in the Northern Pacific

By Joseph Moses Botbol *and* Gerald I. Evenden

Abstract

Tables, graphs, and maps are used to portray the frequency characteristics and spatial distribution of manganese oxide-rich phase geochemical data, to characterize the northern Pacific in terms of publicly available nodule geochemical data, and to develop data portrayal methods that will facilitate data analysis. Source data are a subset of the Scripps Institute of Oceanography's Sediment Data Bank. The study area is bounded by 0° N., 40° N., 120° E., and 100° W. and is arbitrarily subdivided into 14 20° by 20° geographic subregions.

Frequency distributions of trace metals characterized in the original raw data are graphed as ogives, and salient parameters are tabulated. All variables are transformed to enrichment values relative to median concentration within their host subregions. Scatter plots of all pairs of original variables and their enrichment transforms are provided as an aid to the interpretation of correlations between variables. Gridded spatial distributions of all variables are portrayed as gray-scale maps.

The use of tables and graphs to portray frequency statistics and gray-scale maps to portray spatial distributions is an effective way to prepare for and facilitate multivariate data analysis.

INTRODUCTION

Future exploitation potential of reserves of strategic minerals in manganese oxide-rich phase ocean crusts and (or) nodules, hereinafter referred to as crusts and nodules, has long been a subject of national and corporate interest (McKelvey, 1986; Johnson and others, 1985). In past years, numerous scientific and economic studies have been conducted. Consequently, data have been accumulated that have contributed significantly to the definition and description of the nature of crusts, nodules, and their environments. These data are available in a form that supports detailed studies dealing with geological attributes of marine mineral deposits (Frazer and Fisk, 1980; DeYoung and others, 1984; Commeau and others, 1984).

This report is the first part of a two-part study on modeling of marine manganese oxide-rich phase mineral deposits. Herein are presented tabular and graphical statistical summaries and maps of the spatial distributions of chemical components in oceanic manganese nodules. The two principal purposes of this report are (1) to assemble publicly available geochemical data and generate descriptive statistics and data transformation methods that can be used to characterize the manganese oxide-rich phase mineral deposits of the northern Pacific and (2) to present data portrayal methods that will facilitate multivariate data analysis.

In 1985, at the inception of this project, the most widely known, comprehensive, and commonly available data base dealing specifically with manganese oxide-rich phase data was the Scripps Institute of Oceanography's (SIO) Sediment Data Bank (Frazer and Fisk, 1980) that deals with nodule geochemistry. Because of its consistent and well-organized nature, this data base was selected as an ideal basis for timely development of statistical data analysis and portrayal methods.

All data subsets were retrieved by using the Geologic Retrieval and Synopsis Program (GRASP) (Bowen and Botbol, 1975) on a UNIX-based microcomputer system (UNIX is a trade mark of Bell Laboratories, Murray Hill, N.J.). Statistical summaries were derived from procedures that were incorporated into GRASP and from computer programs that were written specifically for this application. Cartography and statistical graphics were produced entirely by the MAPGEN and PLOTGEN computer graphics systems (Evenden, 1988).

Acknowledgments

The authors gratefully acknowledge the assistance of Frank Manheim for contributions to data interpretation, Candice Lane-Bostwick for assistance with the data base,

Manuscript approved for publication, July 1, 1988.

Janet Fredericks for assistance in computer programming, and Allen Clark and Richard B. McCammon for their review of this manuscript.

RAW DATA

A northern Pacific Ocean subset of the SIO Sediment Data Bank was used for this study. Many of these data are the same as described by McKelvey and others (1983). The study area is bounded by 0° N., 40° N.,120° E., and 100° W. For this study, the area was arbitrarily subdivided into 14 20° by 20° geographic subregions. Each record in the SIO Sediment Data Bank contains the information that describes one ocean bottom sample; the retrieved subset that is used in this report makes use of the following variables: water depth above sample, geographic coordinates, and contents (in weight percent) of Co, Ni, Mn, Fe, Cu, Zn, Pb, Al, and Si. The reader should note that many of the variables are not present in all samples.

The fact that the SIO Sediment Data Bank is a relational data base of marine manganese nodule attributes implies that each record of the data base represents the chemical composition of a single marine manganese nodule. There are, however, many records in the data base whose chemical composition, location, and depth of occurrence suggest, according to recently developed criteria, that the records are more apt to be crusts than nodules. Inasmuch as the SIO Sediment Data Bank data subset that is used in this study was originally encoded without distinguishing between crust and nodule, no such distinction can be made in this study. Therefore, each unit record is considered only as a sample rich in manganese oxide phases.

Two aspects of the SIO Sediment Data Bank that should be noted are (1) the absence of sample quality control data and (2) the probable sampling of mixed populations. In general, data originally collected primarily for one purpose may often be unsuitable for another purpose, particularly with respect to sample design. The spacing and number of samples collected are critical in establishing quantifiable relations among the variables of interest. Also, evidence of mixed populations is shown in both the frequency distributions and in the scatter plots; the strongest evidence is depth of sample shown in the scatter plots of the depth versus variables (see figs. 37, 38). For the purposes of this study, neither lack of sample quality control data nor presence of mixed populations invalidates the informational content of the data.

FREQUENCY STATISTICS

Raw data frequency statistics are presented here in the form of tabular frequency distributions, ogives (cumulative frequency distributions), and scatter plots of element pairs.

Tabular frequency distribution characteristics and ogives show the frequency behavior of the variables in all of the subregions, and their comparison yields insight into differences in the geochemical landscape. Most importantly, one glimpse of the tables and graphics provides summary information necessary to describe the population(s) thereby enhancing the analyst's ability to recognize immediately differences in the data and, consequently, in the relevant geology. The descriptive statistics consist of the following: number of samples, mean, median, variance, standard deviation, minimum data value, maximum data value, and data range. For the tabular cumulative frequency distribution of all subregions considered collectively, Sturges' rule (from Huntsberger, 1963, p. 10) was used to determine the number of classes.

Scatter plots facilitate visual assessment of correlation between all pairs of variables in all subregions considered collectively, particularly in context with outliers and (or) data extrema.

Enrichment Transforms

The raw data are viewed first in a geochemical landscape of the entire study area, and subregional geochemical trends are then portrayed as geochemical enrichments. Geochemical enrichment of an element is most often measured by the simple ratio of its concentration to some chosen criterion such as crustal abundance. Such a ratio is always a positive number.

For the enrichment computation in this study, 1 is subtracted from the ratio of each datum to the ungrouped median for that variable in its host subregion. This subtraction results in an enrichment metric that is negative if the sample is impoverished and positive if the sample is enriched in a given element. Elemental content equal to that of the criterion has an enrichment of zero. Medians were selected rather than means because the median is less subject to perturbations by data extrema.

Small Samples

Many of the variables have low sample density in some subregions, and, in general, one should interpret these data with caution. Of major concern in the cartographic portrayal of small sample populations is the difficulty in establishing an area-of-influence to be used in the determination of reliable, quantitative interpolated data values.

Correlation Between Variables

Traditional product-moment linear correlation coefficients are not presented in this report because the distributions of the data values are not sufficiently well defined and

both nonlinear correlations and outliers seriously affect the correlation coefficient. For example, consider the zinc versus manganese scatter plot in figure 22 in which the outliers have been removed and the bivariate correlation is depicted as a high-density curvilinear dot pattern. The linear correlation coefficient for this pair of variables as shown is 0.65. However, the linear correlation coefficient for the entire zinc population, including the three outliers that were dropped from the distribution, is 0.11, a very dramatic reduction attributable to the 3 highest of almost 700 observations.

Therefore, rather than forcing the interpretations of the bivariate distributions to fit the constraints of a linear model, an arbitrary, ordinal, threefold classification of the scatter plot patterns is used. A visual estimate of the density and alignment of the points in the plot classifies correlations implicit in the scatter plot patterns as strong, moderate, or weak.

Spatial Distribution

To portray the spatial distributions of the data, a 28 by 77 grid was fit to the entire study area, and both raw data and enrichments were interpolated by using a 5-grid-unit search radius. The sizes of the grid mesh and search radius were selected on the basis of maximum areal coverage and minimum noise and smoothing. The interpolation weighting function used was a function of the inverse squared distance. Gray levels for each variable approximately correspond to the deciles of raw data frequency distribution.

A transparency in the pocket of this report shows continental and subregion boundaries and 200-mile limits within the study area. The transparency is to be used as a direct overlay on the gray-level and sample location maps.

FREQUENCY DISTRIBUTION CHARACTERISTICS

This section of the report discusses the frequency characteristics and spatial distribution of each variable and its enrichment transform in both sample space and variable space. The following are provided for each variable:

1. A table showing the cumulative frequency distribution and its salient parameters for all samples in the entire northern Pacific study area;
2. A table showing the salient frequency parameters in each subregion;
3. Graphs of ogives for each subregion and all subregions considered collectively;
4. Scatter plots of the raw data values for each variable versus raw data for all other variables;
5. Scatter plots of enrichment transforms for each variable versus enrichments of all other variables; and
6. Spot maps showing original sample locations and gray-scale maps of gridded spatial distributions of both raw and enrichment transformed data.

The data will be discussed one variable at a time. Discussion of the attributes of each variable will be in the following order:

1. Nature and occurrence of the data extrema as presented in the tables;
2. Salient features in the figure of ogives;
3. Salient features of raw data and enrichment scatter plots; and
4. Spatial distribution of data and enrichments as presented on the maps.

Each of the discussions is immediately followed by the relevant tables, graphs, and maps.

Cobalt

Cobalt concentration ranges from 0.01 percent in subregions 00, 04, 05, 06, 07, and 12 to 1.64 percent in subregion 03 (compare tables 1 and 2). Except for subregion 11, the aggregate of ogives in figure 1 shows a narrow range of Co contents up to approximately the 80th percentile, at which point the concentration range increases dramatically. The ogive for subregion 11 more closely approximates a parabola than an S-shaped curve, and because of its high range of cobalt concentrations and low sample density (N = 22), it is a viable candidate for further investigation.

In figure 2, cobalt shows a moderate positive correlation with both lead and iron. No correlation is apparent between cobalt and any of the other variables. This is also true of the enrichments (see fig. 3).

As shown in figure 4, high cobalt concentrations form an east-trending zone in the center of the study area at about 20° N. latitude. One lobe of this zone trends southward into subregions 9 and 10, and another lobe trends southward into subregion 11. Lowest cobalt concentrations occupy the northeast corner of subregion 05, almost all of subregion 07, and small areas of subregions 00, 01, 02, 03, and 12.

Cobalt enrichment is distributed similarly to the raw data except that the zones of highest positive enrichment are less continuous and the zones of moderately positive enrichment are broader than the distribution of raw-data values in those zones.

Table 1. Descriptive statistics for the distribution of Co concentration in Mn oxide-rich phases in the northern Pacific study area

Number of nonblank observations = 1,167

Number of classes (by Sturges' Rule) = 11
Class size = 0.14

Mean = 0.26
Median (ungrouped data) = 0.22
Variance = 0.03
Standard deviation = 0.18

Minimum value = 0.01
Maximum value = 1.64
Range = 1.63

Frequency distribution			
Class	Count	%	Cumulative %
0.01 —	275	23.56	23.56
0.16 —	604	51.76	75.32
0.31 —	182	15.60	90.92
0.45 —	45	3.86	94.77
0.60 —	20	1.71	96.49
0.75 —	19	1.63	98.11
0.90 —	13	1.11	99.23
1.05 —	3	0.26	99.49
1.20 —	2	0.17	99.66
1.34 —	2	0.17	99.83
1.49 —	2	0.17	100.00
1.64 —			

Table 2. Descriptive statistics for the distribution of Co concentration in Mn oxide-rich phases of subregions in the northern Pacific study area

Subregion	00	01	02	03	04	05	06
Number of samples	8	33	40	50	52	39	89
Mean	0.17	0.30	0.38	0.37	0.34	0.21	0.17
Median (ungrouped)	0.21	0.22	0.31	0.25	0.28	0.17	0.13
Variance	0.01	0.03	0.05	0.10	0.06	0.02	0.02
Standard deviation	0.10	0.19	0.23	0.33	0.26	0.16	0.15
Minimum value	0.01	0.05	0.04	0.07	0.01	0.01	0.01
Maximum value	0.36	0.78	1.04	1.64	1.17	0.90	1.00
Range	0.35	0.73	1.00	1.57	1.16	0.89	0.99

Subregion	13	12	11	10	09	08	07
Number of samples	26	20	22	219	367	139	63
Mean	0.24	0.27	0.52	0.31	0.22	0.25	0.15
Median (ungrouped)	0.24	0.33	0.40	0.26	0.21	0.24	0.13
Variance	0.01	0.01	0.15	0.04	0.00	0.00	0.02
Standard deviation	0.13	0.13	0.39	0.20	0.08	0.09	0.16
Minimum value	0.03	0.01	0.09	0.03	0.03	0.05	0.01
Maximum value	0.54	0.51	1.50	1.34	0.58	0.70	1.10
Range	0.51	0.50	1.41	1.31	0.55	0.65	1.09

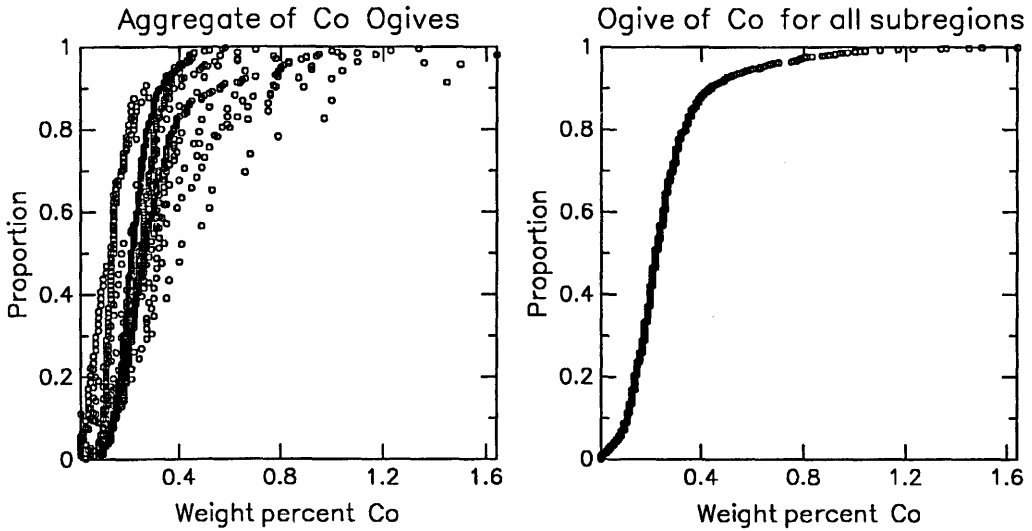

EXPLANATION

Below are ogives of Co content in manganese oxide-rich samples from 14 subregions (SR00–SR13) of a Pacific Ocean study area bounded by 0° N., 40° N., 120° E., and 100° W. All data are from the Scripps Institute of Oceanography's Sediment Data Bank. The relative geographic positions of the subregions are as depicted by the positions of the ogives below. Each datum on each ogive is represented by a circle.

In the upper left of this figure are two summary ogives showing frequency relations for the entire study area. The aggregate of Co ogives superimposes the individual subregion ogives, and the ogive of Co content for all subregions is a pooled, sorted plot of Co content of all subregions considered collectively.

The proportion of each datum is calculated as follows:

$$p = i / (N + 1)$$

where:

p = proportion of population ≤ corresponding Co content,
i = integer rank of datum in population, and
N = number of data points in the array.

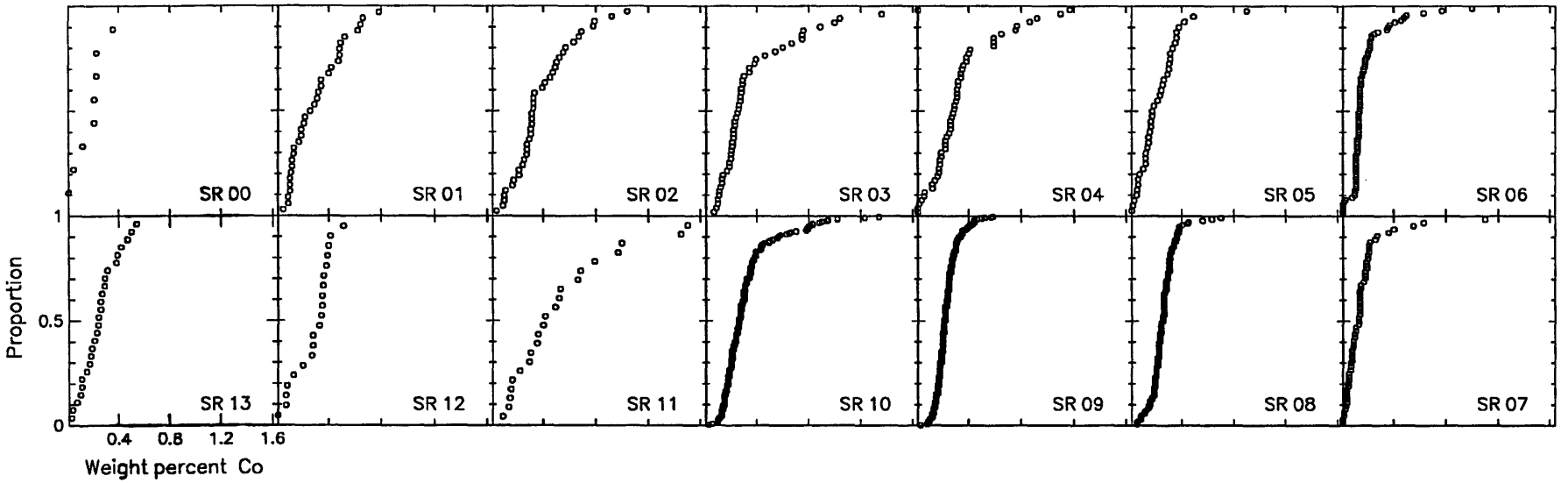

Figure 1. Ogives of Co concentration in northern Pacific subregions.

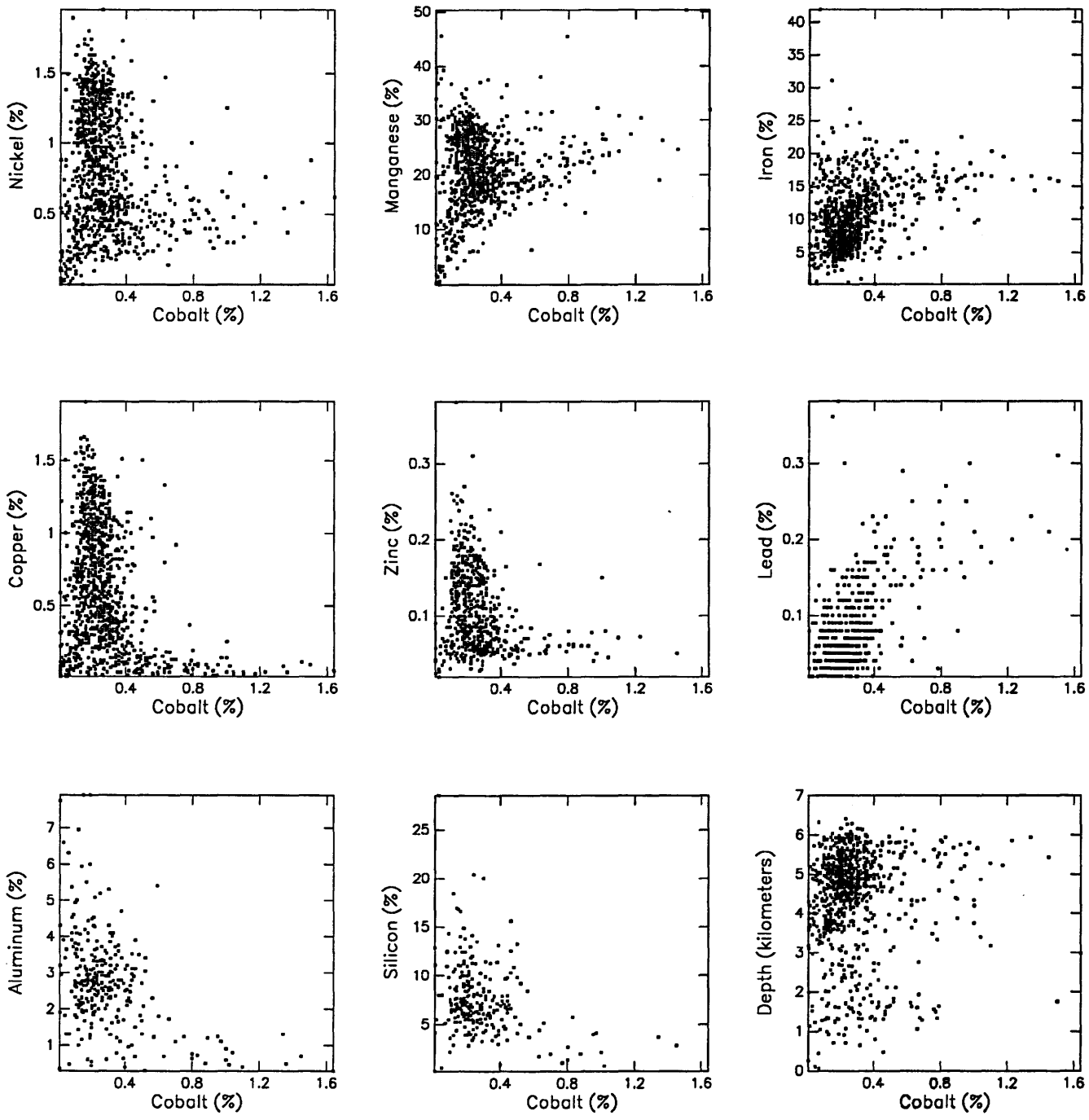

Figure 2. Scatter plots of Co content versus content of Ni, Mn, Fe, Cu, Zn, Pb, Al, Si, and depth in northern Pacific Mn oxide-rich phases.

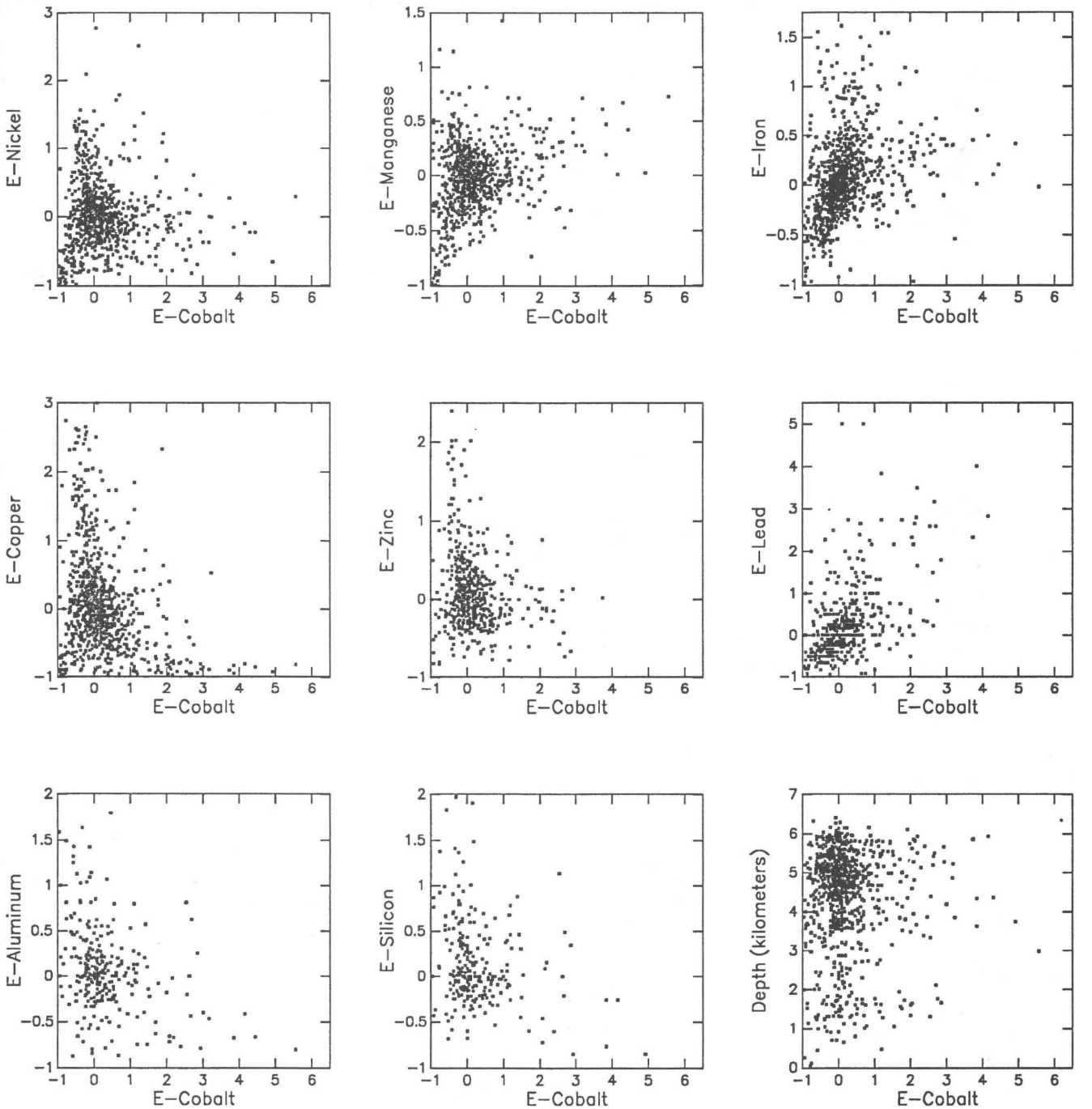

Figure 3. Scatter plots of Co enrichment (E) versus enrichment of Ni, Mn, Fe, Cu, Zn, Pb, Al, Si, and depth in northern Pacific Mn oxide-rich phases.

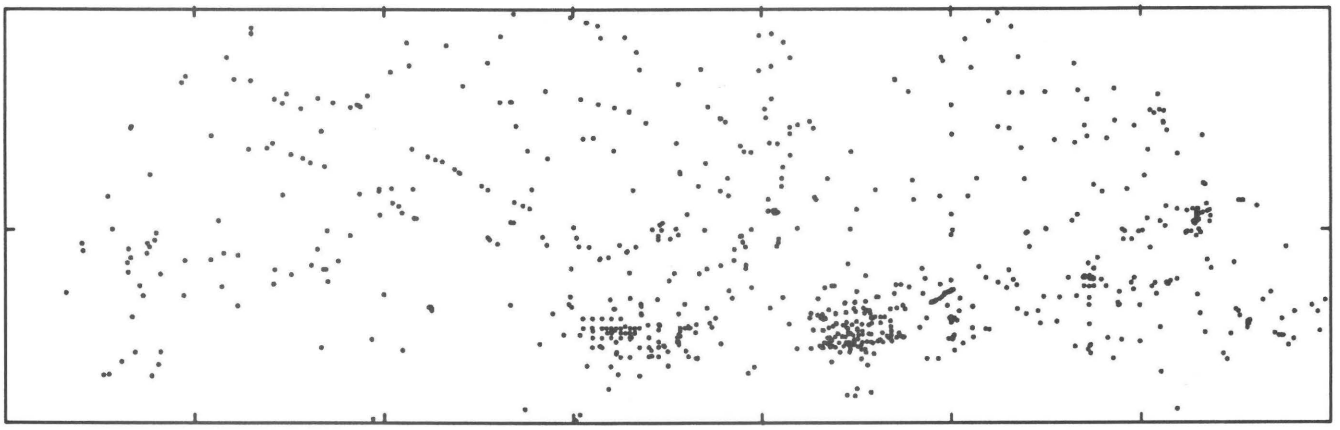

A

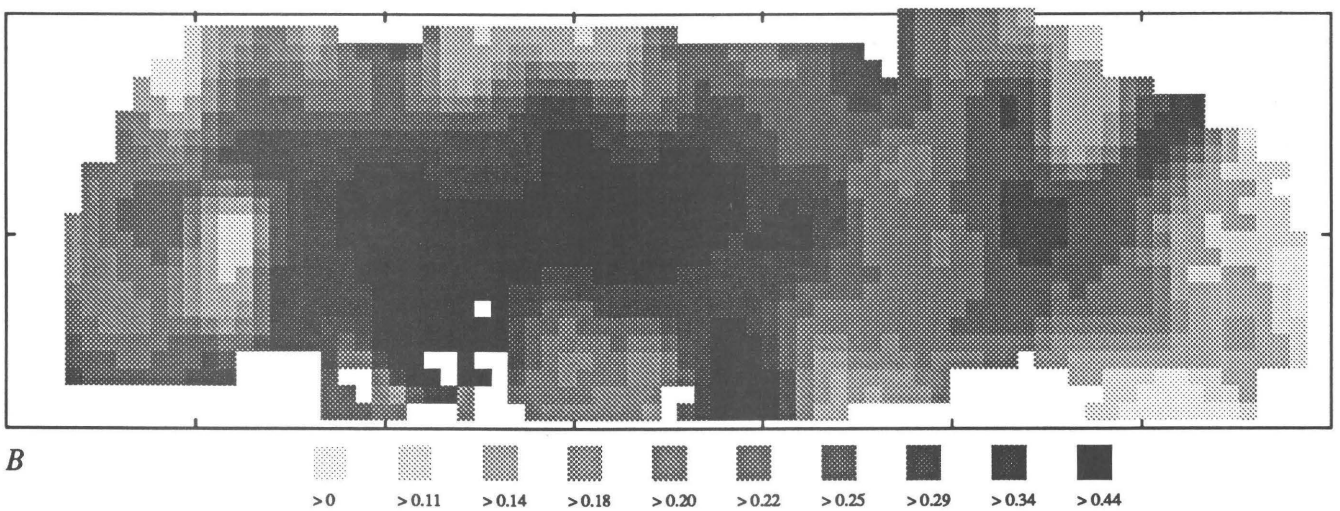

B

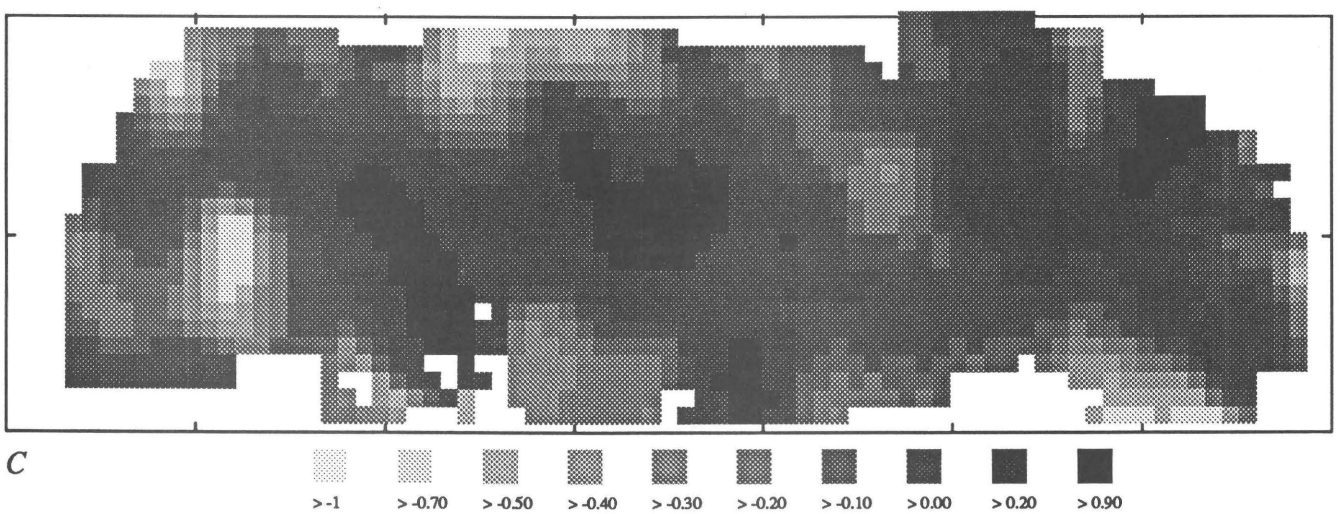

C

Figure 4. *A*, Sample locations. *B*, Distribution of Co content (weight percent). *C*, Enrichment in Mn oxide-rich phases of the northern Pacific study area. Subregion boundaries are provided by overlay in pocket.

Nickel

Nickel concentration ranges from 0.01 percent in subregion 04 to 1.95 percent in subregion 08 (compare tables 3 and 4). The aggregate of ogives in figure 5 shows a partition in the pattern of ogives; subregions 06, 07, 08, and 09 have much higher nickel values than those of the rest of the subregions. This partition of high nickel value is also shown in the spatial distribution of nickel concentration as shown in figure 8.

In the scatter plots (compare figs. 6 and 7), nickel shows a strong correlation with manganese, copper, and zinc. Although somewhat less well defined, this is also true for the enrichments of these variables. Nickel and nickel enrichment also show a strong negative correlation with iron. Nickel enrichment shows a very weak negative correlation with lead enrichment.

In figure 8, high nickel concentrations are found in the southeast corner of the study area in subregions 05, 06, 07, 08, and 09. None of the other subregions has nickel concentration above the overall median of 0.92 percent. The high values in 07, 08, and 09 correspond to the trace of the Clarion-Clipperton Zone.

The spatial distribution of high nickel enrichment forms a broad elliptical halo around a low enrichment nucleus that is roughly coincident with the east-west boundaries between subregions 03 and 10, and 04 and 09. The positive nickel enrichment area defined by subregions 05, 06, 07, 08, and 09 ranges from slightly enriched to slightly impoverished.

Table 3. Descriptive statistics for the distribution of Ni concentration in Mn oxide-rich phases in the northern Pacific study area

Number of nonblank observations = 1,228

Number of classes (by Sturges' Rule) = 11
Class size = 0.17

Mean = 0.87
Median (ungrouped data) = 0.92
Variance = 0.17
Standard deviation = 0.42

Minimum value = 0.01
Maximum value = 1.95
Range = 1.94

Frequency distribution			
Class	Count	%	Cumulative %
0.01 — 0.19	47	3.83	3.83
0.19 — 0.36	120	9.77	13.60
0.36 — 0.54	169	13.76	27.36
0.54 — 0.72	149	12.13	39.50
0.72 — 0.89	111	9.04	48.53
0.89 — 1.07	140	11.40	59.93
1.07 — 1.24	198	16.12	76.06
1.24 — 1.42	187	15.23	91.29
1.42 — 1.60	89	7.25	98.53
1.60 — 1.77	15	1.22	99.76
1.77 — 1.95	3	0.24	100.00

Table 4. Descriptive statistics for the distributions of Ni concentration in Mn oxide-rich phases of subregions in the northern Pacific study area

Subregion	00	01	02	03	04	05	06
Number of samples	8	33	40	50	56	40	127
Mean	0.33	0.38	0.49	0.52	0.46	0.62	0.94
Median (ungrouped)	0.34	0.33	0.46	0.48	0.44	0.52	1.09
Variance	0.04	0.05	0.03	0.05	0.06	0.11	0.13
Standard deviation	0.20	0.23	0.19	0.24	0.26	0.33	0.36
Minimum value	0.03	0.07	0.09	0.10	0.01	0.03	0.05
Maximum value	0.64	1.16	0.97	1.15	1.36	1.45	1.69
Range	0.61	1.09	0.88	1.05	1.35	1.42	1.64
Subregion	13	12	11	10	09	08	07
Number of samples	28	20	22	219	370	148	67
Mean	0.36	0.36	0.61	0.68	1.12	1.22	0.89
Median (ungrouped)	0.28	0.31	0.55	0.60	1.19	1.27	1.00
Variance	0.05	0.06	0.06	0.09	0.09	0.07	0.21
Standard deviation	0.23	0.25	0.24	0.31	0.31	0.27	0.46
Minimum value	0.03	0.03	0.28	0.08	0.15	0.11	0.04
Maximum value	1.30	1.17	1.17	1.54	1.74	1.95	1.89
Range	1.27	1.14	0.89	1.46	1.59	1.84	1.85

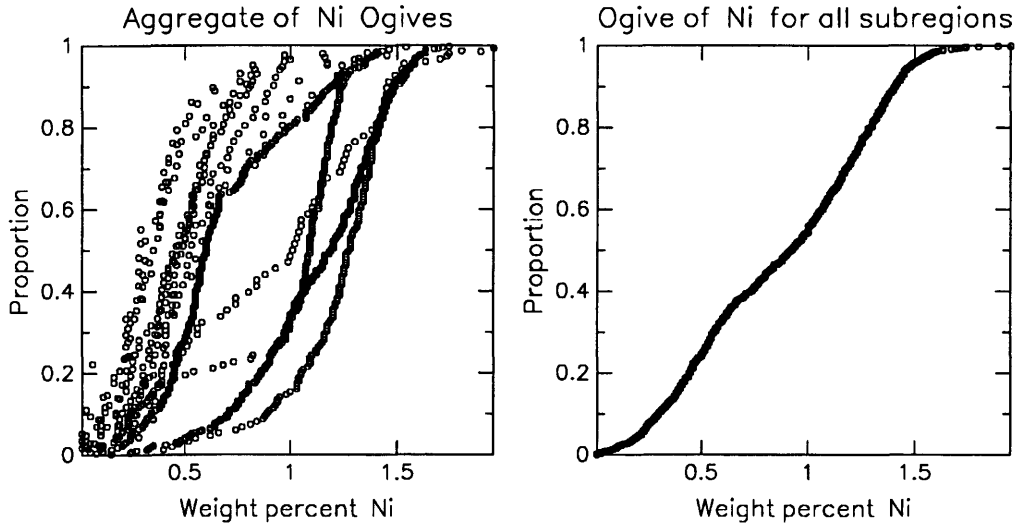

EXPLANATION

Below are ogives of Ni content in manganese oxide-rich samples from 14 subregions (SR00–SR13) of a Pacific Ocean study area bounded by 0° N., 40° N., 120° E., and 100° W. All data are from the Scripps Institute of Oceanography's Sediment Data Bank. The relative geographic positions of the subregions are as depicted by the positions of the ogives below. Each datum on each ogive is represented by a circle.

In the upper left of this figure are two summary ogives showing frequency relations for the entire study area. The aggregate of Ni ogives superimposes the individual subregion ogives, and the ogive of Ni content for all subregions is a pooled, sorted plot of Ni content of all subregions considered collectively.

The proportion of each datum is calculated as follows:

$$p = i / (N + 1)$$

where:

p = proportion of population ≤ corresponding Ni content,
i = integer rank of datum in population, and
N = number of data points in the array.

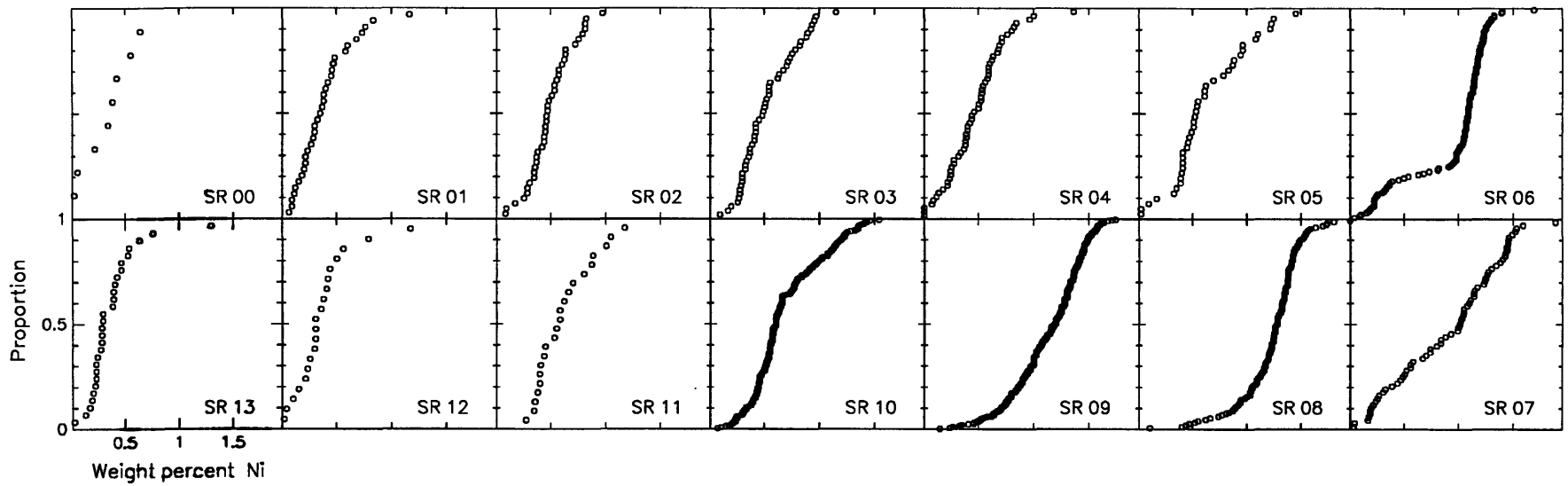

Figure 5. Ogives of Ni concentration in northern Pacific subregions.

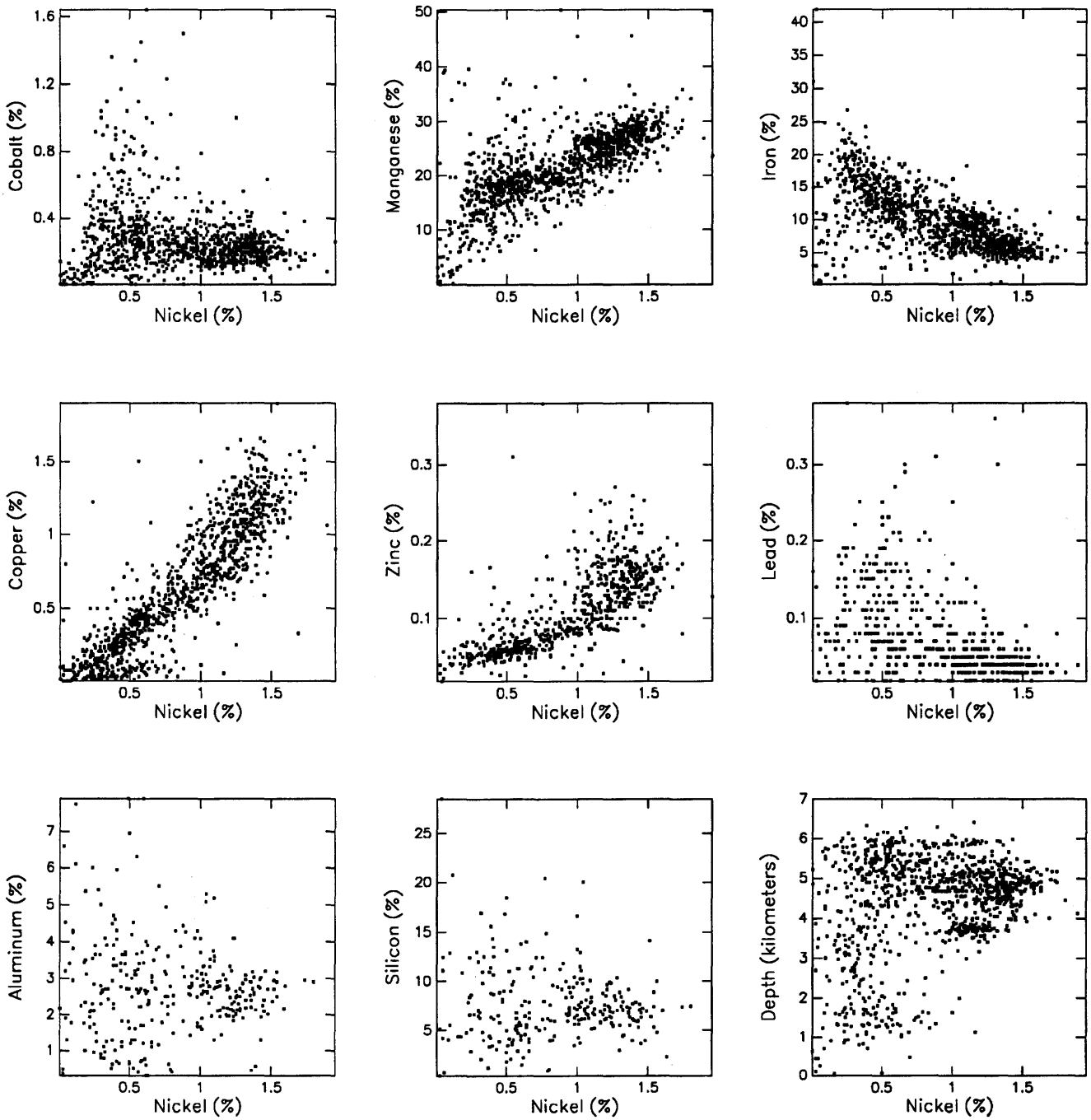

Figure 6. Scatter plots of Ni content versus content of Co, Mn, Fe, Cu, Zn, Pb, Al, Si, and depth in northern Pacific Mn oxide-rich phases.

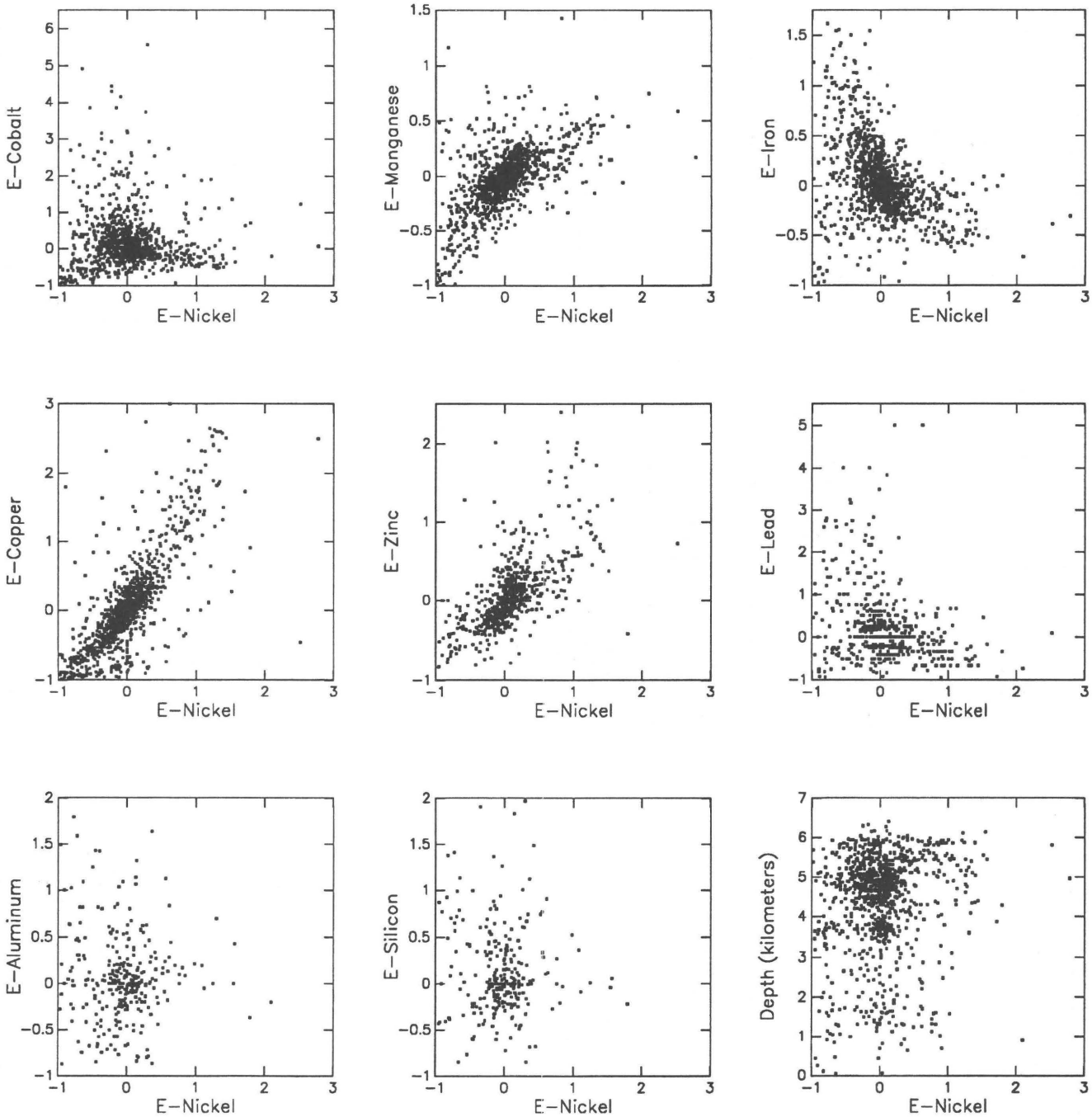

Figure 7. Scatter plots of Ni enrichment (E) versus enrichment of Co, Mn, Fe, Cu, Zn, Pb, Al, Si, and depth in northern Pacific Mn oxide-rich phases.

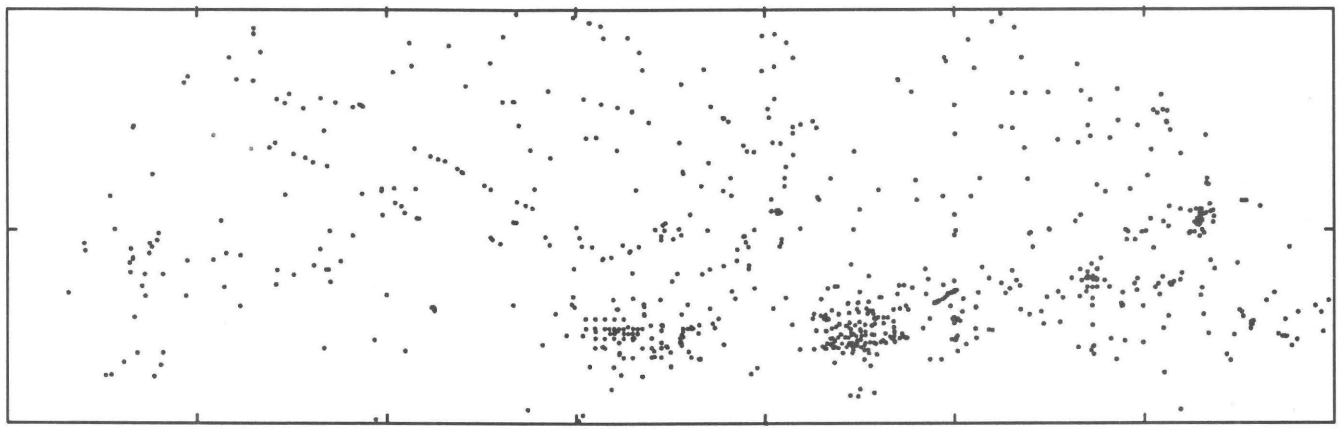

A

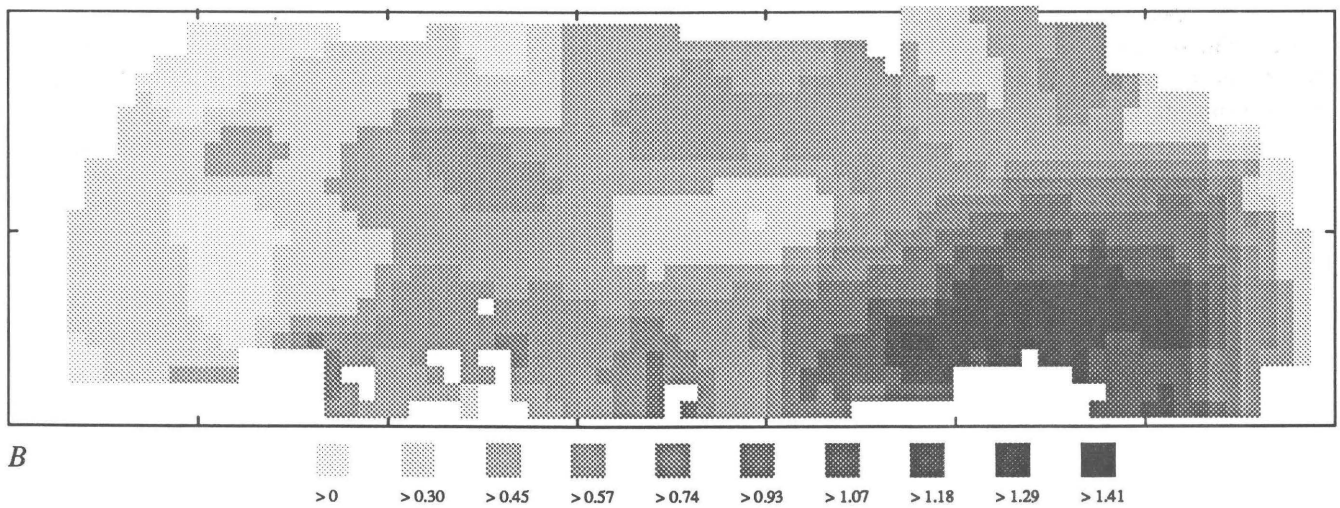

B

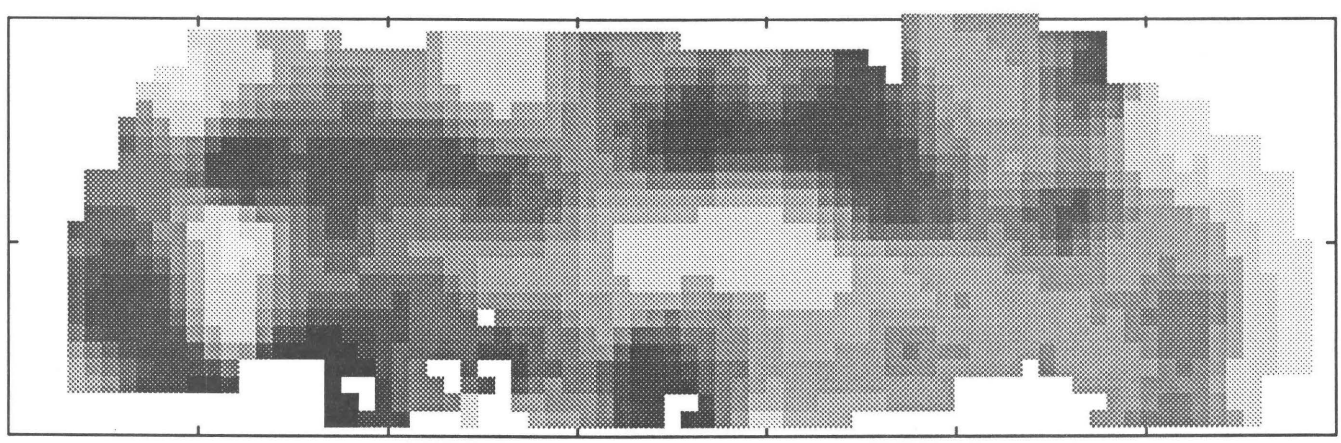

C

Figure 8. *A*, Sample locations. *B*, Distribution of Ni content (weight percent). *C*, Enrichment in Mn oxide-rich phases of the northern Pacific study area. Subregion boundaries are provided by overlay in pocket.

Manganese

Manganese concentration ranges from 0.07 percent in subregion 13 to 50.29 percent in subregion 11 (compare tables 5 and 6). The aggregate of ogives in figure 9 shows the vestige of two clusters of ogives: a cluster of higher grade distributions from subregions 06, 07, 08, and 09 and a rather narrow, lower grade band that falls within the remaining nine ogives.

The scatter plots in figure 10 show that manganese has a very strong positive correlation with nickel and copper and a strong curvilinear correlation with zinc. These relations are somewhat subdued in the counterpart scatter plots of the enrichments (see fig. 11). Manganese has a moderate negative correlation with iron and is weakly negatively correlated with aluminum and silicon. These negative correlations appear to be slightly more well defined in the scatter plots of the enrichments.

As shown in figure 12, manganese concentrations occur in two distinct areas; one area is defined by the subregions 06, 07, 08, and 09, and the other area is located almost entirely in subregion 11. The former group was also defined by the higher grade partition evident in the aggregate of ogives.

Excepting the area of high manganese concentration in subregion 11, distribution of manganese concentration is almost identical to that of nickel (see fig. 8). This also is true of the distribution of the manganese enrichments.

Table 5. Descriptive statistics for the distribution of Mn concentration in Mn oxide-rich phases in the northern Pacific study area

	Frequency distribution			
	Class	Count	%	Cumulative %
Number of nonblank observations = 1,218	0.07 — 4.64	18	1.48	1.48
Number of classes (by Sturges' Rule) = 11	4.64 — 9.20	34	2.79	4.27
Class size = 4.56	9.20 — 13.77	74	6.08	10.34
Mean = 21.56	13.77 — 18.34	227	18.64	28.98
Median (ungrouped data) = 22.00	18.34 — 22.90	312	25.62	54.60
Variance = 41.80	22.90 — 27.47	347	28.49	83.09
Standard deviation = 6.46	27.47 — 32.03	178	14.61	97.70
Minimum value = 0.07	32.03 — 36.60	15	1.23	98.93
Maximum value = 50.29	36.60 — 41.17	10	0.82	99.75
Range = 50.23	41.17 — 45.73	2	0.16	99.92
	45.73 — 50.30	1	0.08	100.00

Table 6. Descriptive statistics for the distributions of Mn concentration in Mn oxide-rich phases of subregions in the northern Pacific study area

Subregion	00	01	02	03	04	05	06
Number of samples	8	33	40	50	57	40	127
Mean	21.08	15.73	17.62	18.16	15.64	15.31	25.16
Median (ungrouped)	18.17	16.54	19.01	18.41	16.00	15.33	26.20
Variance	53.77	31.44	23.05	24.24	40.56	40.70	21.22
Standard deviation	7.33	5.60	4.80	4.92	6.36	6.38	4.60
Minimum value	14.65	1.90	2.20	6.73	0.17	0.60	11.70
Maximum value	39.29	26.29	25.70	31.79	28.00	27.00	39.56
Range	24.64	24.40	23.50	25.07	27.83	26.40	27.86
Subregion	13	12	11	10	09	08	07
Number of samples	28	20	22	219	365	144	65
Mean	15.24	14.35	22.01	19.76	23.27	25.55	24.10
Median (ungrouped)	15.20	15.00	18.74	18.85	23.95	26.40	25.79
Variance	31.50	24.55	89.11	24.60	24.09	25.96	80.69
Standard deviation	5.61	4.95	9.44	4.96	4.90	5.09	8.98
Minimum value	0.07	5.00	10.87	1.90	2.60	2.50	1.70
Maximum value	32.59	27.20	50.29	34.20	36.43	37.50	45.59
Range	32.52	22.20	39.43	32.29	33.83	35.00	43.89

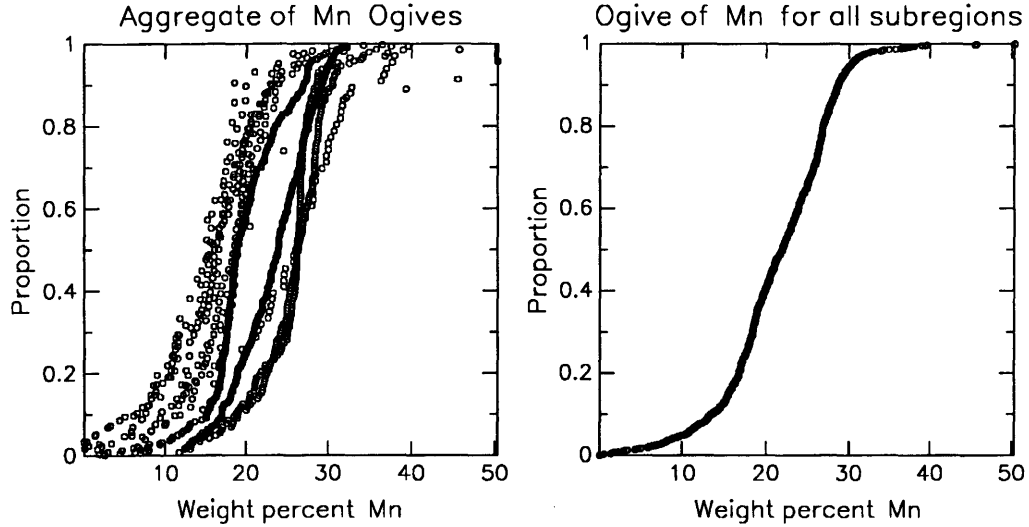

EXPLANATION

Below are ogives of Mn content in manganese oxide-rich samples from 14 subregions (SR00–SR13) of a Pacific Ocean study area bounded by 0° N., 40° N., 120° E., and 100° W. All data are from the Scripps Institute of Oceanography's Sediment Data Bank. The relative geographic positions of the subregions are as depicted by the positions of the ogives below. Each datum on each ogive is represented by a circle.

In the upper left of this figure are two summary ogives showing frequency relations for the entire study area. The aggregate of Mn ogives superimposes the individual subregion ogives, and the ogive of Mn content for all subregions is a pooled, sorted plot of Mn content of all subregions considered collectively.

The proportion of each datum is calculated as follows:

$$p = i / (N + 1)$$

where:

p = proportion of population ≤ corresponding Mn content,
i = integer rank of datum in population, and
N = number of data points in the array.

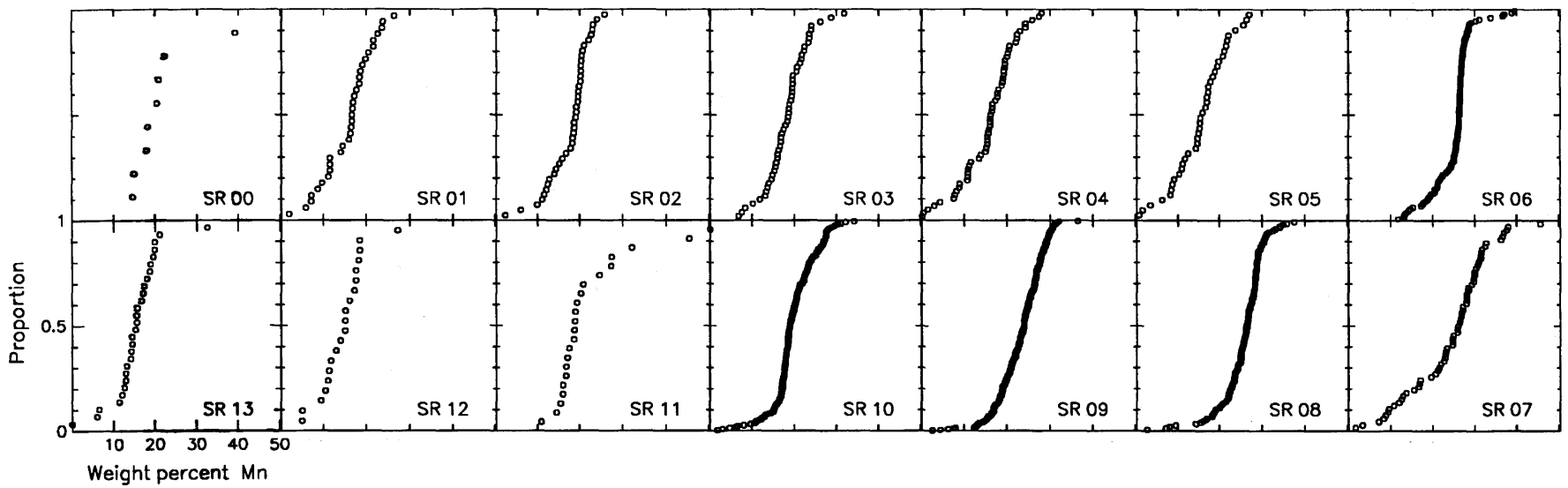

Figure 9. Ogives of Mn concentration in northern Pacific subregions.

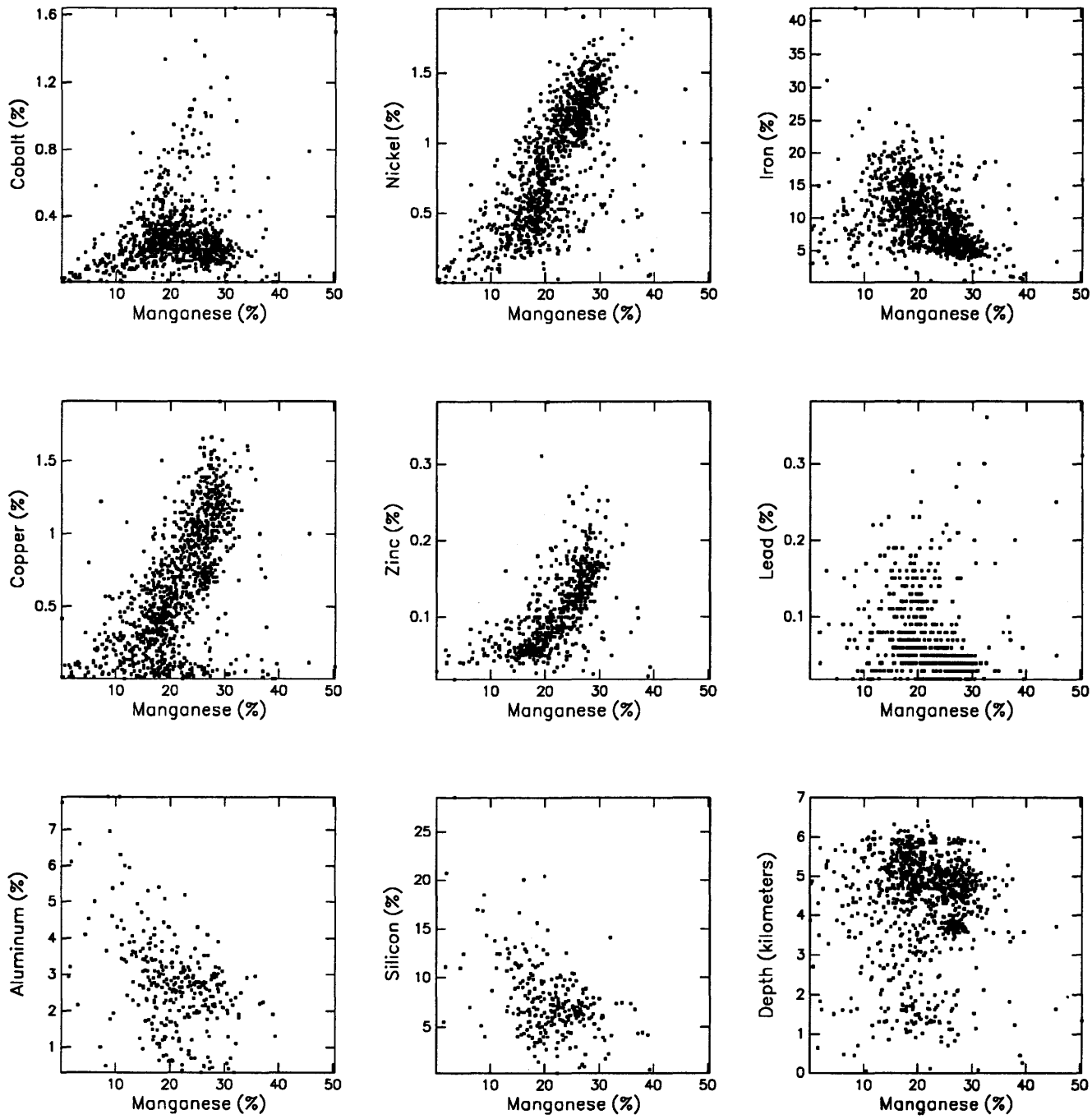

Figure 10. Scatter plots of Mn content versus content of Co, Ni, Fe, Cu, Zn, Pb, Al, Si, and depth in northern Pacific Mn oxide-rich phases.

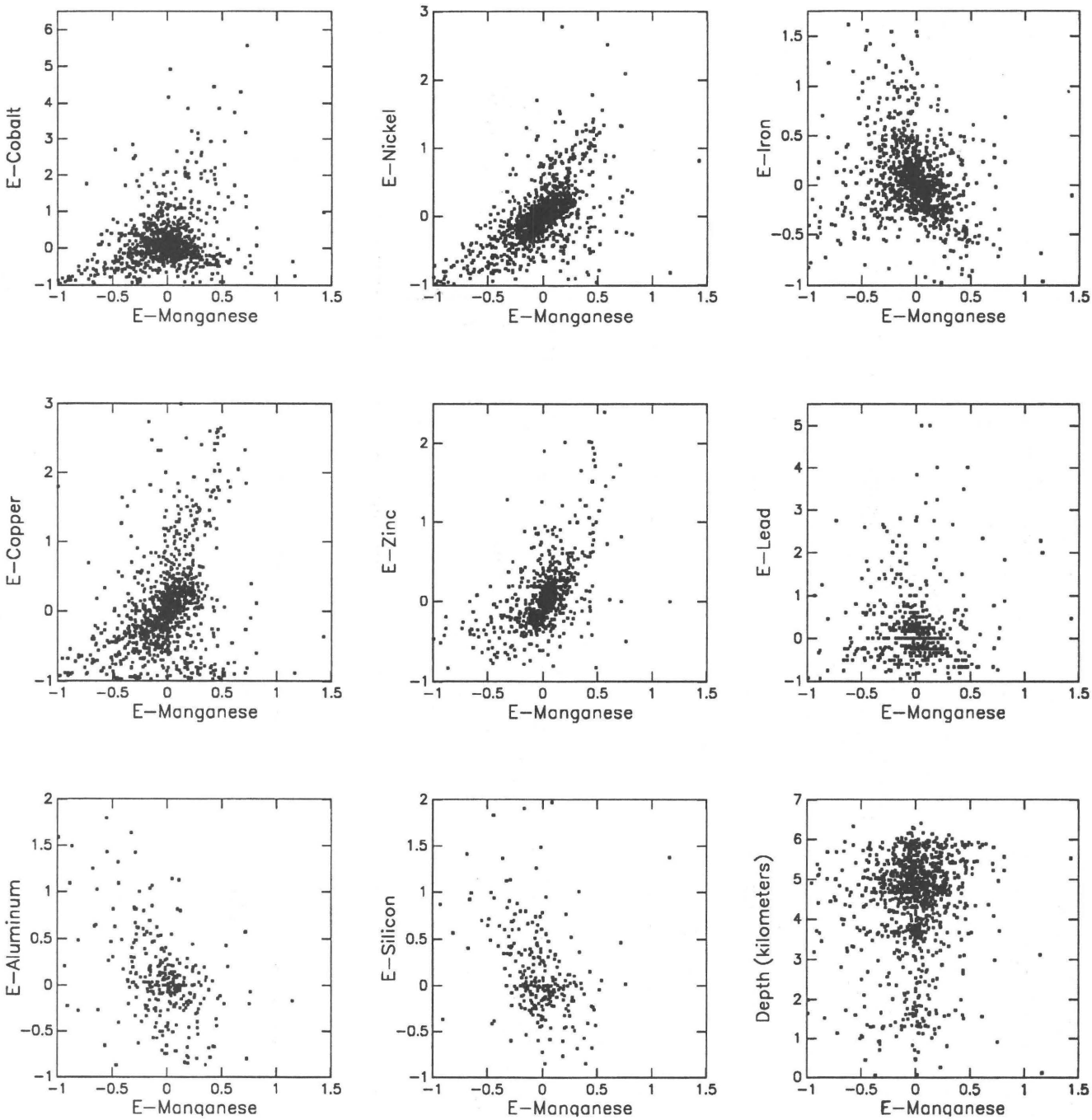

Figure 11. Scatter plots of Mn enrichment (E) versus enrichment of Co, Ni, Fe, Cu, Zn, Pb, Al, Si, and depth in northern Pacific Mn oxide-rich phases.

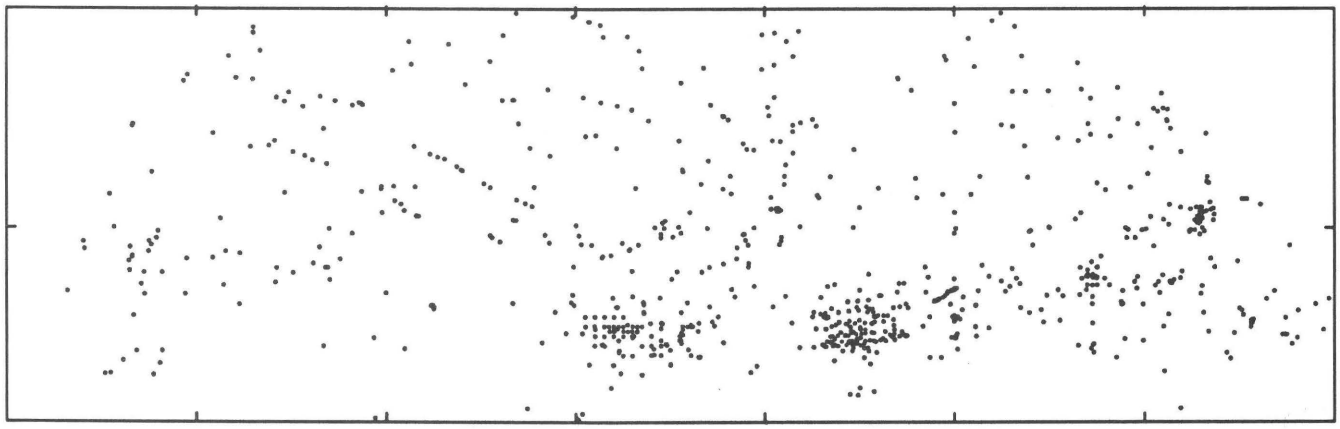

A

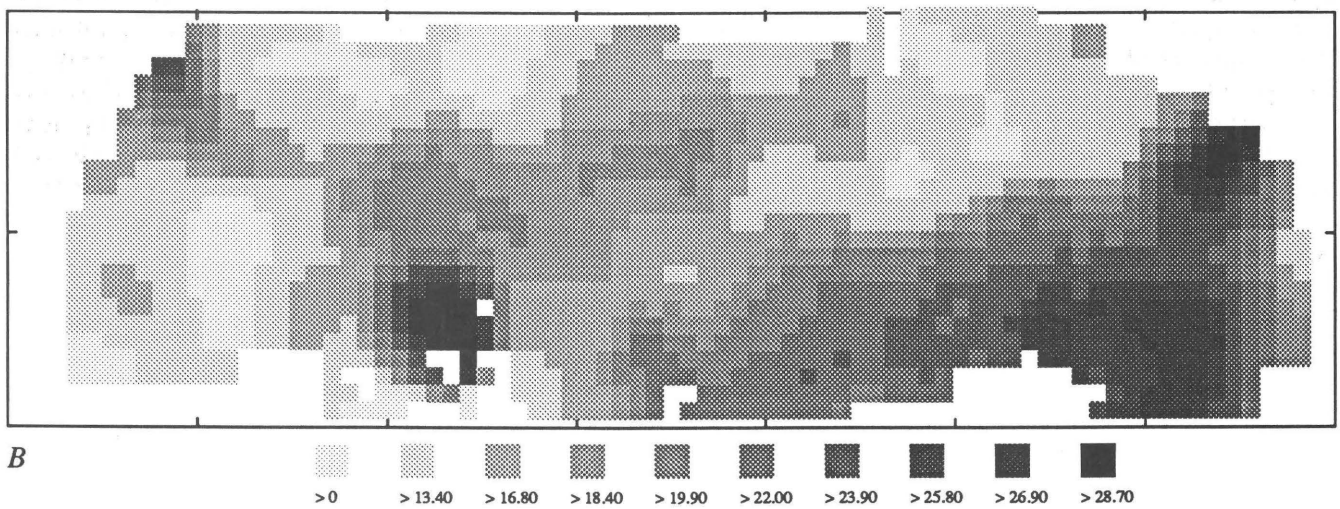

B

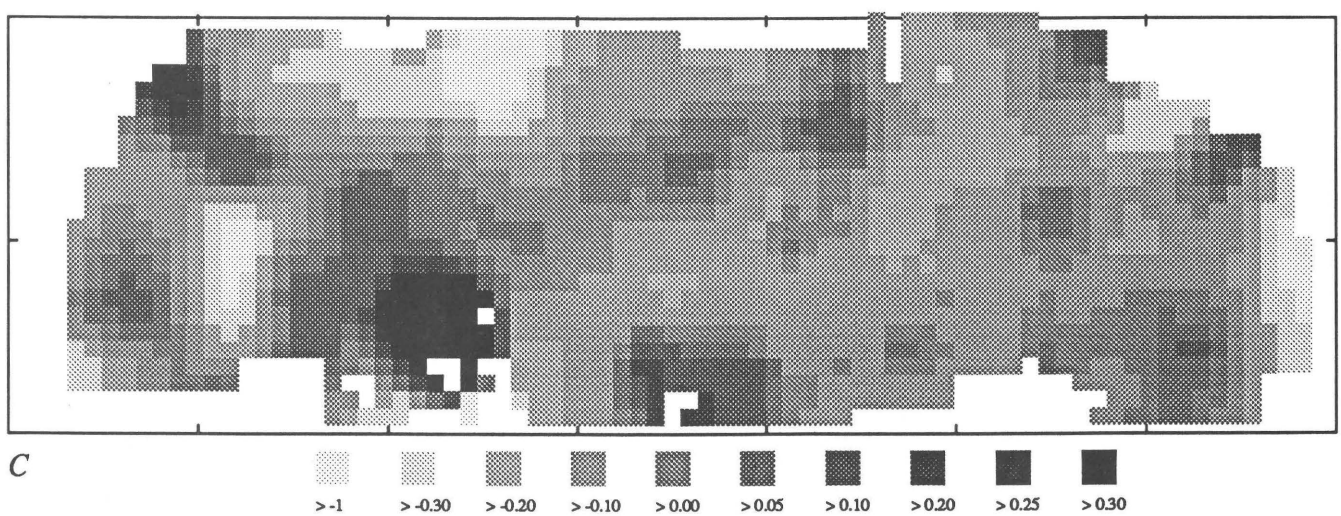

C

Figure 12. *A*, Sample locations. *B*, Distribution of Mn content (weight percent). *C*, Enrichment in Mn oxide-rich phases of the northern Pacific study area. Subregion boundaries are provided by overlay in pocket.

Iron

Iron concentration values range from 0.3 percent in subregion 07 to 41.9 percent in subregion 05 (compare tables 7 and 8). In figure 13, the aggregate of ogives, the frequency distributions of iron in subregions 08 and 09 are almost coincidental and constitute the distinct lower grade boundary of the aggregate pattern.

The scatter plots in figures 14 and 15 show that iron has a strong negative correlation with nickel and copper and a moderate negative correlation with manganese and zinc. In the scatter plots of the enrichments, these correlations appear to be more subdued. Iron has a moderate positive correlation with cobalt and lead. This is also true for their enrichments.

As is substantiated by the strong negative correlation of iron with nickel in the scatter plot, the spatial distribution of iron concentrations are almost exactly the opposite of those of nickel (compare figs. 8 and 16). Low-value iron content is concentrated in a well-defined area centered in subregion 08 and extending laterally into subregions 07 and 09. The distribution of iron enrichments is also opposite to that of nickel.

Table 7. Descriptive statistics for the distribution of Fe concentration in Mn oxide-rich phases in the northern Pacific study area

	Frequency distribution			
	Class	Count	%	Cumulative %
Number of nonblank observations = 1,211	0.30 — 4.08	38	3.14	3.14
Number of classes (by Sturges' Rule) = 11	4.08 — 7.86	444	36.66	39.80
Class size = 3.78	7.86 — 11.65	355	29.31	69.12
Mean = 9.90	11.65 — 15.43	221	18.25	87.37
Median (ungrouped data) = 9.31	15.43 — 19.21	112	9.25	96.61
Variance = 20.19	19.21 — 22.99	32	2.64	99.26
Standard deviation = 4.49	22.99 — 26.77	7	0.58	99.83
Minimum value = 0.30	26.77 — 30.55	0	0.00	99.83
Maximum value = 41.90	30.55 — 34.34	1	0.08	99.92
Range = 41.60	34.34 — 38.12	0	0.00	99.92
	38.12 — 41.90	1	0.08	100.00

Table 8. Descriptive statistics for the distribution of Fe concentration in Mn oxide-rich phases of subregions in the northern Pacific area

Subregion	00	01	02	03	04	05	06
Number of samples	8	33	40	50	56	40	127
Mean	15.02	13.72	13.36	12.78	14.21	11.23	10.67
Median (ungrouped)	18.62	14.80	12.90	11.95	13.90	10.32	10.09
Variance	72.99	15.42	6.00	8.92	27.14	35.09	12.43
Standard deviation	8.54	3.92	2.45	2.98	5.21	5.92	3.52
Minimum value	0.42	2.90	8.20	7.10	3.00	4.50	0.86
Maximum value	24.20	20.00	19.77	20.20	31.00	41.90	22.10
Range	23.78	17.10	11.57	13.11	28.00	37.40	21.24
Subregion	13	12	11	10	09	08	07
Number of samples	28	20	22	219	364	140	64
Mean	16.27	14.93	13.56	10.81	7.22	6.91	9.79
Median (ungrouped)	17.36	14.92	14.47	11.02	6.35	6.64	9.10
Variance	24.63	9.16	9.22	14.95	8.20	4.66	22.30
Standard deviation	4.96	3.02	3.03	3.86	2.86	2.16	4.72
Minimum value	2.97	9.87	6.89	2.37	1.78	0.50	0.30
Maximum value	24.60	19.60	18.50	26.70	23.20	14.93	23.79
Range	21.63	9.73	11.61	24.33	21.42	14.43	23.50

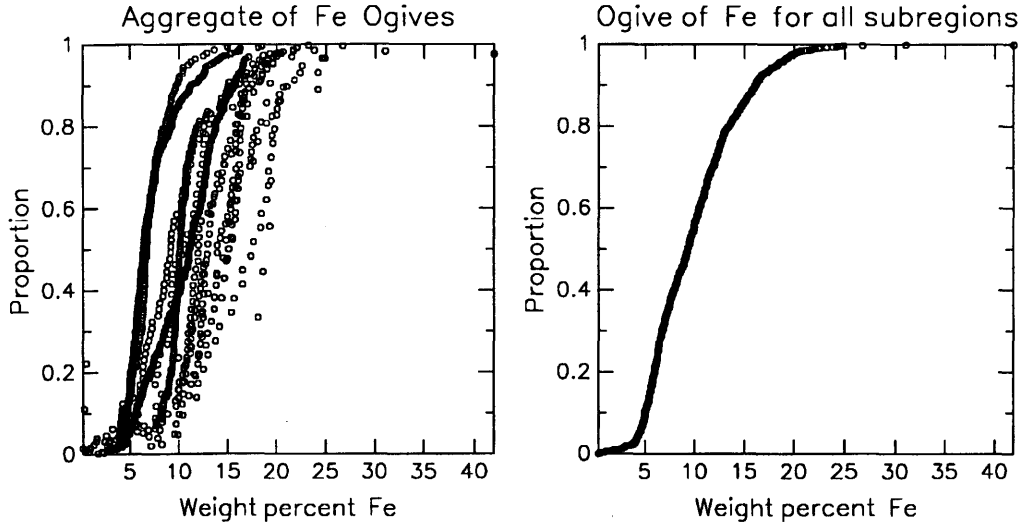

EXPLANATION

Below are ogives of Fe content in manganese oxide-rich samples from 14 subregions (SR00–SR13) of a Pacific Ocean study area bounded by 0° N., 40° N., 120° E., and 100° W. All data are from the Scripps Institute of Oceanography's Sediment Data Bank. The relative geographic positions of the subregions are as depicted by the positions of the ogives below. Each datum on each ogive is represented by a circle.

In the upper left of this figure are two summary ogives showing frequency relations for the entire study area. The aggregate of Fe ogives superimposes the individual subregion ogives, and the ogive of Fe content for all subregions is a pooled, sorted plot of Fe content of all subregions considered collectively.

The proportion of each datum is calculated as follows:

$$p = i / (N + 1)$$

where:

p = proportion of population ≤ corresponding Fe content,
i = integer rank of datum in population, and
N = number of data points in the array.

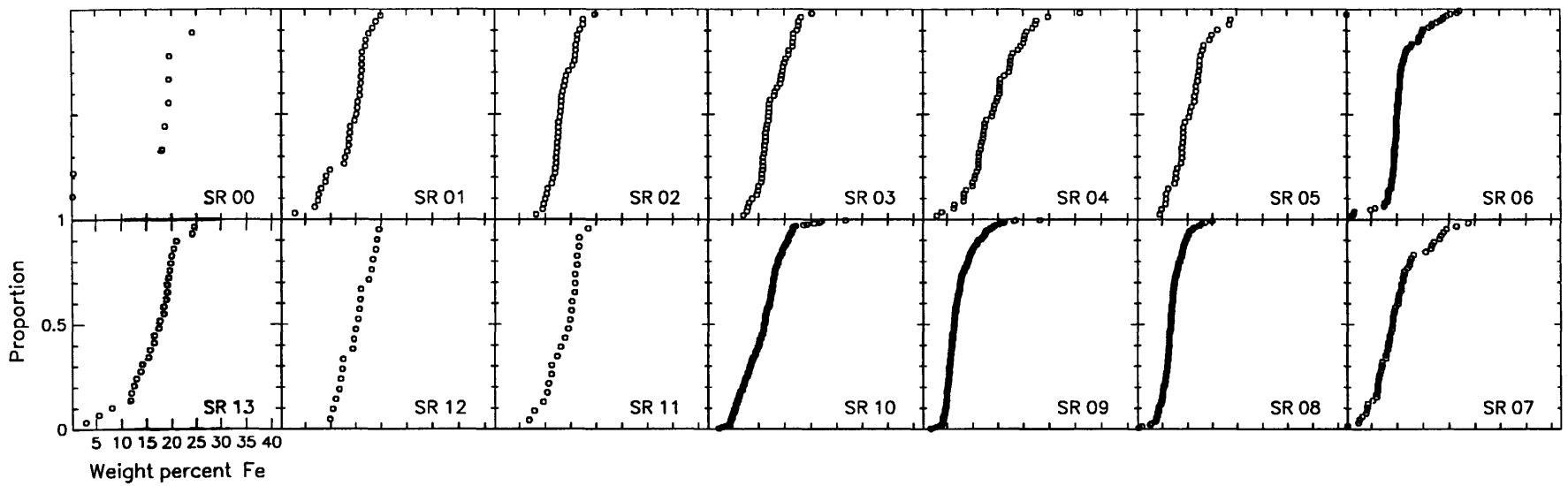

Figure 13. Ogives of Fe concentration in northern Pacific subregions.

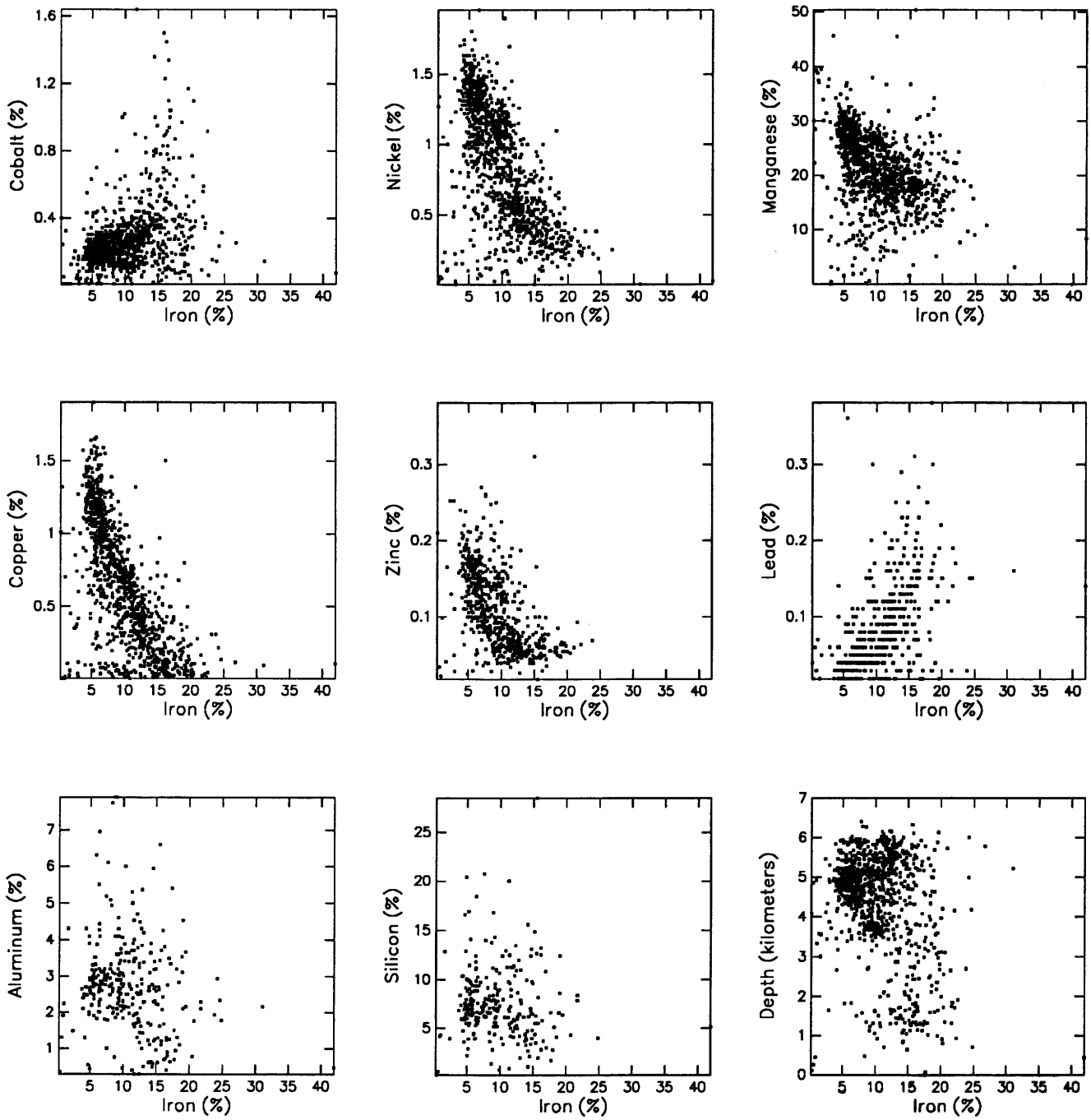

Figure 14. Scatter plots of Fe content versus content of Co, Ni, Mn, Cu, Zn, Pb, Al, Si, and depth in northern Pacific Mn oxide-rich phases.

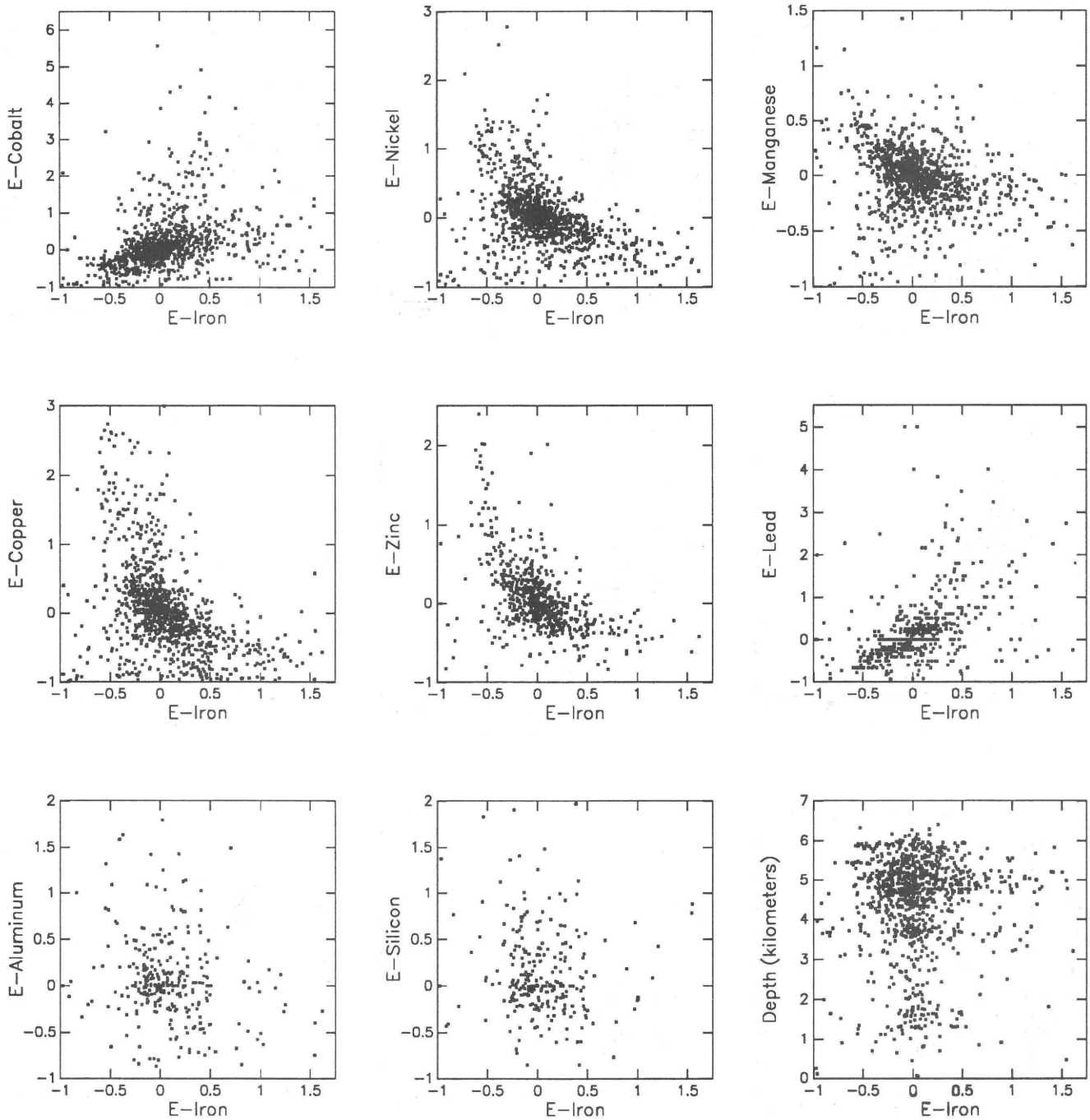

Figure 15. Scatter plots of Fe enrichment (E) versus enrichment of Co, Ni, Mn, Cu, Zn, Pb, Al, Si, and depth in northern Pacific Mn oxide-rich phases.

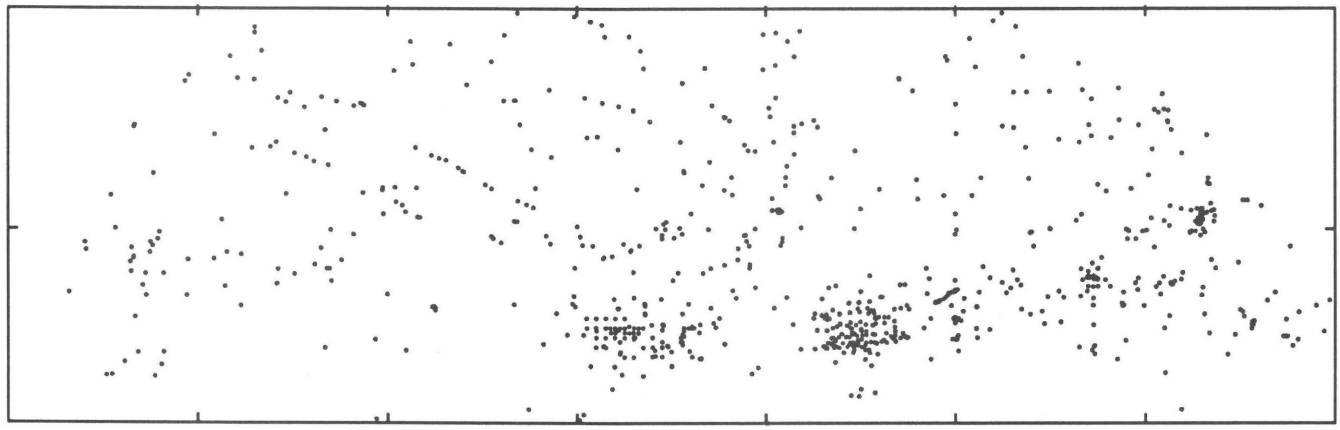

A

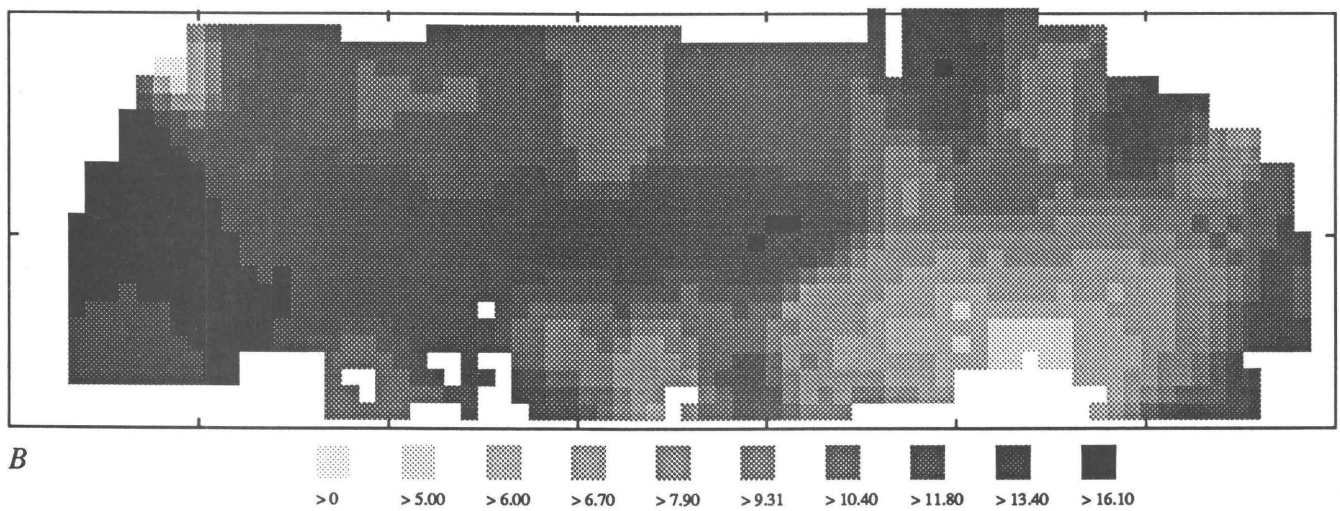

B

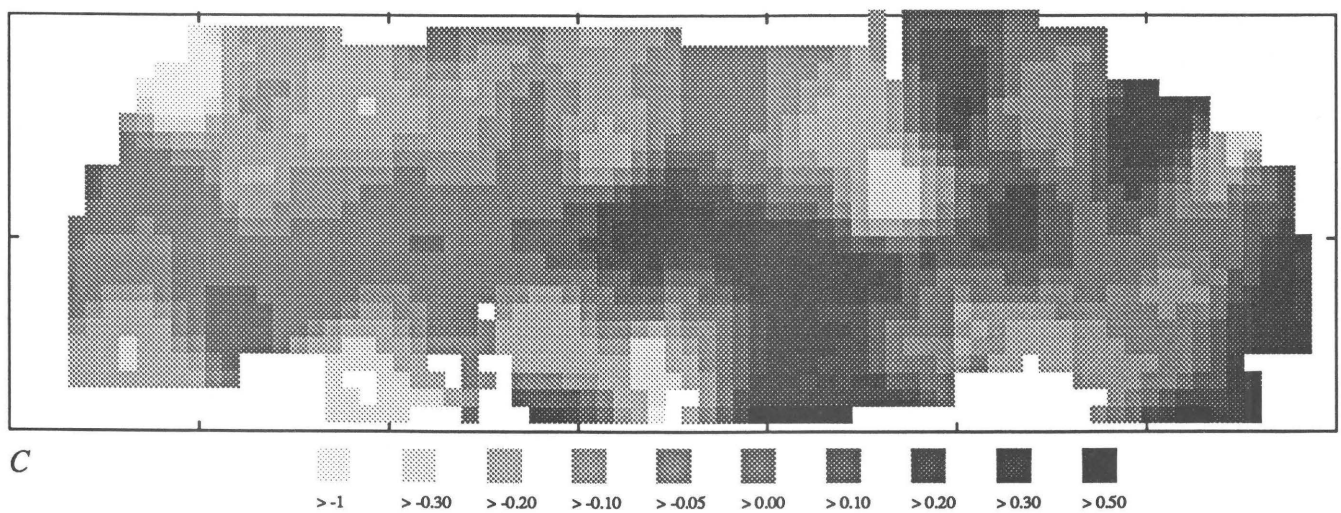

C

Figure 16. *A*, Sample locations. *B*, Distribution of Fe content (weight percent). *C*, Enrichment in Mn oxide-rich phases of the northern Pacific study area. Subregion boundaries are provided by overlay in pocket.

Copper

Copper concentration ranges from 0.01 percent in subregions 00, 04, and 06 to 1.9 percent in subregion 10 (compare tables 9 and 10). In figure 17, the aggregate of ogives shows four distinct ogive patterns: (1) the similarity of the ogives for subregions 08 and 09, (2) the similarity of ogives for subregions 06 and 07, (3) the uniqueness of subregion 10, and (4) the clustering of the patterns for all other subregions.

Scatter plots in figures 18 and 19 show that copper has a strong positive correlation with manganese, nickel, and zinc; a strong negative correlation with iron; and a weak negative correlation with lead. This is also true of the enrichments of these variables.

In figure 20, most of the high copper content is localized in subregions 07, 08, and 09 in the vicinity of the trace of the Clarion-Clipperton Zone. Subregion 10, however, appears quite distinct and, as illustrated in the map of enrichments, exhibits a high degree of increase in high copper content (above the 70th percentile).

Areas of high enrichment occur in a halolike pattern around a nucleus of low enrichment near the intersection of subregions 03, 04, 09, and 10. The enrichment also shows a persistent moderate high in the areas included by subregions 07, 08, and 09. Subregions 10 and 11 constitute an isolated area of high enrichment.

Table 9. Descriptive statistics for the distribution of Cu concentration in Mn oxide-rich phases in the northern Pacific study area

	Frequency distribution			
	Class	Count	%	Cumulative %
Number of nonblank observations = 1,218	0.01 — 0.18	193	15.85	15.85
Number of classes (by Sturges' Rule) = 11	0.18 — 0.35	158	12.97	28.82
Class size = 0.17	0.35 — 0.53	160	13.14	41.95
Mean = 0.65	0.53 — 0.70	150	12.32	54.27
Median (ungrouped data) = 0.64	0.70 — 0.87	159	13.05	67.32
Variance = 0.16	0.87 — 1.04	127	10.43	77.75
Standard deviation = 0.40	1.04 — 1.21	145	11.90	89.66
Minimum value = 0.01	1.21 — 1.38	80	6.57	96.22
Maximum value = 1.90	1.38 — 1.56	36	2.96	99.18
Range = 1.89	1.56 — 1.73	9	0.74	99.92
	1.73 — 1.90	1	0.08	100.00

Table 10. Descriptive statistics for the distributions of Cu concentration in Mn oxide-rich phases of subregions in the northern Pacific study area

Subregion	00	01	02	03	04	05	06
Number of samples	8	32	37	50	52	39	127
Mean	0.17	0.14	0.23	0.30	0.27	0.40	0.55
Median (ungrouped)	0.09	0.11	0.20	0.28	0.27	0.31	0.67
Variance	0.02	0.01	0.02	0.03	0.04	0.05	0.07
Standard deviation	0.16	0.10	0.15	0.19	0.21	0.23	0.27
Minimum value	0.01	0.04	0.02	0.03	0.01	0.10	0.01
Maximum value	0.50	0.50	0.53	0.70	1.10	1.03	1.04
Range	0.49	0.46	0.51	0.67	1.09	0.93	1.03
Subregion	13	12	11	10	09	08	07
Number of samples	28	20	22	218	370	148	67
Mean	0.22	0.23	0.30	0.56	0.91	0.99	0.67
Median (ungrouped)	0.15	0.18	0.19	0.43	0.95	1.04	0.72
Variance	0.03	0.03	0.05	0.16	0.10	0.08	0.13
Standard deviation	0.19	0.17	0.22	0.40	0.32	0.29	0.36
Minimum value	0.02	0.05	0.09	0.02	0.04	0.05	0.04
Maximum value	0.98	0.80	0.82	1.90	1.66	1.60	1.50
Range	0.96	0.75	0.73	1.88	1.62	1.55	1.46

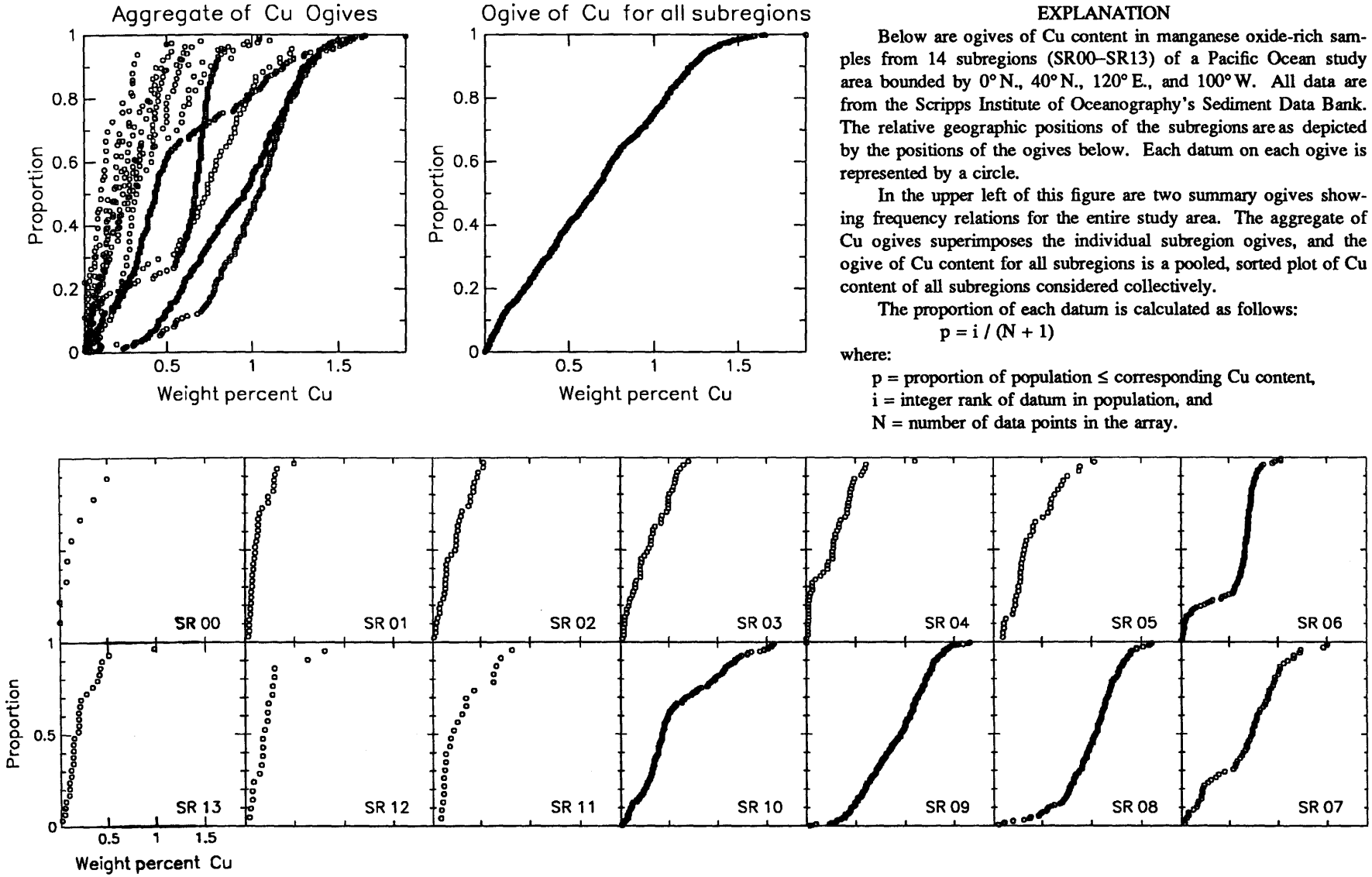

EXPLANATION

Below are ogives of Cu content in manganese oxide-rich samples from 14 subregions (SR00–SR13) of a Pacific Ocean study area bounded by 0° N., 40° N., 120° E., and 100° W. All data are from the Scripps Institute of Oceanography's Sediment Data Bank. The relative geographic positions of the subregions are as depicted by the positions of the ogives below. Each datum on each ogive is represented by a circle.

In the upper left of this figure are two summary ogives showing frequency relations for the entire study area. The aggregate of Cu ogives superimposes the individual subregion ogives, and the ogive of Cu content for all subregions is a pooled, sorted plot of Cu content of all subregions considered collectively.

The proportion of each datum is calculated as follows:

$$p = i / (N + 1)$$

where:

p = proportion of population ≤ corresponding Cu content,
i = integer rank of datum in population, and
N = number of data points in the array.

Figure 17. Ogives of Cu concentration in northern Pacific subregions.

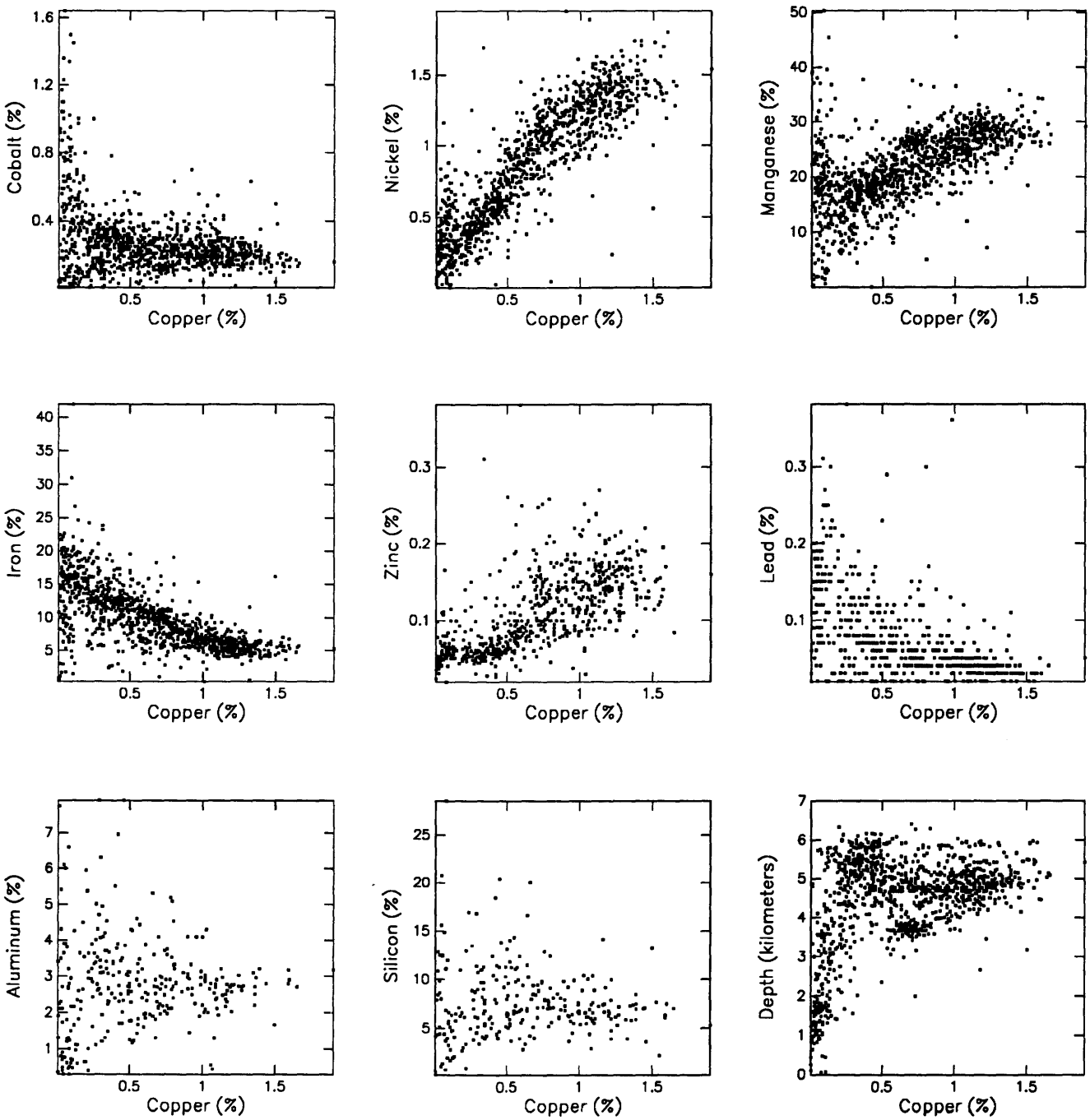

Figure 18. Scatter plots of Cu content versus content of Co, Ni, Mn, Fe, Zn, Pb, Al, Si, and depth in northern Pacific Mn oxide-rich phases.

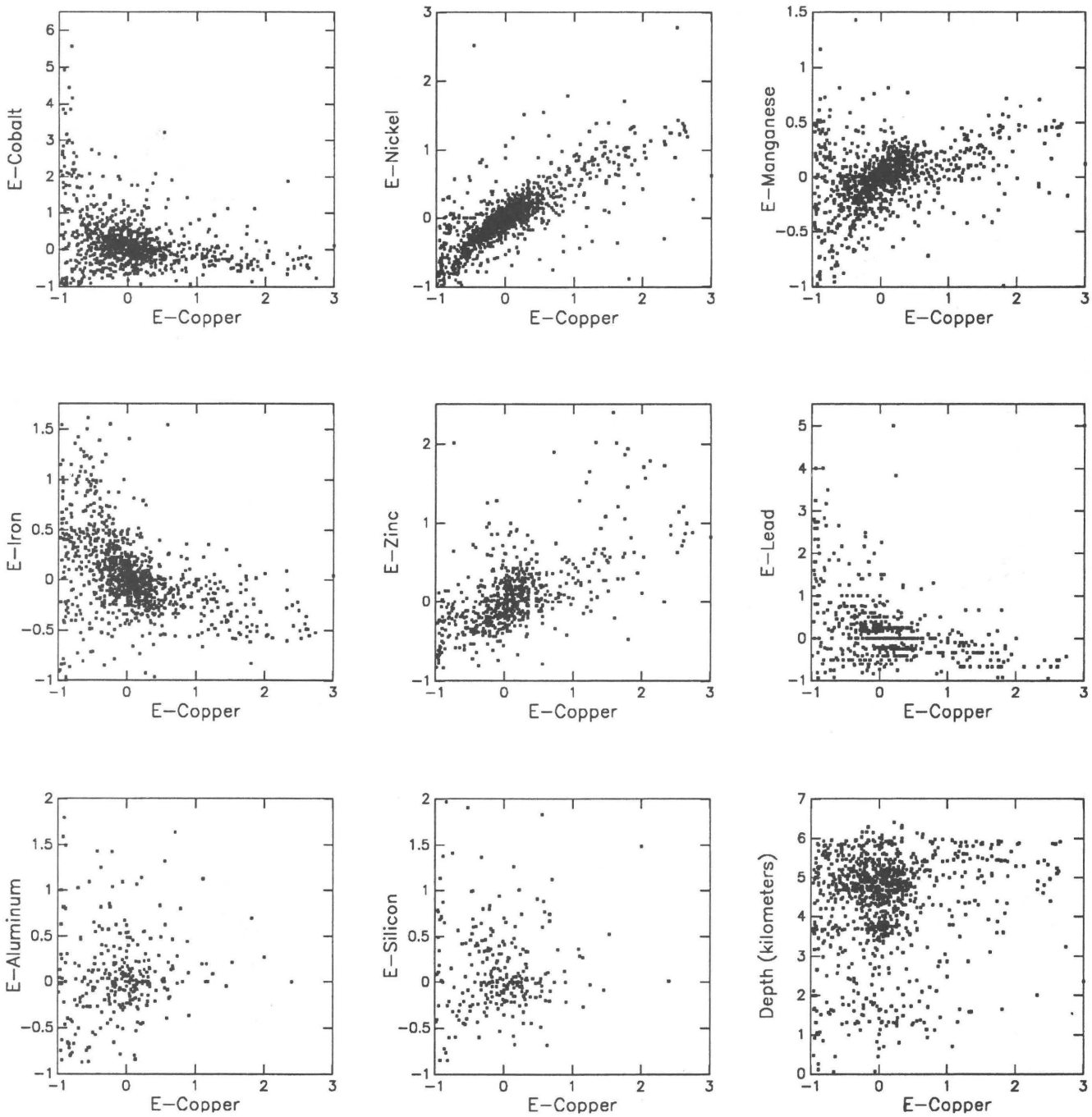

Figure 19. Scatter plots of Cu enrichment (E) versus enrichment of Co, Ni, Mn, Fe, Zn, Pb, Al, Si, and depth in northern Pacific Mn oxide-rich phases.

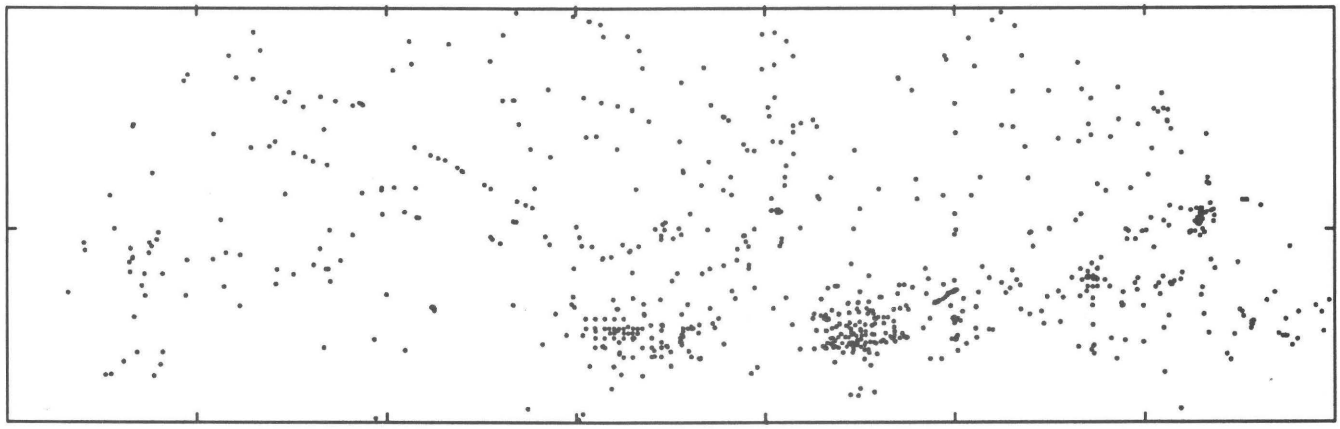

A

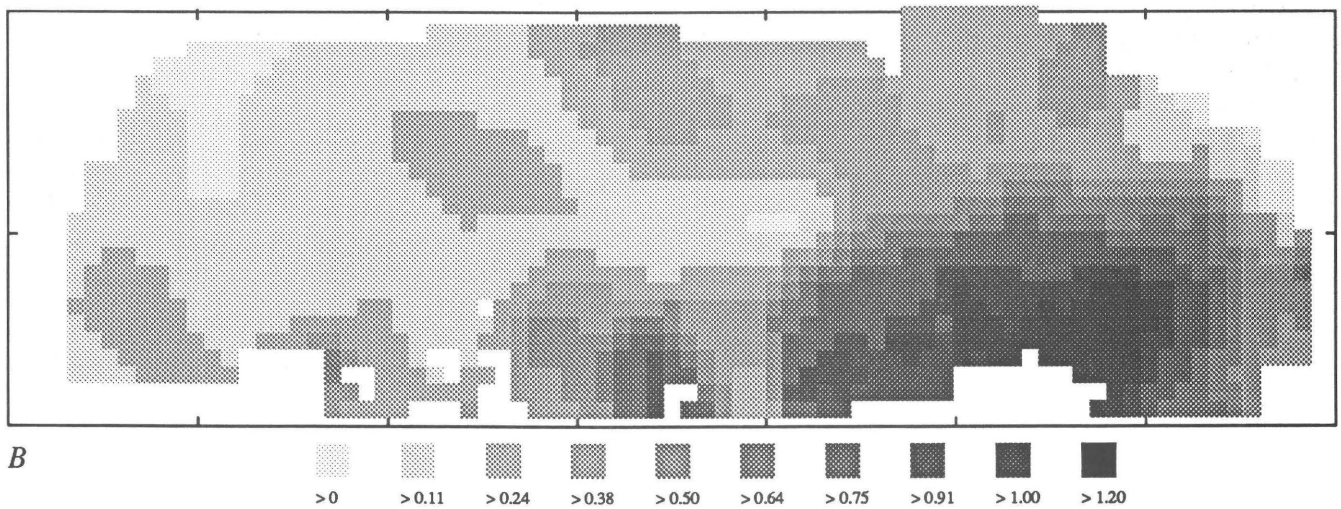

B

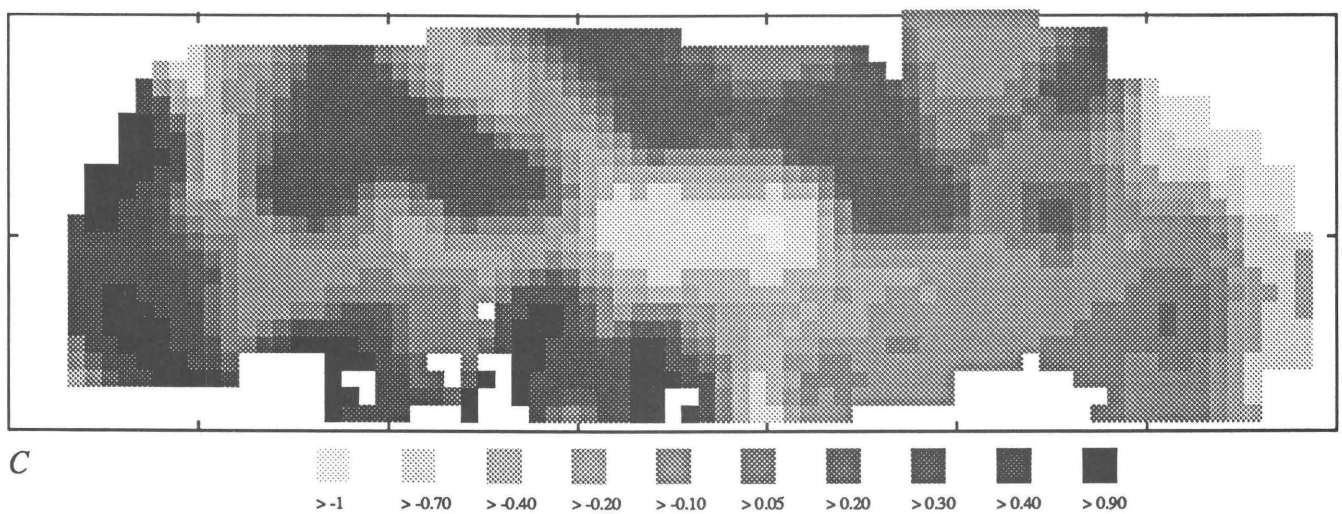

C

Figure 20. *A*, Sample locations. *B*, Distribution of Cu content (weight percent). *C*, Enrichment in Mn oxide-rich phases of the northern Pacific study area. Subregion boundaries are provided by overlay in pocket.

Zinc

Subregion 07 hosts both the highest and the lowest zinc concentrations of the entire study area, 1.07 percent and 0.01 percent, respectively (compare tables 11 and 12). The frequency distribution for the entire study region shows that zinc is skewed toward the positive such that more than 97 percent of the samples have concentrations of less than 0.23 percent. In figure 21, the aggregate of zinc ogives shows that the distribution of zinc content in subregions 06, 07, 08, and 09 are clustered and that they have a wider range of high Zn content values than the other subregions.

The scatter plots in figures 22 and 23 show zinc to have strong positive correlation with copper, manganese, and nickel, and a moderate negative correlation with iron and lead. The same is true for the enrichments of these variables.

In figure 24, three distinct areas of high zinc concentration are shown. One is centered about subregion 07, which is in immediate proximity to the eastern Pacific hydrothermally active areas. The trend of the second is truncated at the northern boundary of subregions 03 and 04. The third zone is centered about the boundary between subregions 01 and 12, projects into subregion 11, and is unresolved at its southernmost extent. Zinc enrichment exhibits a far more pervasive positive pattern than does that of zinc concentration. The distribution of positive zinc enrichment forms a broad halo around two negative enrichment nuclei located at the boundaries between subregions 03 and 10 and subregions 05 and 08. In almost all relevant subregions, zinc enrichment increases with distance north or south from the 20° N. central latitude of the study area.

Table 11. Descriptive statistics for the distribution of Zn concentration in Mn oxide-rich phases in the northern Pacific study area

	Frequency distribution			
	Class	Count	%	Cumulative %
Number of nonblank observations = 696	0.02 — 0.12	434	62.36	62.36
Number of classes (by Sturges' Rule) = 10	0.12 — 0.23	248	35.63	97.99
Class size = 0.10	0.23 — 0.33	11	1.58	99.57
Mean = 0.11	0.33 — 0.44	1	0.14	99.71
Median (ungrouped data) = 0.10	0.44 — 0.54	0	0.00	99.71
Variance = 0.003	0.54 — 0.65	0	0.00	99.71
Standard deviation = 0.06	0.65 — 0.75	1	0.14	99.86
Minimum value = 0.01	0.75 — 0.86	0	0.00	99.86
Maximum value = 1.07	0.86 — 0.96	0	0.00	99.86
Range = 1.05	0.96 — 1.07	1	0.14	100.00

Table 12. Descriptive statistics for the distributions of Zn concentration in Mn oxide-rich phases of subregions in the northern Pacific study area

Subregion	00	01	02	03	04	05	06
Number of samples	2	16	25	27	15	21	78
Mean	0.04	0.06	0.06	0.09	0.06	0.06	0.12
Median (ungrouped)	0.03	0.06	0.06	0.06	0.05	0.06	0.13
Variance	0.00	0.00	0.00	0.00	0.00	0.00	0.00
Standard deviation	0.01	0.01	0.01	0.07	0.02	0.02	0.05
Minimum value	0.03	0.04	0.04	0.04	0.04	0.03	0.02
Maximum value	0.06	0.10	0.12	0.38	0.16	0.10	0.26
Range	0.02	0.06	0.07	0.34	0.12	0.07	0.23
Subregion	13	12	11	10	09	08	07
Number of samples	14	2	7	166	179	106	38
Mean	0.05	0.38	0.06	0.08	0.12	0.13	0.13
Median (ungrouped)	0.05	0.04	0.05	0.07	0.12	0.14	0.11
Variance	0.00	0.11	0.00	0.00	0.00	0.00	0.02
Standard deviation	0.01	0.34	0.01	0.04	0.03	0.04	0.15
Minimum value	0.02	0.04	0.05	0.02	0.04	0.03	0.01
Maximum value	0.07	0.73	0.09	0.23	0.25	0.27	1.07
Range	0.04	0.69	0.04	0.21	0.20	0.23	1.05

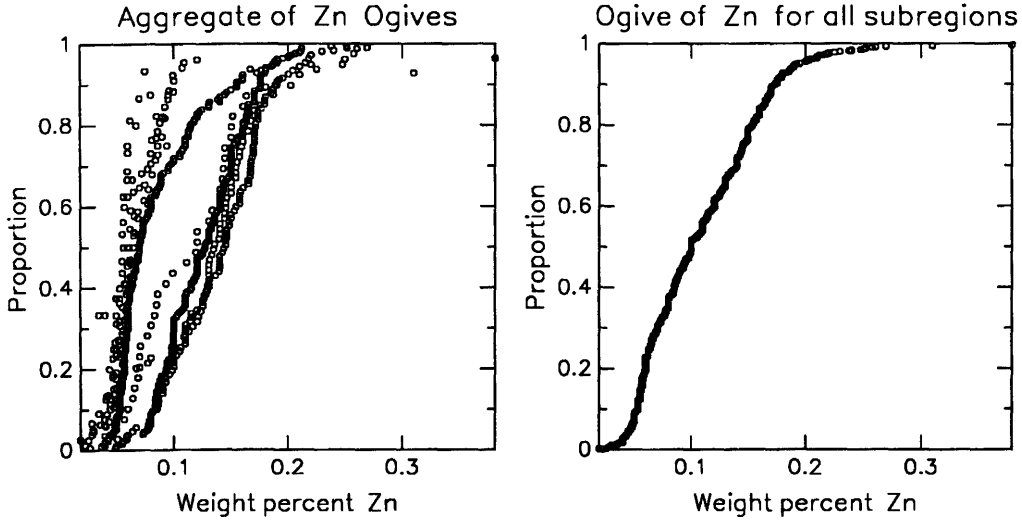

EXPLANATION

Below are ogives of Zn content in manganese oxide-rich samples from 14 subregions (SR00–SR13) of a Pacific Ocean study area bounded by 0° N., 40° N., 120° E., and 100° W. All data are from the Scripps Institute of Oceanography's Sediment Data Bank. The relative geographic positions of the subregions are as depicted by the positions of the ogives below. Each datum on each ogive is represented by a circle.

In the upper left of this figure are two summary ogives showing frequency relations for the entire study area. The aggregate of Zn ogives superimposes the individual subregion ogives, and the ogive of Zn content for all subregions is a pooled, sorted plot of Zn content of all subregions considered collectively.

The proportion of each datum is calculated as follows:

$$p = i / (N + 1)$$

where:

p = proportion of population ≤ corresponding Zn content,
i = integer rank of datum in population, and
N = number of data points in the array.

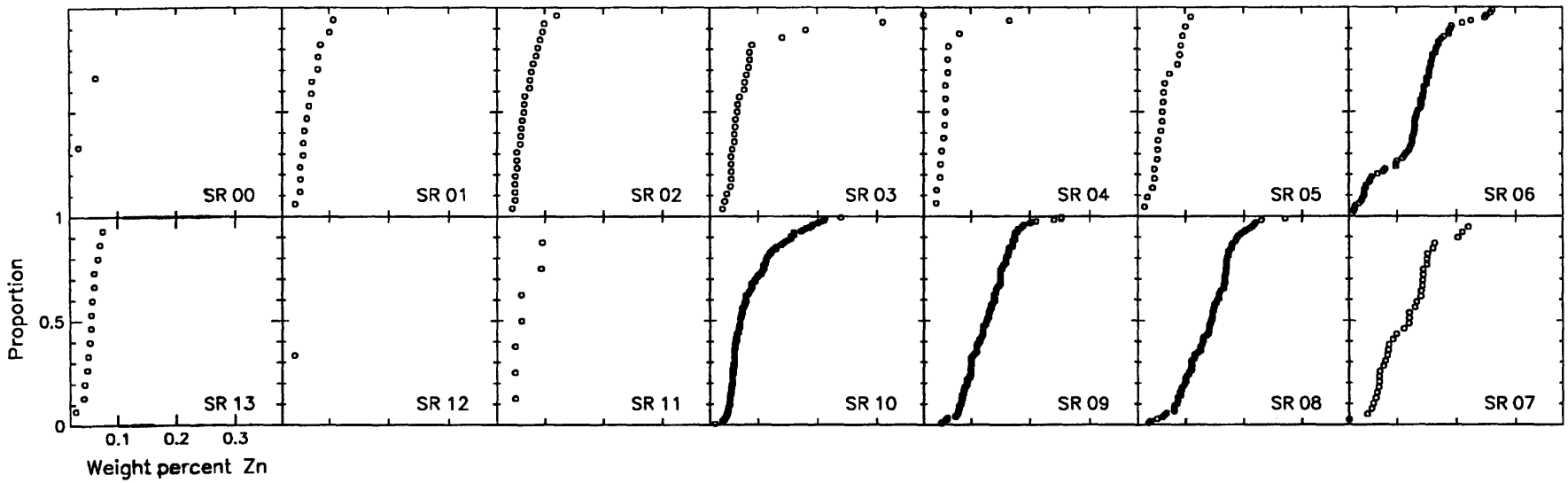

Figure 21. Ogives of Zn concentration in northern Pacific subregions.

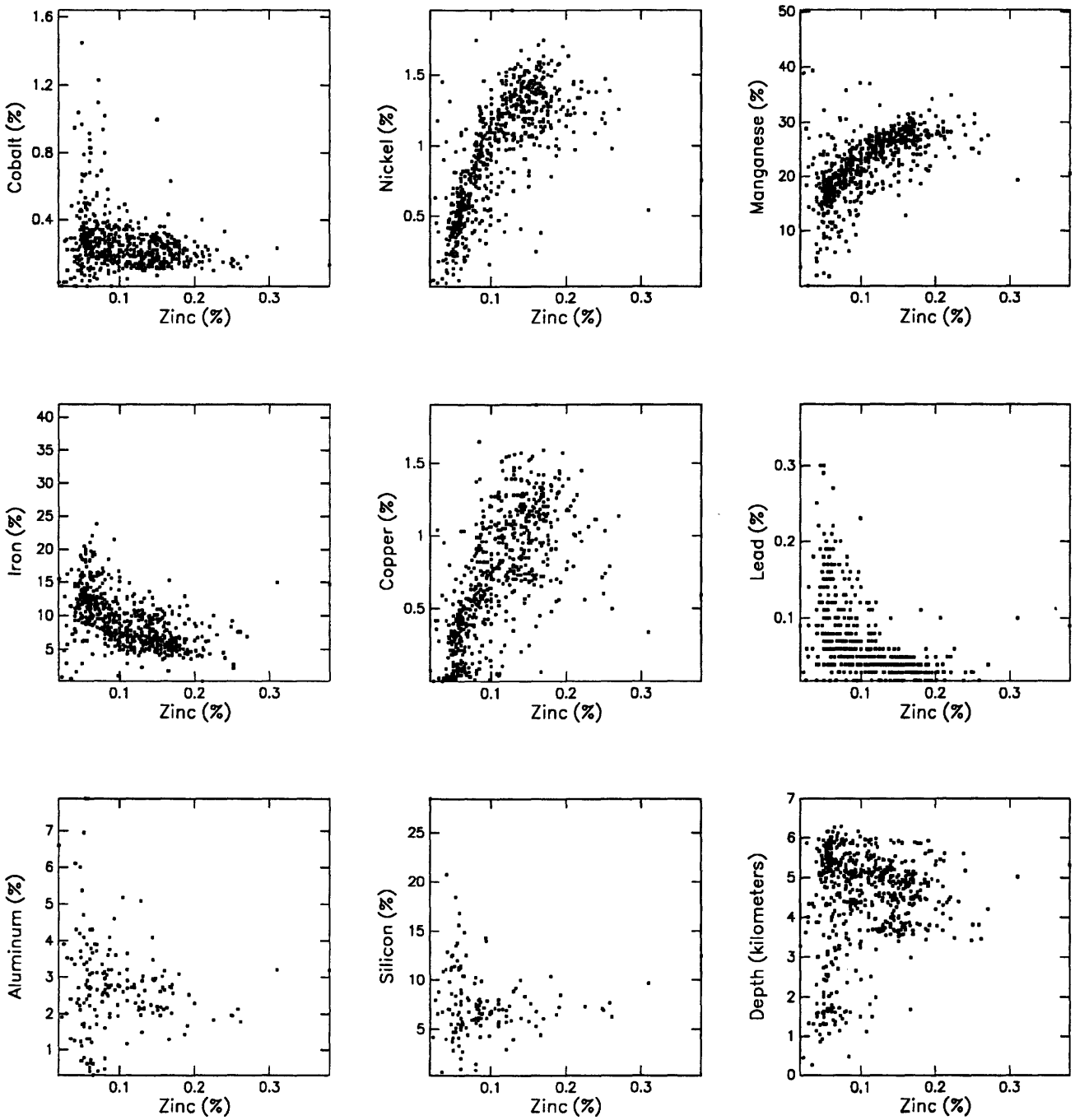

Figure 22. Scatter plots of Zn content versus content of Co, Ni, Mn, Fe, Cu, Pb, Al, Si, and depth in northern Pacific Mn oxide-rich phases.

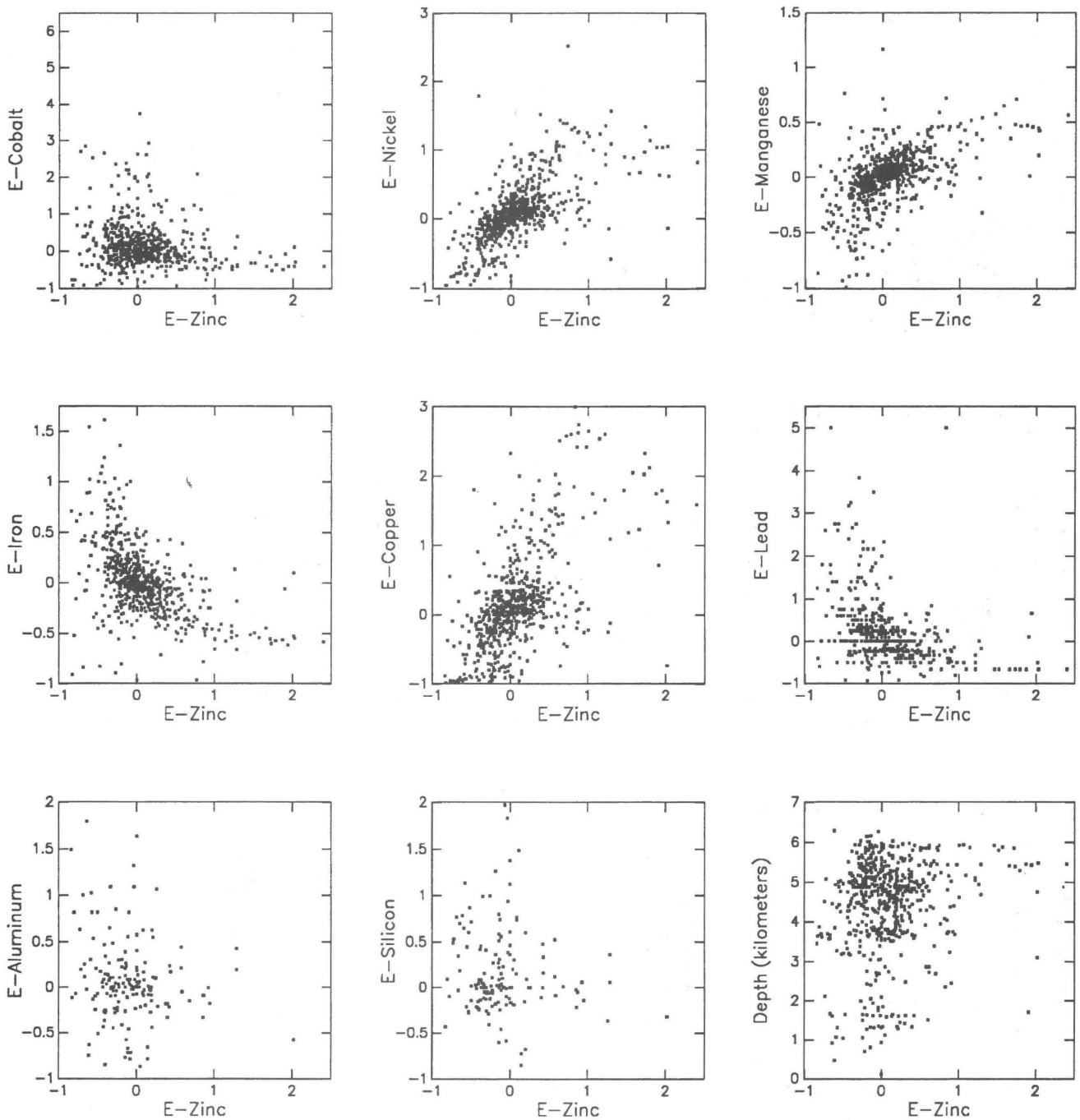

Figure 23. Scatter plots of Zn enrichment (E) versus enrichment of Co, Ni, Mn, Fe, Cu, Pb, Al, Si, and depth in northern Pacific Mn oxide-rich phases.

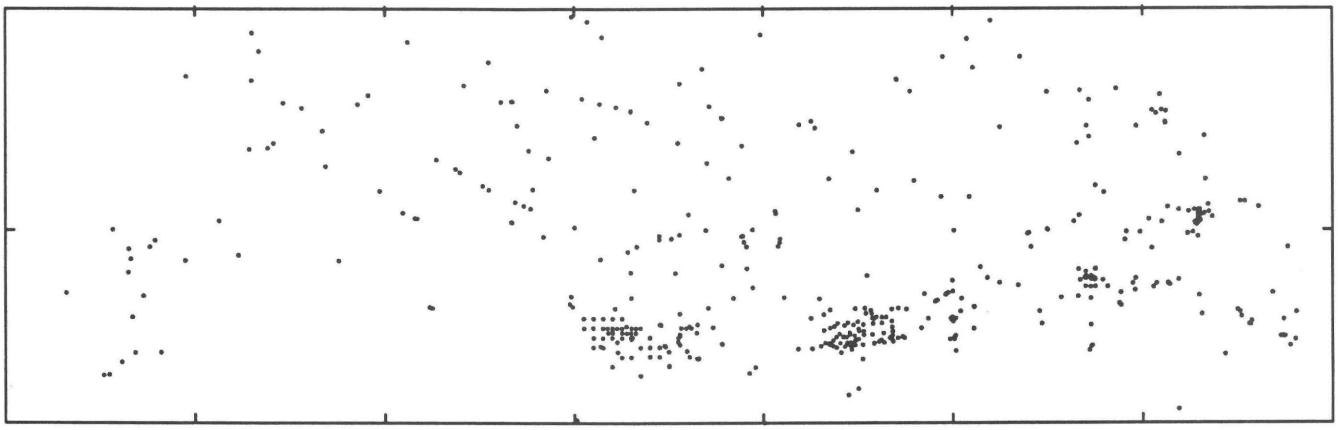

A

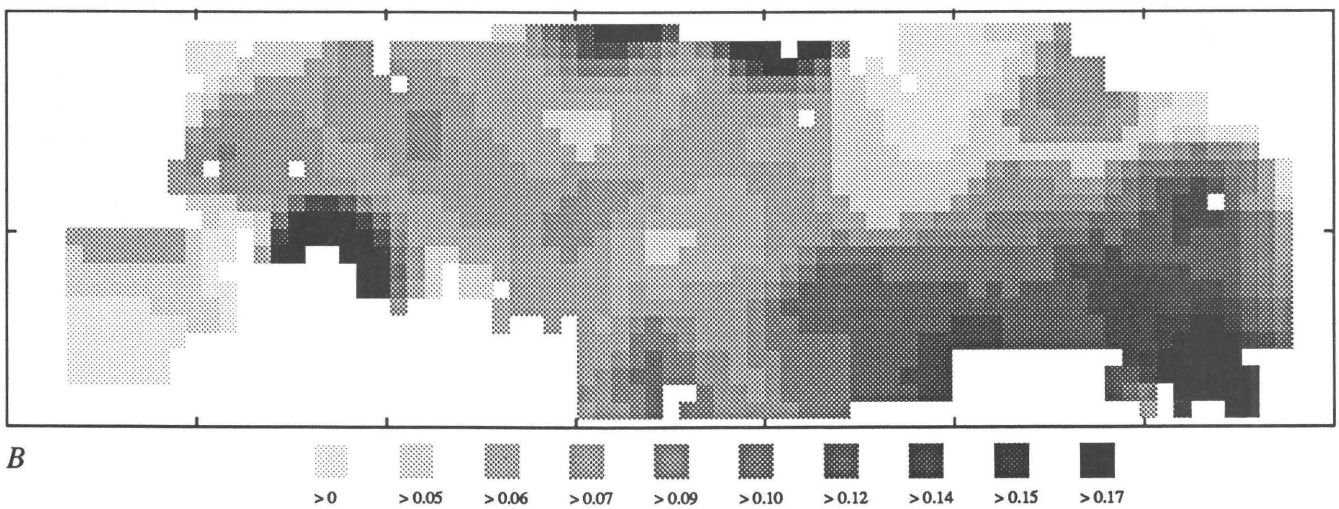

B

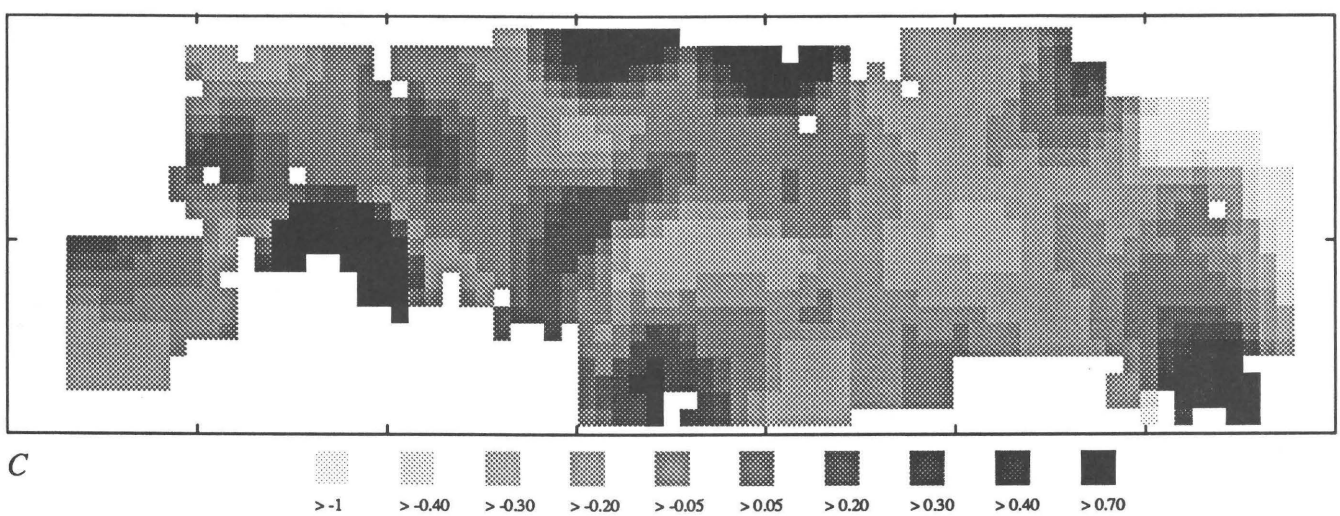

C

Figure 24. *A*, Sample locations. *B*, Distribution of Zn content (weight percent). *C*, Enrichment in Mn oxide-rich phases of the northern Pacific study area. Subregion boundaries are provided by overlay in pocket.

Lead

Lead ranges in concentration from 0.01 percent in subregions 02, 06, 07, 09, 10, 11, and 13 to 0.41 percent in subregion 06 (compare tables 13 and 14). In figure 25, ogives of subregions 01 through 05 and 11 through 13 constitute a cluster of higher values than the remaining subregions. Of this cluster, subregion 11 is the most anomalous in shape, but it, like the ogives of subregions 00, 12, and 13, is composed of very few data points and therefore must be interpreted with caution.

As shown in figures 26 and 27, lead has a moderate positive correlation with cobalt and iron. This correlation appears equally as moderate for their enrichments. Lead has a moderate negative correlation with zinc and a weak negative correlation with copper. These relations are slightly enhanced in their enrichment transforms.

Three major zones of lead concentration are shown in figure 28: an isolated zone within subregion 13, an isolated zone in subregion 06, and a wide east-trending band with highest content centered about the 20° N. parallel and extending into subregions 01 through 04, and 09 through 12. The major zone of high lead enrichment is an east-trending zone centered about the 20° N. parallel and extending from 180° W. to 150° W. Additional areas of high enrichment occur in subregions 05 and 06.

Table 13. Descriptive statistics for the distribution of Pb concentration in Mn oxide-rich phases in the northern Pacific study area

	Frequency distribution			
	Class	Count	%	Cumulative %
Number of nonblank observations = 629	0.01 — 0.05	318	50.56	50.56
Number of classes (by Sturges' Rule) = 10	0.05 — 0.09	163	25.91	76.47
Class size = 0.04	0.09 — 0.13	64	10.17	86.65
Mean = 0.07	0.13 — 0.17	48	7.63	94.28
Median (ungrouped data) = 0.05	0.17 — 0.21	19	3.02	97.30
Variance = 0.003	0.21 — 0.25	9	1.43	98.73
Standard deviation = 0.05	0.25 — 0.29	2	0.32	99.05
Minimum value = 0.01	0.29 — 0.33	3	0.48	99.52
Maximum value = 0.41	0.33 — 0.37	1	0.16	99.68
Range = 0.40	0.37 — 0.41	2	0.32	100.00

Table 14. Descriptive statistics for the distributions of Pb concentration in Mn oxide-rich phases of subregions in the northern Pacific study area

Subregion	00	01	02	03	04	05	06
Number of samples	3	21	26	18	17	18	56
Mean	0.06	0.11	0.13	0.10	0.11	0.10	0.07
Median (ungrouped)	0.02	0.11	0.14	0.10	0.11	0.09	0.05
Variance	0.00	0.00	0.00	0.00	0.00	0.00	0.00
Standard deviation	0.04	0.04	0.04	0.03	0.03	0.04	0.07
Minimum value	0.02	0.04	0.01	0.06	0.03	0.02	0.01
Maximum value	0.12	0.18	0.23	0.23	0.17	0.17	0.41
Range	0.10	0.14	0.22	0.17	0.14	0.15	0.40
Subregion	13	12	11	10	09	08	07
Number of samples	17	4	11	162	146	86	44
Mean	0.11	0.08	0.18	0.07	0.05	0.05	0.05
Median (ungrouped)	0.11	0.08	0.17	0.06	0.04	0.05	0.04
Variance	0.00	0.00	0.00	0.00	0.00	0.00	0.00
Standard deviation	0.08	0.04	0.08	0.05	0.03	0.02	0.03
Minimum value	0.01	0.02	0.01	0.01	0.01	0.02	0.01
Maximum value	0.36	0.15	0.31	0.29	0.38	0.17	0.20
Range	0.35	0.13	0.30	0.28	0.37	0.15	0.19

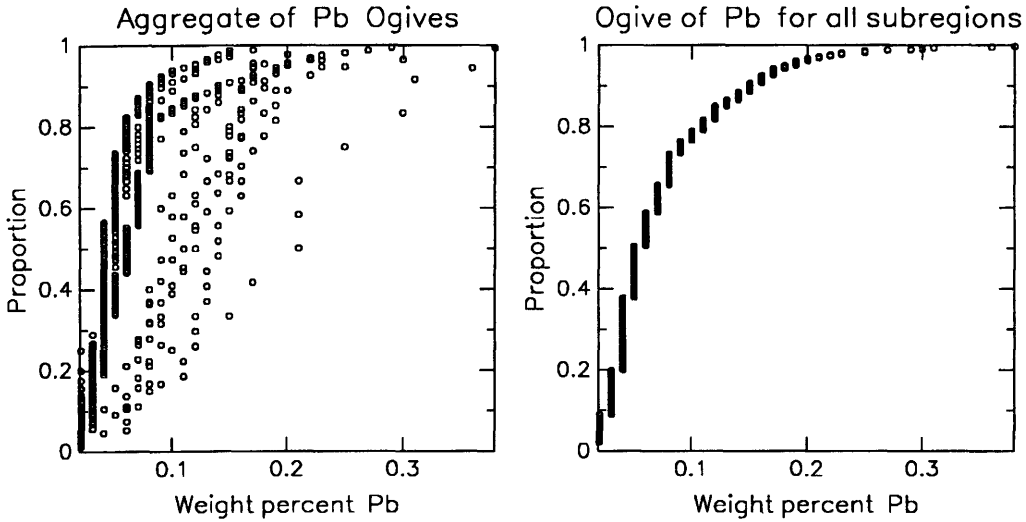

EXPLANATION

Below are ogives of Pb content in manganese oxide-rich samples from 14 subregions (SR00–SR13) of a Pacific Ocean study area bounded by 0°N., 40°N., 120°E., and 100°W. All data are from the Scripps Institute of Oceanography's Sediment Data Bank. The relative geographic positions of the subregions are as depicted by the positions of the ogives below. Each datum on each ogive is represented by a circle.

In the upper left of this figure are two summary ogives showing frequency relations for the entire study area. The aggregate of Pb ogives superimposes the individual subregion ogives, and the ogive of Pb content for all subregions is a pooled, sorted plot of Pb content of all subregions considered collectively.

The proportion of each datum is calculated as follows:

$$p = i / (N + 1)$$

where:

p = proportion of population ≤ corresponding Pb content,
i = integer rank of datum in population, and
N = number of data points in the array.

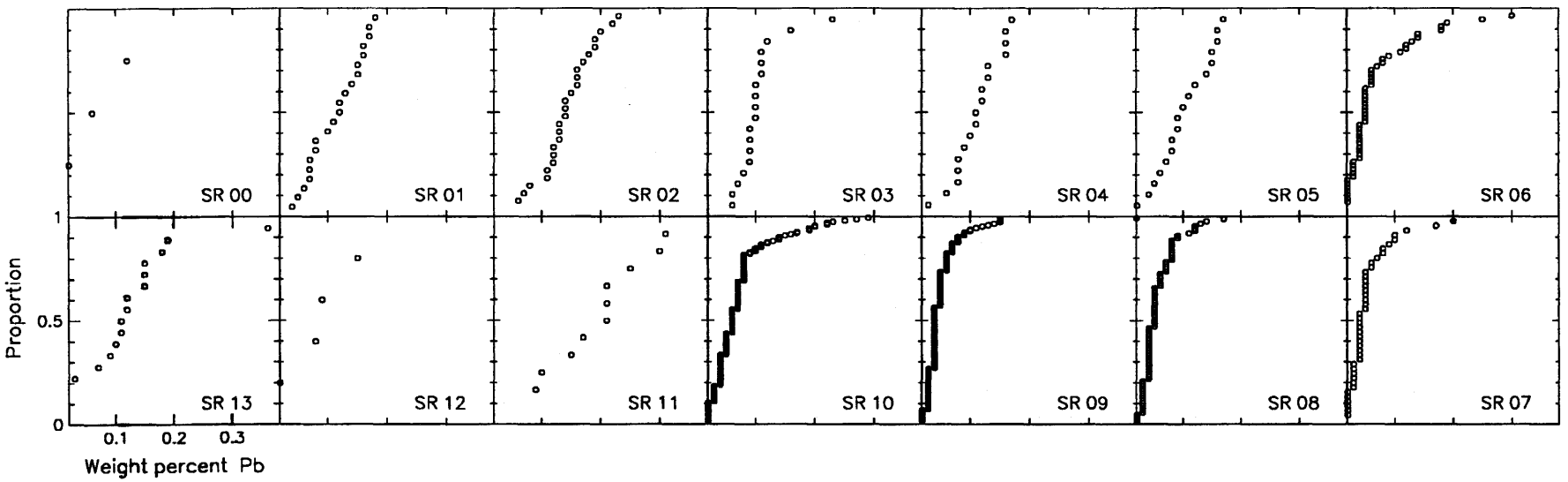

Figure 25. Ogives of Pb concentration in northern Pacific subregions.

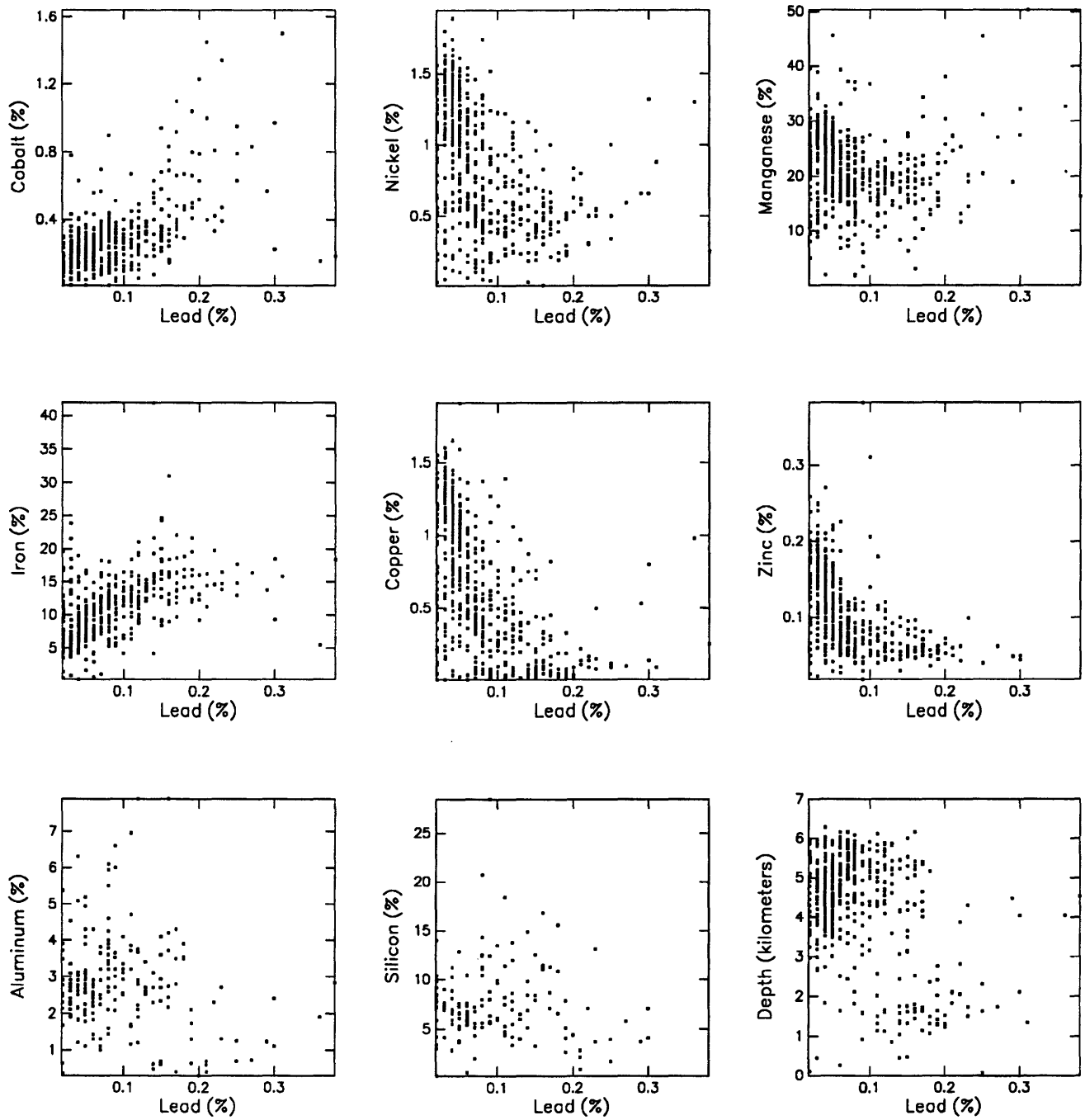

Figure 26. Scatter plots of Pb content versus content of Co, Ni, Mn, Fe, Cu, Zn, Al, Si, and depth in northern Pacific Mn oxide-rich phases.

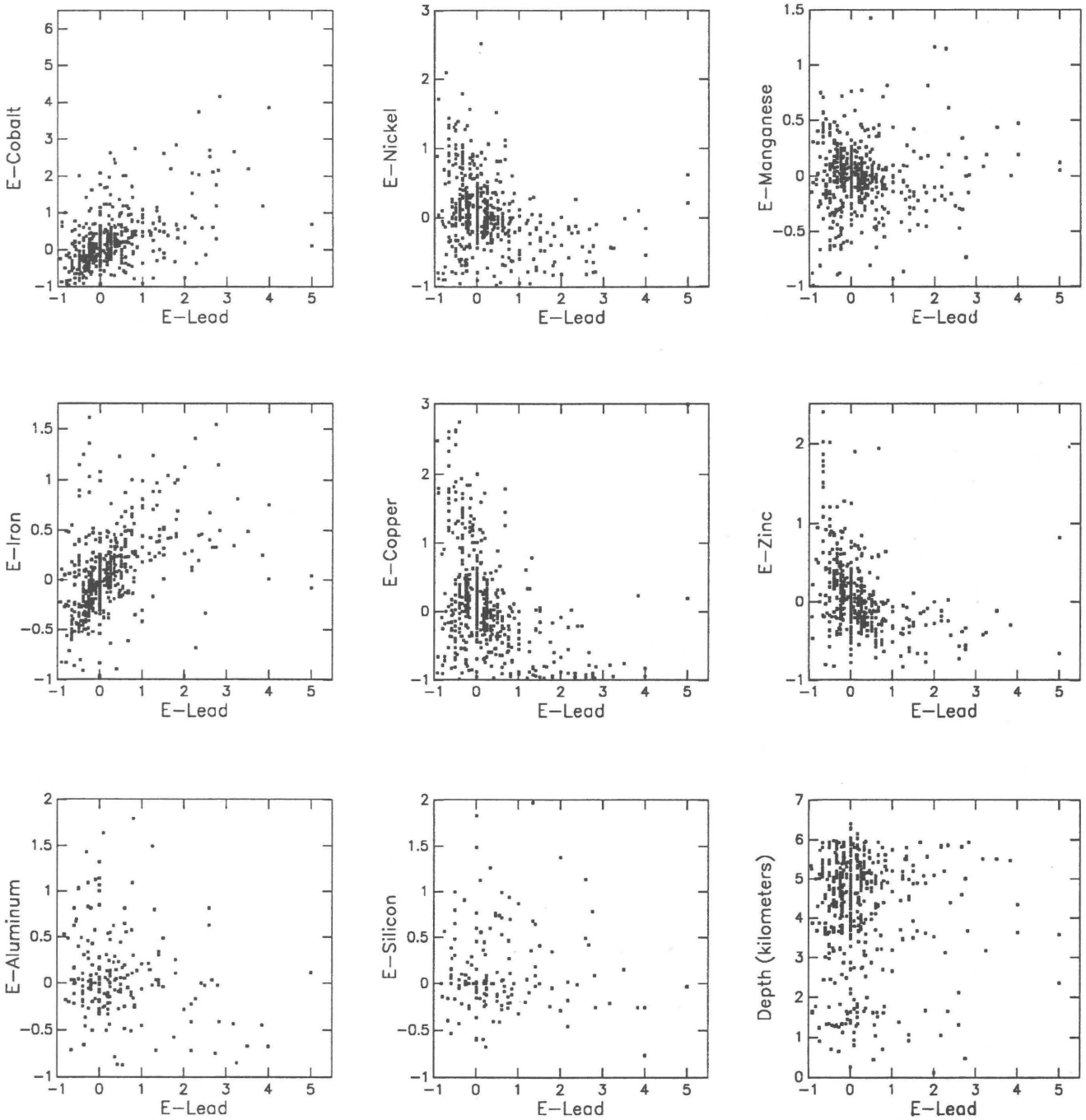

Figure 27. Scatter plots of Pb enrichment (E) versus enrichment of Co, Ni, Mn, Fe, Cu, Zn, Al, Si, and depth in northern Pacific Mn oxide-rich phases.

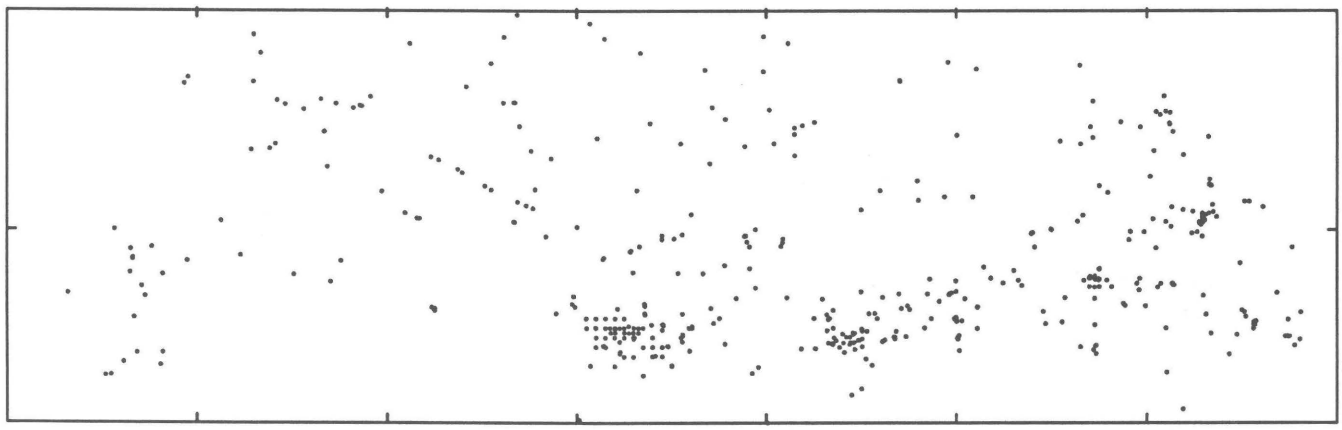

A

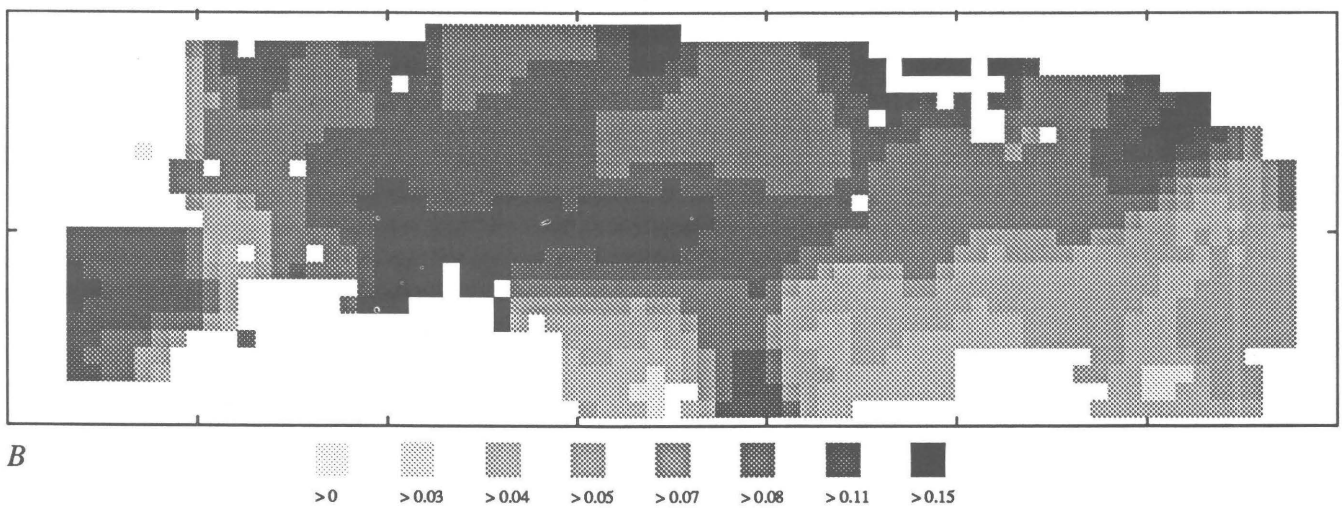

B

>0 >0.03 >0.04 >0.05 >0.07 >0.08 >0.11 >0.15

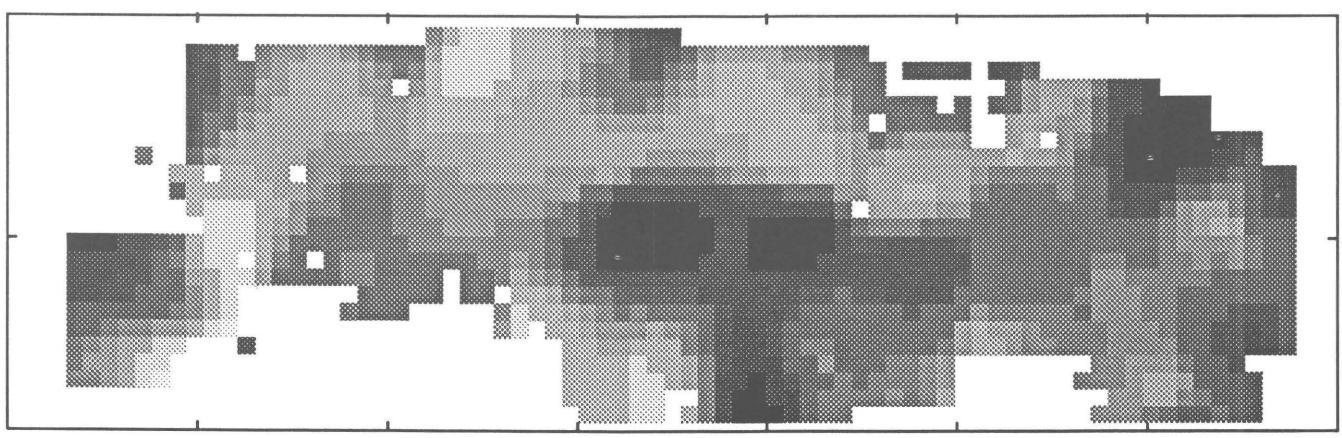

C

>-1 >-0.50 >-0.30 >-0.10 >0.00 >0.10 >0.20 >0.50 >0.60 >1.30

Figure 28. *A*, Sample locations. *B*, Distribution of Pb content (weight percent). *C*, Enrichment in Mn oxide-rich phases of the northern Pacific study area. Subregion boundaries are provided by overlay in pocket.

Aluminum

Aluminum concentration ranges from 0.3 percent in subregions 02 and 03 to 7.9 percent in subregions 04 and 05 (compare tables 15 and 16). The aggregate of ogives in figure 29 shows no unique partitions, and the sampling density of the western part of the study area is quite low.

In figure 30, aluminum shows a strong positive correlation with silicon, and in figure 31, this correlation is also true with their enrichments. A weak negative correlation appears to exist between aluminum and manganese as well as between their enrichments. No other scatter plot for aluminum and aluminum enrichment shows any visibly distinct positive or negative correlations.

Figure 32 shows three well-defined areas of high aluminum concentration. The major one is centered in the southeastern part of subregion 04; a minor one is centered in the northern part of subregion 01, and another minor one is centered in subregion 05. Zones of aluminum enrichment approximately correspond to the zones of high concentration.

Table 15. Descriptive statistics for the distribution of Al concentration in Mn oxide-rich phases in the northern Pacific study area

	Frequency distribution			
	Class	Count	%	Cumulative %
Number of nonblank observations = 313	0.30 — 1.14	31	9.90	9.90
Number of classes (by Sturges' Rule) = 9	1.14 — 1.99	46	14.70	24.60
Class size = 0.84	1.99 — 2.83	112	35.78	60.38
Mean = 2.70	2.83 — 3.68	75	23.96	84.35
Median (ungrouped data) = 2.68	3.68 — 4.52	30	9.58	93.93
Variance = 1.59	4.52 — 5.37	8	2.56	96.49
Standard deviation = 1.26	5.37 — 6.21	5	1.60	98.08
Minimum value = 0.30	6.21 — 7.06	3	0.96	99.04
Maximum value = 7.90	7.06 — 7.90	3	0.96	100.00
Range = 7.60				

Table 16. Descriptive statistics for the distributions of Al concentration in Mn oxide-rich phases of subregions in the northern Pacific study area

Subregion	00	01	02	03	04	05	06
Number of samples	3	10	7	14	24	16	43
Mean	1.77	3.12	2.31	1.97	3.49	3.92	2.40
Median (ungrouped)	0.35	2.92	2.30	1.50	3.00	3.78	2.15
Variance	1.93	2.87	0.96	1.37	3.57	3.19	0.85
Standard deviation	1.39	1.69	0.98	1.17	1.88	1.78	0.92
Minimum value	0.35	0.62	0.30	0.30	0.94	0.48	0.70
Maximum value	3.66	6.10	3.43	3.64	7.90	7.90	6.00
Range	3.31	5.48	3.13	3.34	6.96	7.42	5.30
Subregion	13	12	11	10	09	08	07
Number of samples	6	10	6	49	62	41	22
Mean	2.52	3.22	1.95	2.12	2.72	2.92	2.86
Median (ungrouped)	2.28	2.77	0.70	2.22	2.76	2.80	2.65
Variance	0.30	0.65	3.43	1.10	0.61	0.58	1.70
Standard deviation	0.54	0.80	1.85	1.05	0.78	0.76	1.30
Minimum value	1.90	2.08	0.39	0.47	0.44	1.44	0.40
Maximum value	3.54	4.52	5.30	5.00	4.43	5.18	6.60
Range	1.64	2.44	4.91	4.53	3.99	3.74	6.20

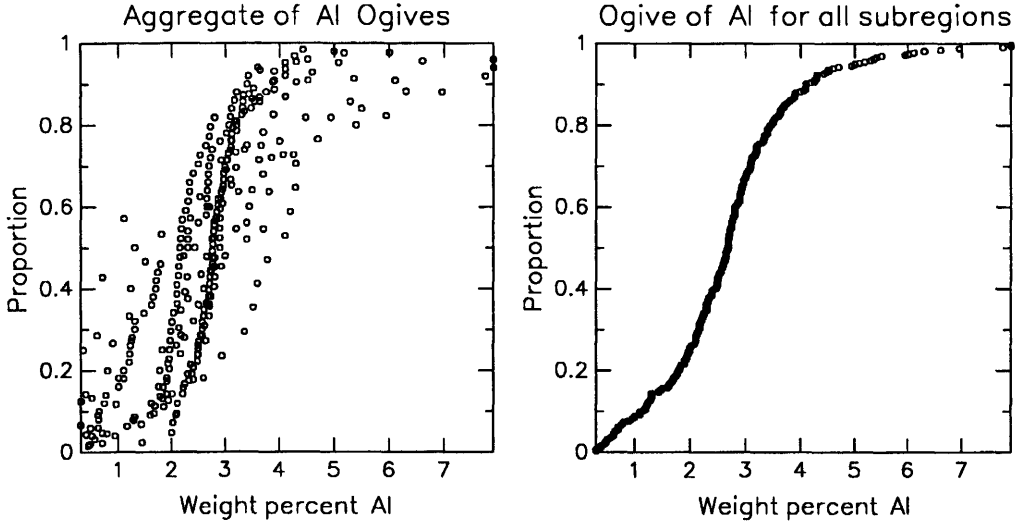

EXPLANATION

Below are ogives of Al content in manganese oxide-rich samples from 14 subregions (SR00–SR13) of a Pacific Ocean study area bounded by 0° N., 40° N., 120° E., and 100° W. All data are from the Scripps Institute of Oceanography's Sediment Data Bank. The relative geographic positions of the subregions are as depicted by the positions of the ogives below. Each datum on each ogive is represented by a circle.

In the upper left of this figure are two summary ogives showing frequency relations for the entire study area. The aggregate of Al ogives superimposes the individual subregion ogives, and the ogive of Al content for all subregions is a pooled, sorted plot of Al content of all subregions considered collectively.

The proportion of each datum is calculated as follows:

$$p = i / (N + 1)$$

where:

p = proportion of population ≤ corresponding Al content,
i = integer rank of datum in population, and
N = number of data points in the array.

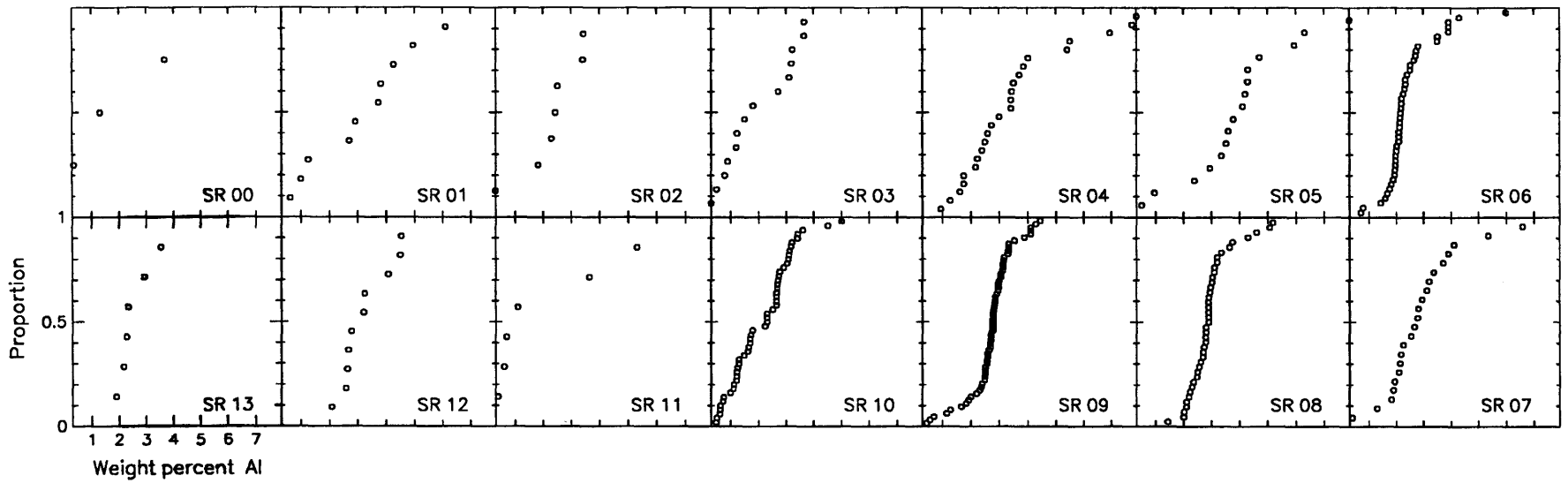

Figure 29. Ogives of Al concentration in northern Pacific subregions.

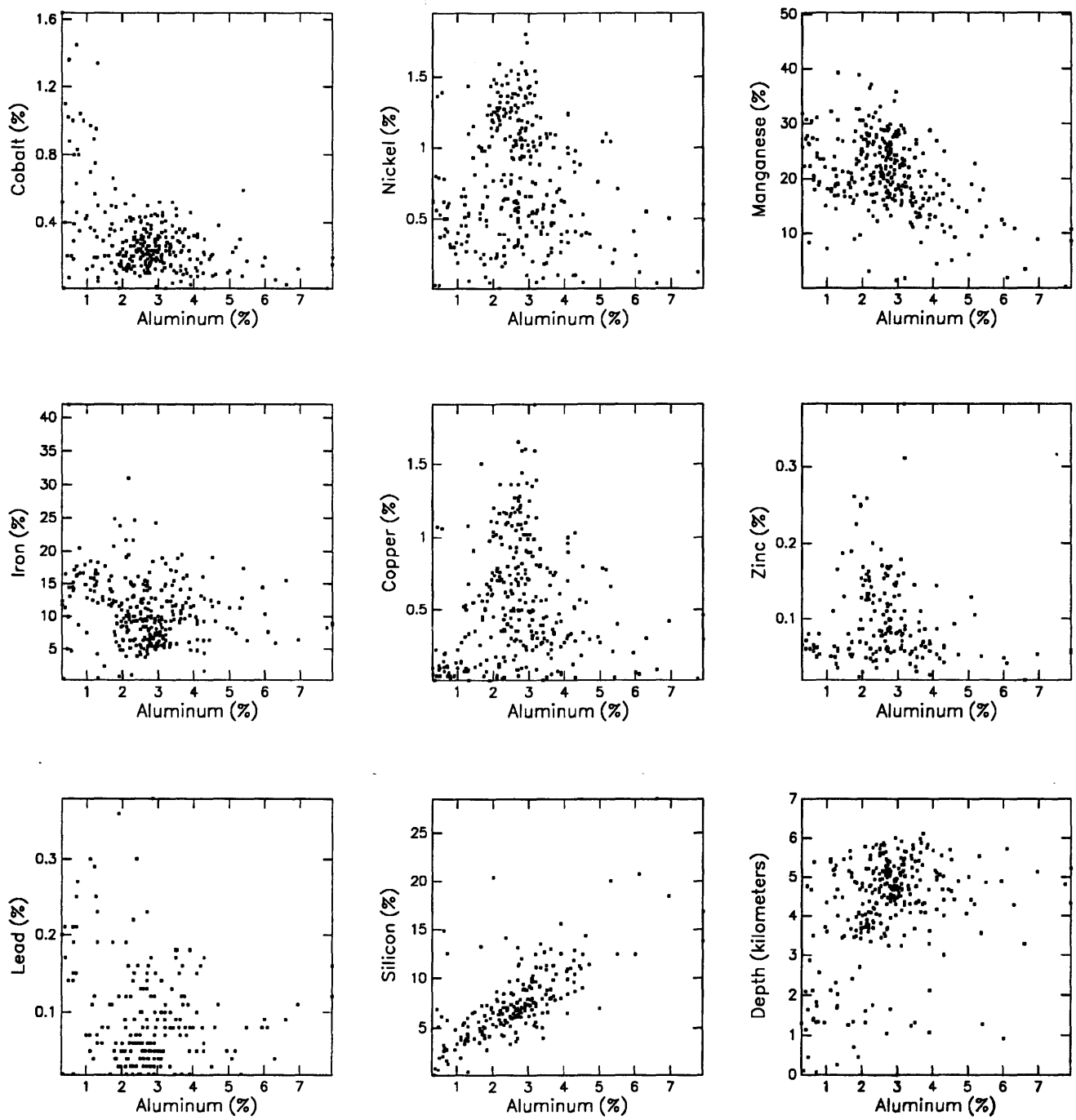

Figure 30. Scatter plots of Al content versus content of Co, Ni, Mn, Fe, Cu, Zn, Pb, Si, and depth in northern Pacific Mn oxide-rich phases.

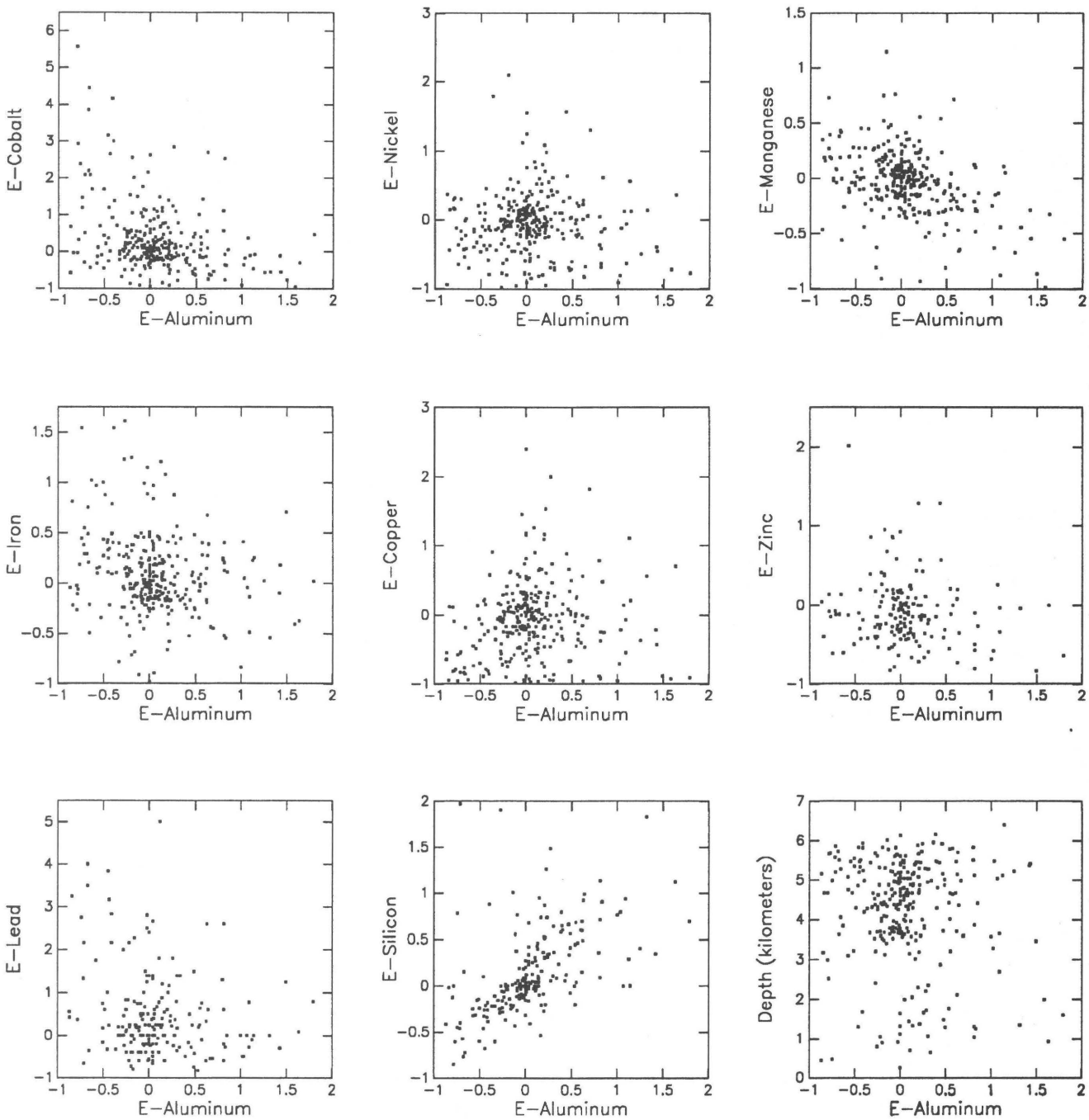

Figure 31. Scatter plots of Al enrichment (E) versus enrichment of Co, Ni, Mn, Fe, Cu, Zn, Pb, Si, and depth in northern Pacific Mn oxide-rich phases.

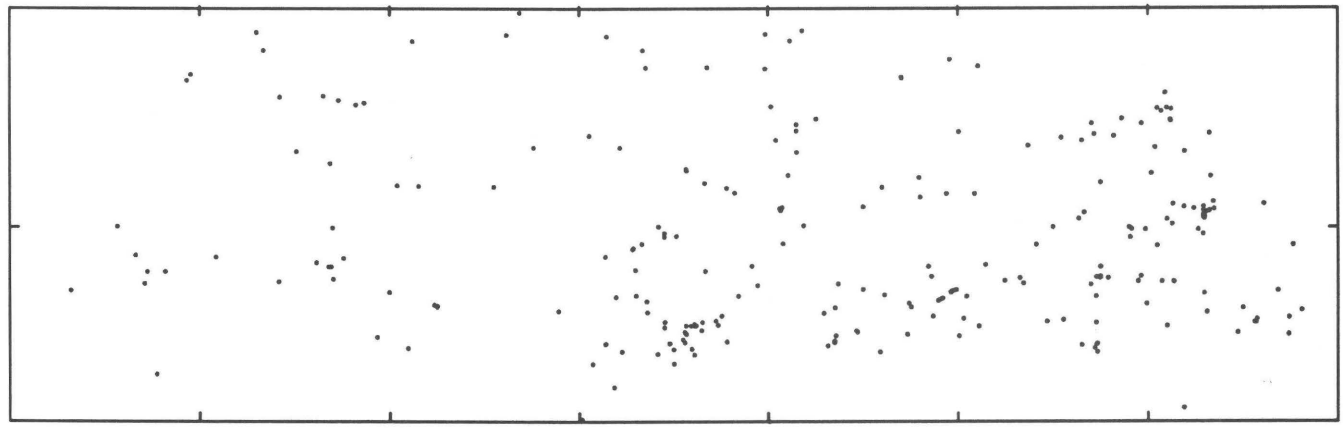

A

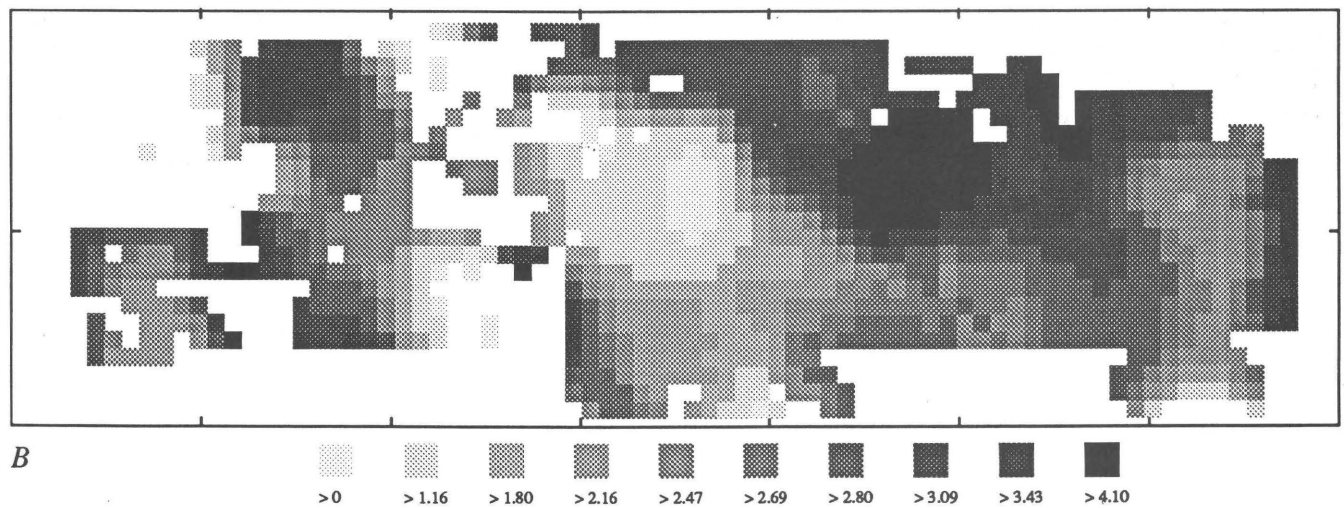

B

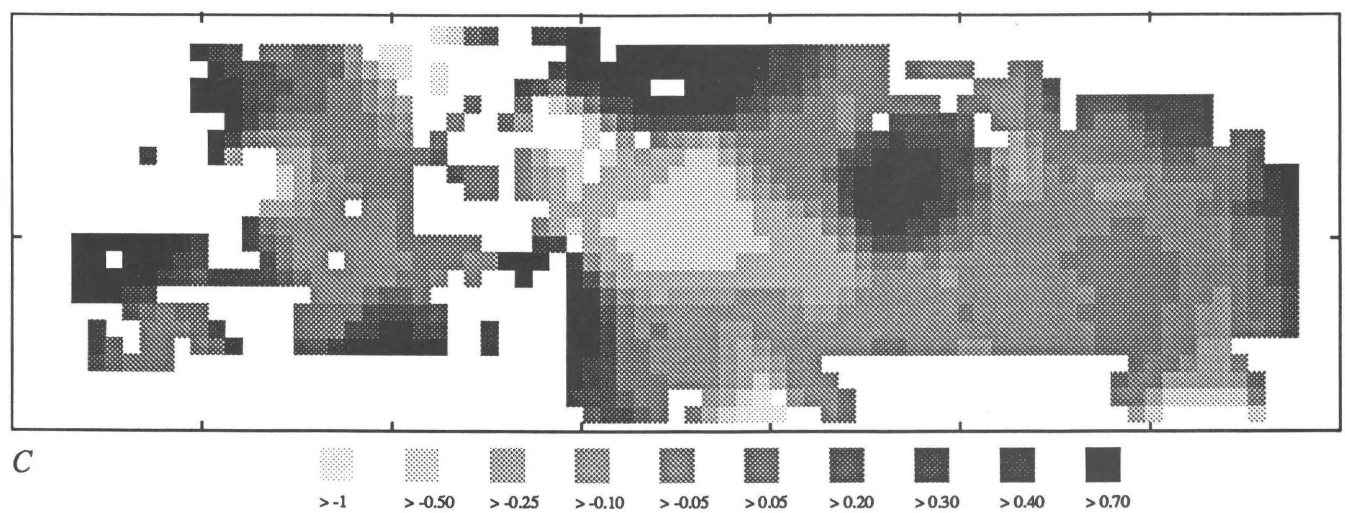

C

Figure 32. *A*, Sample locations. *B*, Distribution of Al content (weight percent). *C*, Enrichment in Mn oxide-rich phases of the northern Pacific study area. Subregion boundaries are provided by overlay in pocket.

Silicon

Silicon concentration ranges in value from 0.24 percent in subregion 00 to 28.5 percent in subregion 07 (compare tables 17 and 18). Lack of data precludes substantive interpretation of the ogives that represent the silicon content (fig. 33) of most of the subregions. Vestiges of discontinuities and (or) wide ranges in concentration exist in subregions 01, 04, 07, and 11.

As shown in figures 34 and 35, silicon shows a strong positive correlation with aluminum and a weak negative correlation with manganese. Enrichments of these variables are correlated essentially the same, but they are a bit more scattered. No visibly detectable correlations exist between silicon or silicon enrichment and any of the other variables.

In figure 36, one major well-defined zone of high silicon concentration exists. It trends northward, is centered in subregion 04, and extends laterally into subregions 03 and 05. The distribution of silicon enrichment is similar to that of silicon concentration.

Table 17. Descriptive statistics for the distribution of Si concentration in Mn oxide-rich phases in the northern Pacific study area

	Frequency distribution			
	Class	Count	%	Cumulative %
Number of non-blank observations = 268	0.24 —			
		19	7.09	7.09
Number of classes (by Sturges' Rule) = 9	3.38 —			
Class size = 3.14		96	35.82	42.91
	6.52 —			
		94	35.07	77.99
Mean = 7.55	9.66 —			
Median (ungrouped data) = 6.91		39	14.55	92.54
Variance = 13.24	12.80 —			
Standard deviation = 3.63		12	4.48	97.01
	15.94 —			
Minimum value = 0.24		4	1.49	98.51
Maximum value = 28.50	19.08 —			
Range = 28.26		3	1.12	99.63
	22.22 —			
		0	0.00	99.63
	25.36 —			
		1	0.37	100.00
	28.50 —			

Table 18. Descriptive statistics for the distributions of Si concentration in Mn oxide-rich phases of subregions in the northern Pacific study area

Subregion	00	01	02	03	04	05	06
Number of samples	2	3	4	7	14	14	27
Mean	0.40	10.73	6.83	10.08	8.73	9.217.80	
Median (ungrouped)	0.24	3.30	5.99	9.66	6.50	8.69	7.30
Variance	0.02	53.65	0.93	7.24	21.98	10.35	11.17
Standard deviation	0.16	7.32	0.96	2.69	4.68	3.21	3.34
Minimum value	0.24	3.30	5.78	6.14	2.79	4.80	1.10
Maximum value	0.57	20.70	7.98	13.10	18.41	16.83	15.60
Range	0.33	17.40	2.20	6.96	15.62	12.03	14.50
Subregion	13	12	11	10	09	08	07
Number of samples	3	8	6	49	100	23	8
Mean	6.46	8.13	6.47	5.48	7.84	7.79	9.39
Median (ungrouped)	6.35	6.46	2.80	5.00	7.03	7.22	5.94
Variance	0.01	6.73	42.94	6.34	9.01	4.14	57.62
Standard deviation	0.10	2.59	6.55	2.51	3.00	2.03	7.59
Minimum value	6.35	5.13	0.90	0.75	2.20	5.20	4.21
Maximum value	6.60	12.42	20.00	14.85	20.43	14.35	28.50
Range	0.25	7.29	19.10	14.10	18.23	9.15	24.29

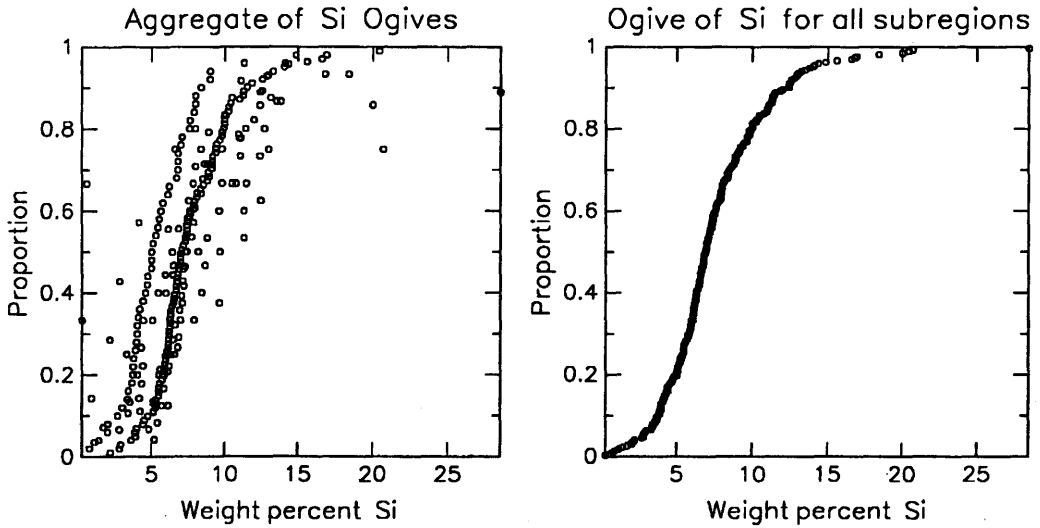

EXPLANATION

Below are ogives of Si content in manganese oxide-rich samples from 14 subregions (SR00–SR13) of a Pacific Ocean study area bounded by 0° N., 40° N., 120° E., and 100° W. All data are from the Scripps Institute of Oceanography's Sediment Data Bank. The relative geographic positions of the subregions are as depicted by the positions of the ogives below. Each datum on each ogive is represented by a circle.

In the upper left of this figure are two summary ogives showing frequency relations for the entire study area. The aggregate of Si ogives superimposes the individual subregion ogives, and the ogive of Si content for all subregions is a pooled, sorted plot of Si content of all subregions considered collectively.

The proportion of each datum is calculated as follows:

$$p = i / (N + 1)$$

where:

p = proportion of population ≤ corresponding Si content,
i = integer rank of datum in population, and
N = number of data points in the array.

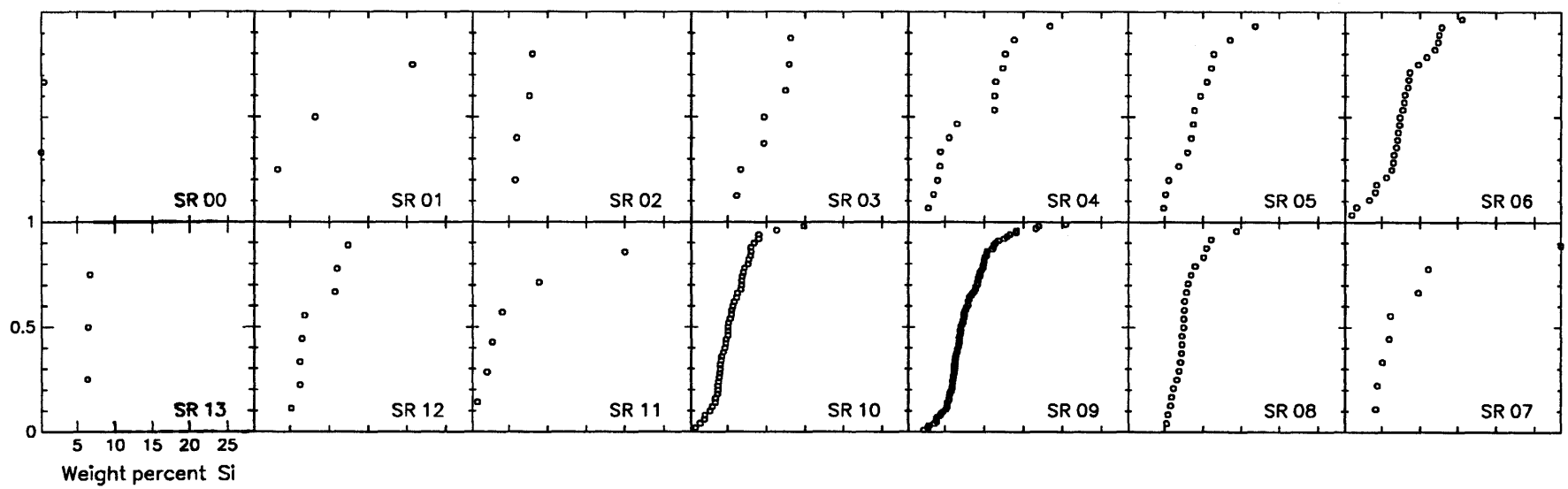

Figure 33. Ogives of Si concentration in northern Pacific subregions.

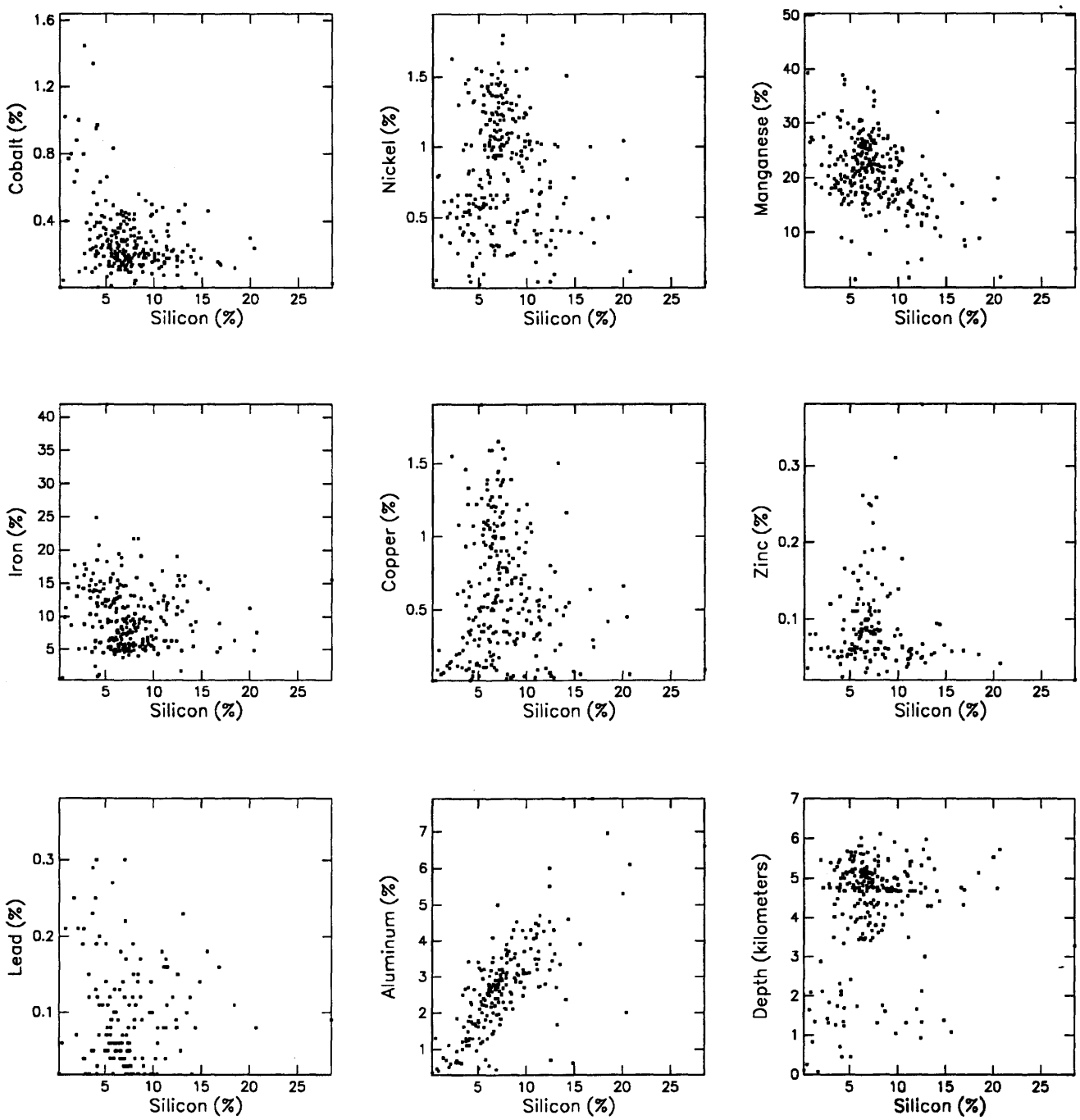

Figure 34. Scatter plots of Si content versus content of Co, Ni, Mn, Fe, Cu, Zn, Pb, Al, and depth in northern Pacific Mn oxide-rich phases.

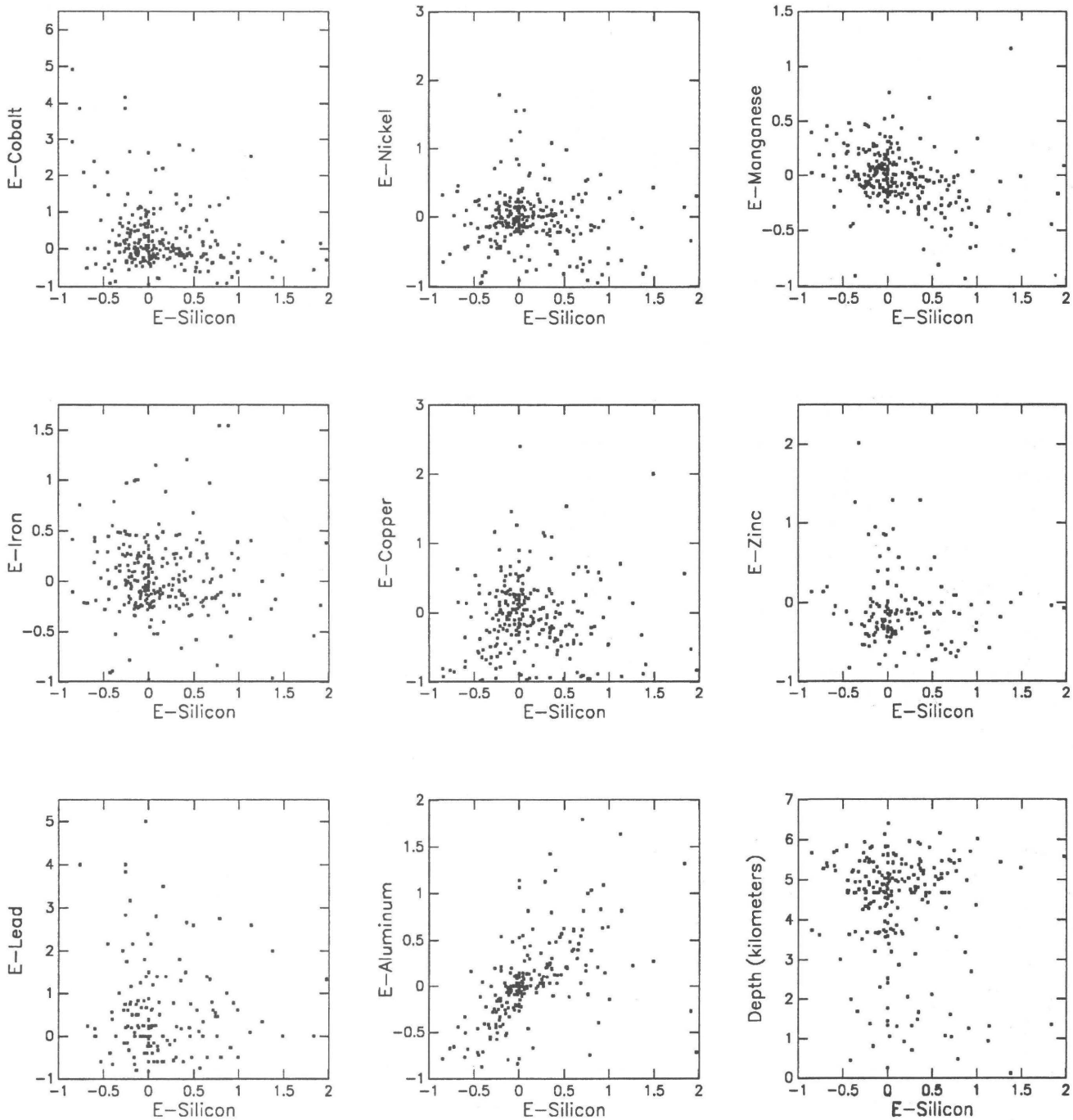

Figure 35. Scatter plots of Si enrichment (E) versus enrichment of Co, Ni, Mn, Fe, Cu, Zn, Pb, Al, and depth in northern Pacific Mn oxide-rich phases.

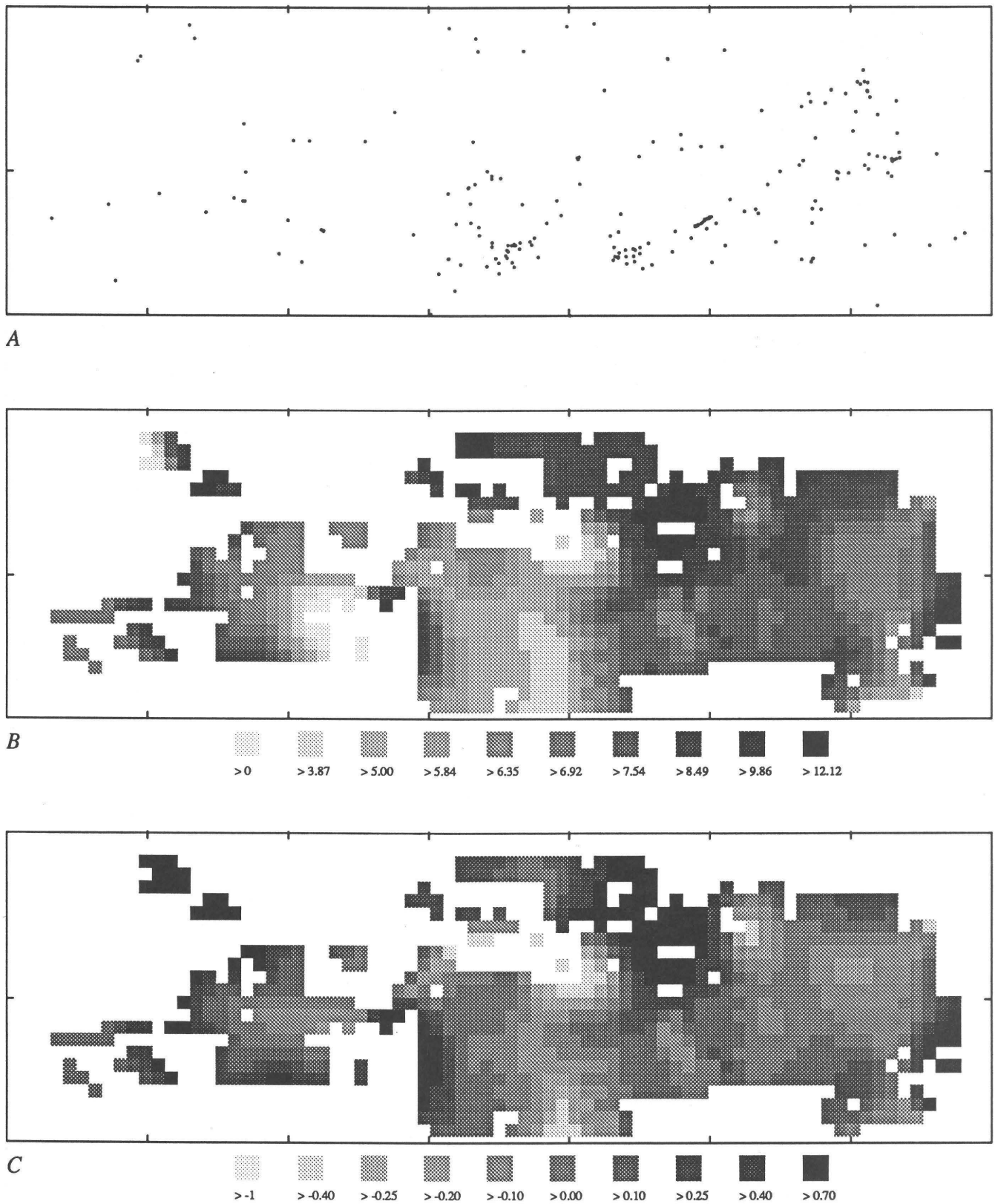

Figure 36. *A*, Sample locations. *B*, Distribution of Si content (weight percent). *C*, Enrichment in Mn oxide-rich phases of the northern Pacific study area. Subregion boundaries are provided by overlay in pocket.

Depth

The scatter plots for depth are provided to illustrate the dichotomy that exists in all distributions (compare figs. 37 and 38). On each scatter plot, a weak to moderately well-defined partition occurs at approximately 3,000 m. Most known crusts occur in the shallower parts of the ocean at less than 3,000 m, and the data may reflect a possible crust versus nodule classification conflict.

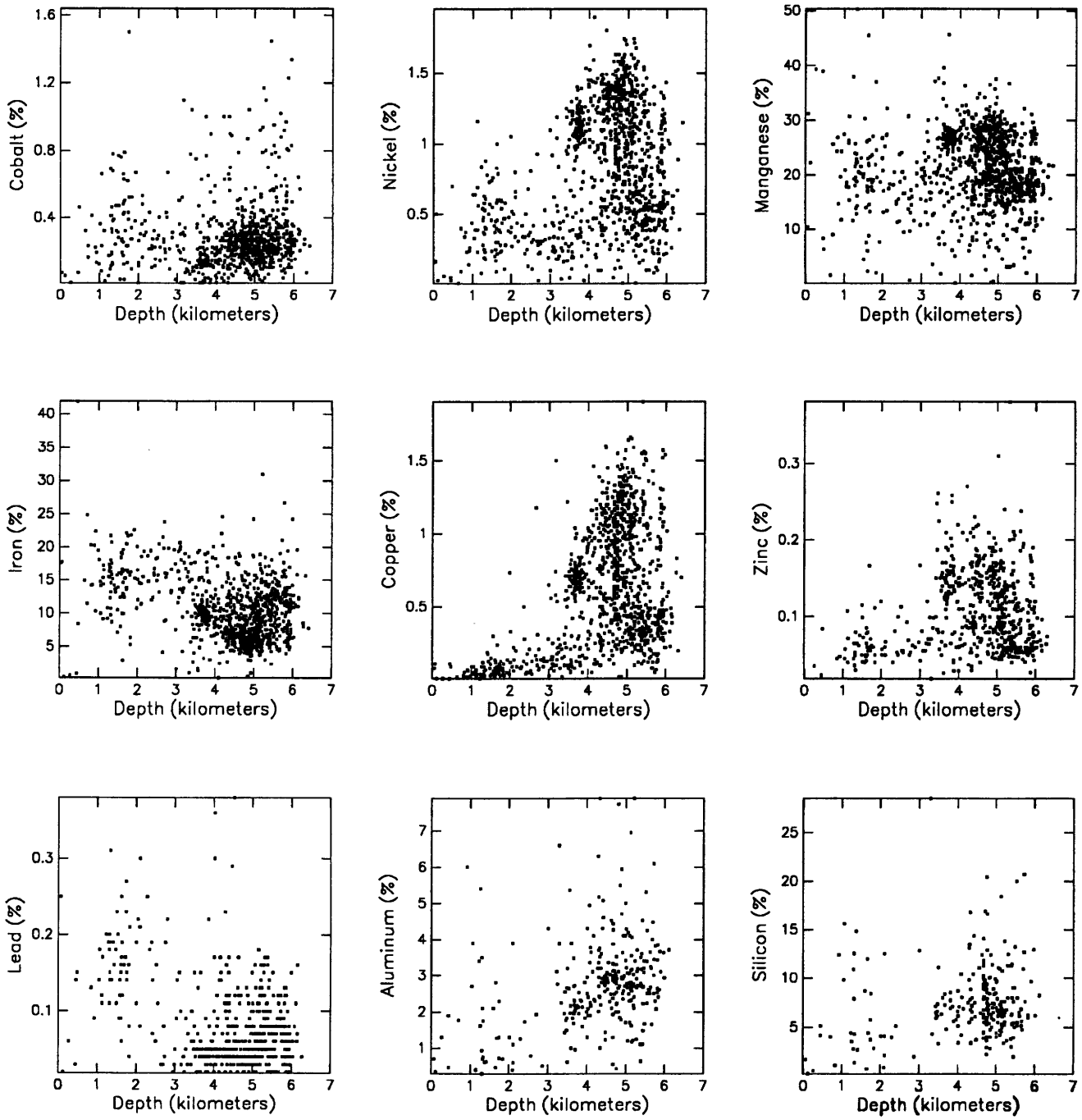

Figure 37. Scatter plots of depth versus content of Co, Ni, Mn, Fe, Cu, Zn, Pb, Al, and Si in northern Pacific Mn oxide-rich phases.

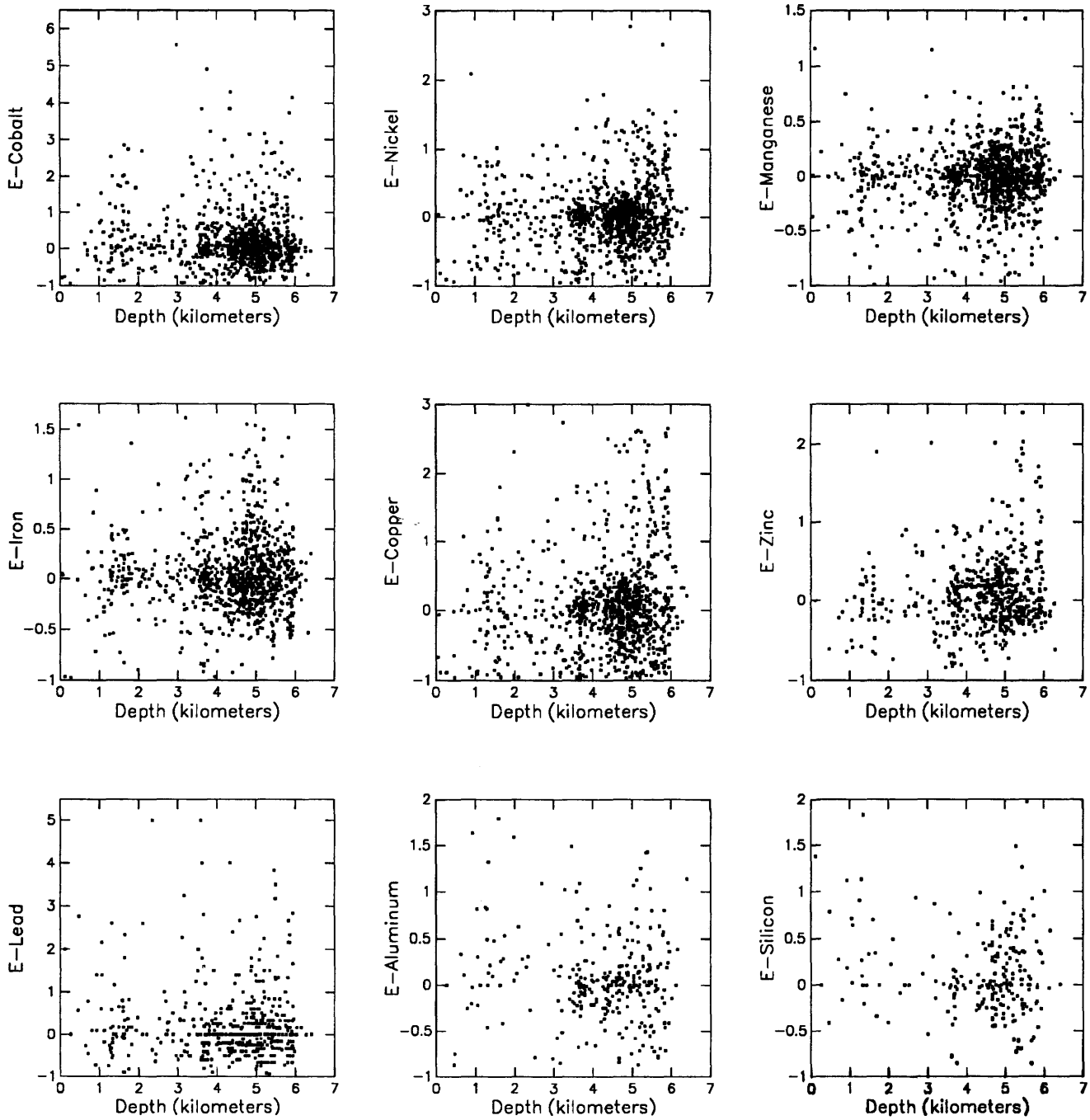

Figure 38. Scatter plots of depth versus enrichment (E) of Co, Ni, Mn, Fe, Cu, Zn, Pb, Al, and Si in northern Pacific Mn oxide-rich phases.

CONCLUSIONS

Tabular, graphic, and cartographic portrayals of preliminary descriptive statistics and data provide a substantial background of information that clearly illustrates conditions and relations that will definitely affect subsequent data analysis and that might otherwise go unnoticed. Of particular importance is the direct relation between tabular and graphic statistics and spatial distributions.

For example, the strong positive correlation of nickel and copper (compare figs. 8 and 20) in their scatter plots is also manifest in their almost identical spatial distributions. The inverse correlation between iron and copper is shown by spatial distributions that are exactly opposite to one another (compare figs. 16 and 20).

Another interesting relation is that between aluminum and silicon (compare figs. 32 and 36). These elements show a strong scatter plot correlation, and yet their spatial distributions are by no means similar except in various parts of the eastern half of the study region. This relation is most likely due to very low sample densities of both elements and the preponderance of the silicon analyses being in the eastern half of the study area.

The gray-scale maps used to portray spatial distributions proved to be very effective at rapid, accurate, and distinct presentation of the data and have high visual impact. The transparent overlay serves to reduce or eliminate annotative clutter from the gray-scale maps. Both the gray-scale maps and the overlay are patterned after the graphics in the Provisional Geochemical Atlas of Northern Ireland (Webb and others, 1973).

FUTURE WORK

All of the data and statistics presented in this report constitute the first part of a multivariate deposit modeling study. The ultimate objective of the study is to use the data and relations as presented in this report to develop models composed of criteria suitable for use in the identification and definition of marine manganese oxide-rich phase mineral deposits. Futher, the techniques used in the establishment of the manganese oxide-rich phase models will serve as guides to analytical methods used to define other types of marine deposits such as heavy metals, precious metals, and nonmetallics.

REFERENCES

Bowen, R.W., and Botbol, J.M., 1975, The geologic retrieval and synopsis program (GRASP): U.S. Geological Survey Professional Paper 966, 87 p.

Commeau, R.F., Clark, A., Johnson, C., Manheim, F.T., Aruscavage, P.J., and Lane, C.M., 1984, Ferromanganese crust resources in the Pacific and Atlantic oceans: Proceedings of Oceans, IEEE Ocean Engineering Society, p. 421–430.

DeYoung, J.H., Jr., Sutphin, D.M., and Cannon, W.F., 1984, International strategic minerals inventory summary report—manganese: U.S. Geological Survey Circular 930–A, 22 p.

Evenden, G.I., 1988, MAPGEN—computer program for generating maps: U.S. Geological Survey unpublished Administrative Report, Woods Hole, Mass.

———1988, PLOTGEN—computer program for generating graphics: U.S. Geological Survey unpublished Administrative Report, Woods Hole, Mass.

Frazer, J.Z., and Fisk, M.B., 1980, Availability of copper, nickel, cobalt, and manganese from ocean ferromanganese nodules (III): La Jolla, Calif., Scripps Institution of Oceanography, SIO reference 80–16 (prepared for U.S. Bureau of Mines), 117 p.

Huntsberger, D.V., 1963, Elements of statistical inference: Boston, Allyn and Bacon, 291 p.

Johnson, C.J., Clark A.L., and Otto, J.M., 1985, Pacific Ocean minerals; the next 20 years, *in* Johnson, C.J., and Clark, A.L., eds., Pacific mineral resources; physical, economic, and legal issues: Proceedings of the Pacific marine mineral resources training course, Honolulu, Hawaii, East-West Resource Systems Institute, p. 21–40.

McKelvey, V.E., 1986, Subsea mineral resources: U.S. Geological Survey Bulletin 1629–A, 106 p.

McKelvey, V.E., Wright, N.A., and Bowen, R.W., 1983, Analysis of the world distribution of metal-rich subsea manganese nodules: U.S. Geological Survey Circular 886, 55 p.

Webb, J.S., 1973, Provisional geochemical atlas of Northern Ireland: London, Applied Geochemistry Research Group, Imperial College of Science and Technology, Technical Communication no. 60, 30 p.